An experimental investigation of the spin dynamics of dipolar spin ice

by

Luke Yaraskavitch

A thesis
presented to the University of Waterloo
in fulfillment of the
thesis requirement for the degree of
Master of Science
in
Physics

Waterloo, Ontario, Canada, 2012

I hereby declare that I am the sole author of this thesis. This is a true copy of the thesis, including any required final revisions, as accepted by my examiners.

I understand that my thesis may be made electronically available to the public.

Abstract

The low temperature spin dynamics of the canonical dipolar spin ice materials is examined. The ac susceptibility of dipolar spin ice materials $Ho_2Ti_2O_7$ and $Dy_2Ti_2O_7$ is measured to lower temperatures and frequencies than previous studies. This provides a probe of the dynamics of fractionalized magnetic excitations which have been found to exist and interact as monopole-like particles within the spin ice configuration. Low temperatures and low frequencies access the dilute monopole phase, and provide a valuable stress case scenario to theory which has been used to describe the system to date. The relaxation is found to be well described at the lowest temperatures by an Arrhenius law with single energy barrier for both $Ho_2Ti_2O_7$ and $Dy_2Ti_2O_7$, with similar barriers to relaxation, 10.7 K and 9.79 K respectively. It is also revealed to be distinctly different from predictions of the dipolar spin ice model, based upon simulations of both a Coulomb gas and dipolar spin ice on the pyrochlore lattice. These simulations, as well as calculations based on Debye-Hückel theory, do not see Arrhenius behaviour in our temperature range, and do not predict the rate at which dynamics freeze out. It is not currently understood what would be required in order to amend this. The implications for thermal methods of probing spin dynamics is discussed, as well as how this measurement impacts the magnetolyte theory of spin ice. Brief reports are presented in the appendices of specific heat measurements of three spin liquid candidates: $Yb_2Ti_2O_7$, $Tb_2Ti_2O_7$, and $Pr_2Hf_2O_7$. In $Yb_2Ti_2O_7$, measurements of three single crystals, two unique features, a broad anomaly at 195 mK and sharp peak at 265 mK, are found which seem to comprise elements of previous single crystal and polycrystalline measurements. These low temperature features do not correspond to changes in neutron scattering intensity at 400 mK. In $Tb_2Ti_2O_7$, a second order transition is found, corresponding to the emergence of a mode in inelastic neutron scattering. Absence of an ordering transition in the suspected $\langle 111 \rangle$ antiferromagnet $Pr_2Hf_2O_7$ is also shown, with specific heat measured down to 100 mK with no ordering transition.

Acknowledgements

First, I would like to thank my supervisor, Jan Kycia, who has been a great source of ideas, guidance, and hands-on help. The knowledge imparted to me, often accompanied by a great anecdote, has been invaluable. His skill with electronics and dilution fridges is essential, and has been there at some pretty exceptional times to diagnose problems and get the show back on the road. I have benefitted greatly from having a supervisor who is there in all aspects of low temperature research. Jan's enthusiasm for coffee also helped fuel innumerable hours of productive work. Chas Mugford spent an enormous amount of time assisting me when I first joined the lab for my fourth year research project, and the time and patience he invested in working with me and my project was what got me interested in low temperature physics in the first place. I was very lucky to have spent that time working with and learning from Chas. I am very grateful for having worked with Jeff Quilliam, who I have learned a great deal about the study of low temperature magnetic materials from. I had the good fortune of Jeff's mentoring in specific heat and susceptibility measurements, with which I was able to hit the ground running, starting with his assistance with $Pr_2Hf_2O_7$ and our joint $Ho_2Ti_2O_7$ measurement. Between Jeff and Shuchao Meng, I also learned how to operate the dilution refrigerator, and had the benefits of their assistance with every aspect of it. After Jeff graduated, Shuchao was also my fridge wingman, always willing to help out on an evening or weekend with cooldowns and transfers. Jeff Mason always seems to be around to offer a second pair of hands and a place to bounce ideas off of. Halle Revell's SQUID expertise has made her my go-to person when the SQUID will not work, and I am thankful for all of her technical assistance with the SQUID. It has also been great to work on complementary spin ice measurements with her. Recently, thanks to David Pomaranski who has been enthusiastically taking on the specific heat measurements. Thanks to the rest of the Kycia group around at various parts of my time here; Lauren Persaud, Dave Vresk, Borko Djurkovic, and Shaoxoing Li. Thanks to Rob Hill, for being a member of my committee as well as another source of experimental low temperature advice. His graduate students, John Dunn, Will Toews, and Kevin Liu, were also great neighbours; always willing to help and share a laugh. They also had the essential role of purifying helium and feeding our mutual liquid helium habit, as not just any dirty old helium will do. I would also like to thank Michel Gingras for being a member of my committee, and David Hawthorn for being a reader for my defense.

Science Technical Services down the hall have been integral for keeping experiments moving forward through the various technical work they do, and without their skilled help, especially Andrew Dube, Hiruy Haile, and Peter Kessel, progress would have been delayed more than once.

I am grateful for the opportunity I had to collaborate with other condensed matter physicists across the world. Thanks to my McMaster University collaborators, especially Kate Ross and her supervisor Bruce Gaulin with whom I worked on a few of the projects presented in this thesis, and who provided most of the pyrochlore samples I studied. Stefan Kycia and Ariel Gomez at the University of Guelph were very accommodating in their efforts and patience assisting me with alignment of some samples, as well as conducting powder diffraction work. Thanks to Patrik Henelius at the Royal Institute of Technology for taking an interest in my work and the valuable discussions, calculations, and enthusiasm he has contributed to it.

Graduate school would be pretty dull without fellow graduate students to celebrate or commiserate over a coffee or a pint with, and I'm thankful to have had many friends while here. While this encompasses those mentioned above, it includes but is not limited to Jordan Thompson, Mike Wesolowski, Robert Lepage, Chad Daley, Lucas Jones, and, naturally, all the Quantum Matters chums. It has been a privilege to have met, worked with, and become friends with so many people.

My parents get well-deserved thanks for all their continuing love, support, and encouragement through my many years here in Waterloo. Almost as important, the regular shipments of garden produce, baking, maple syrup, and venison always ensured I had a taste of home.

Last but certainly not least, countless thanks to my fiancée, Katie, for her understanding of the crazy lifestyle experimental research in graduate school imposes on one's self. Her love and patience throughout and ensured I got through all this.

Dedication

This is dedicated to my fiancée, Katie, who, near or far, has been amazingly supportive. Thank you for all of your love, patience, and support through my years here. There were some tough spells that came along, and I was and still am lucky to have you to ride them out with me. I couldn't have done it alone.

Table of Contents

List of Tables

List of Figures

Chapter 1

Introduction

Frustration in nature has been a source of fascination for scientists for nearly a century beginning with the identification of a macroscopic number of ground states in water ice. Frustration is defined as the inability of a system to satisfy all of its interactions simultaneously and thus select a unique ground state. Suprisingly, this plays a significant role in several natural systems, including water [1], protein-folding for biological roles [2], supercooled liquids and their glassy state, [3], and magnetism [4]. Much like the well-known arrangements of atoms as solid, liquid, and gas phases, magnetism has analogues in the arrangement of magnetic moments: magnetically ordered, spin glass, spin ice, spin liquid, and paramagnetic states. In many cases, the magnetic system provides a very clean example of these analogous phases of matter, making them ideal systems in which to explore frustration. The reach of current methods of study, particularly methods in low temperature physics and powerful simulation techniques, allow for exhaustive characterization and modelling of these materials. Even so, many are a far cry from being solved systems, and remain extremely rich fields of study with a substantial volume of active research ongoing throughout the condensed matter community.

This thesis is focused around the use of low temperature ac magnetic susceptibility to study frustration in magnetism, specifically on two members of the pyrochlore oxide family. This work will focus on the dynamics of the canonical dipolar spin ice materials, holmium titanate ($Ho_2Ti_2O_7$) and dysprosium titanate ($Dy_2Ti_2O_7$), within the frozen 'ice-rule' regime, which recent work has put forward as a host to fractionalized excitations which behave as magnetic monopoles [5] . Naturally, attempts to verify and characterize this based upon interpretation of existing and new data in the framework of the dipolar spin ice model [6, 7, 8, 9, 10, 11, 12, 13] have followed in short order. Several theoretical and experimental works have focused on dynamics of these monopoles, whether through

comparison to prior ac susceptibility results as a signature of monopole dynamics [6] or matching magnetization decay measurements to a 'magnetolyte' dissociation process [13]. The motivation of this project was to measure ac susceptibility to lower temperatures and frequencies than had been previously measured to establish a benchmark of the low temperature dynamics of spin ice. Data in this regime will provide a test of the predictions of the dipolar spin ice model, as well as a valuable understanding of the time and energy scales involved in the motion of magnetic defects.

Chapter 1 will discuss frustration and the magnetic pyrochlore oxide family, which happen to be excellent candidates for frustration based upon their lattice composition of corner-sharing tetrahedra. Chapter 2 will address water ice and dipolar spin ice, $Ho_2Ti_2O_7$ and $Dy_2Ti_2O_7$. Dipolar spin ice viewed through the context of magnetic monopoles will be next in Chapter 3, discussing the initial recognition of the monopole picture, and the experimental and theoretical works which have followed that realization. Chapter 4 will present the experimental methods used here, the dilution refrigerator and a superconducting quantum interference device (SQUID)-based magnetometer. At the heart of this thesis, Chapter 5 presents ac susceptibility measurements of $Ho_2Ti_2O_7$ and $Dy_2Ti_2O_7$ at low temperatures. This thesis work has revealed Arrhenius relaxation at the lowest temperatures studied in both spin ices. How this fits in the context of the existing monopole work will be discussed. Lastly, Chapter 6 will conclude and summarize what this work has accomplished, and possible fruitful topics for future work.

The appendices contain several specific heat measurements of three other pyrochlores also completed during the course of this Masters which did not fit within the overall context of this thesis. The measurement method is briefly described in Appendix A. The first two, rare earth titatates ytterbium titanate ($Yb_2Ti_2O_7$) and terbium titanate ($Tb_2Ti_2O_7$), were initially tagged as spin liquids, and have been the subject of varying experimental and theoretical reports as to their low temperature state [14]. $Yb_2Ti_2O_7$ has been most recently proposed to be a quantum spin ice by recent experimental and theoretical work [15]. A specific heat study of several samples complementary to neutron scattering work with collaborators [16] is presented in Appendix B. The $Yb_2Ti_2O_7$ study set out to determine the quality of a particular single crystal after early measurements found a clear difference between powder and single crystal samples. This included measuring the same sample upon which neutron scattering was performed. The second material, terbium titanate ($Tb_2Ti_2O_7$), has been most recently characterized as a quantum spin ice candidate as well [17]. The $Tb_2Ti_2O_7$ study is a short description of the measurement of one polycrystalline sample, which is proposed to be a high quality sample exhibiting all of the fundamental features of $Tb_2Ti_2O_7$ [18]. Inconsistency in both polycrystalline and single crystal samples have led to conflicting results and conclusions. We present our measurement on a sample

grown in the same manner as that studied by Takatsu *et al.* [19] in Appendix C. These two materials are somewhat more exotic than the classical spin ice materials, as it seems their proximity to a phase boundary has led to such variability in measured materials. Lastly, in Appendix D, we will discuss specific heat measurements of praseodymium hafnate ($Pr_2Hf_2O_7$), which preliminary study had shown appears to be an Ising antiferromagnet pyrochlore oxide avoiding the predicted long range order state [20].

1.1 Frustration

The two paths to frustration are geometry and randomness [14]. Here, we will be focused on geometrical frustration. The classic toy model example used to convey geometric frustration is that of Ising spins interacting through an antiferromagnetic exchange of energy J_{ex} on vertices of a two-dimensional triangular lattice. This simple Hamiltonian can be written as:

$$H = -J_{\text{ex}} \sum S_i \cdot S_j \tag{1.1}$$

Where J_{ex} is the exchange energy (negative, in the antiferromagnetic case) and S_i is the Ising spin at the ith site (± 1 symbolizing up or down). In the ferromagnetic case (positive J_{ex}), all interactions are easily satisfied by ordering all spins up, or all spins down. In the antiferromagnetic case (negative J_{ex}), any one exchange between two spins can be satisfied, but satisfying the second exchange will require forcing the third to be a coupling of up and up or down and down spins. Thus, we are left with a degenerate ground state manifold with 6 possible states (Fig. 1.1), and a finite residual entropy. This system was investigated early on by Wannier and Houtappel in separate studies [21, 22].

The spinel structure, was also explored by Anderson in 1956 in the context of a finite ground state entropy [23]. In fact, in the nearest neighbour exchange model on the corner-sharing tetrahedral site of this lattice (later recognized as the pyrochlore lattice) he noted an analogue in water ice: the short range order which would occur gave a ground state with a residual entropy just like Pauling's water ice prediction. The ice rules, two long hydrogen-oxygen bonds and two short bonds, were mapped to an equivalent two up-spins and two down-spins per tetrahedron, leaving six possible states. These spins were considered lying in the global z-axis. Anderson also briefly examined frustration in 3-1 state, where along the [111] axis the system decoupled into triangular lattice planes and kagome planes. Subsequent theoretical work examining candidate systems was done. Villain also reported on the multiple ground states of the spinel structure [24]. It is interesting to note the use of the term frustration to describe a system which could not select a unique ground

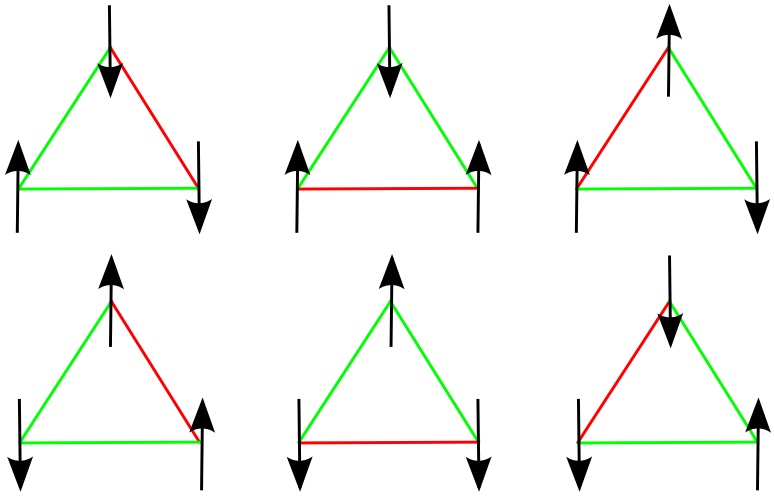

Figure 1.1: Frustration demonstrated on the triangular lattice for antiferromagnetic (negative) J_{ex}. There is six-fold degenerate ground state.

state was ascribed to Anderson, describing glassy phenomena in 1976 [14], well after the initial recognition of absence of a ground state in the triangular lattice.

Naturally, the Hamiltonian in actual materials systems is rarely as simple as the exchange model proposed in the previous paragraph, but regardless, systems that seemingly refuse to select a unique ground state have been observed within the limits of many methods of probing these systems. A classic parametrization of magnetic systems is to use a Curie-Weiss law to estimate the strength of the magnetic interactions, which can be anticipated in many systems as the temperature scale where order may be expected. However, several systems persist in avoiding long range order even at temperatures well below the magnitude of their nearest-neighbour interactions.

Among the multitude of systems studied, the lattice of corner sharing tetrahedra known as the pyrochlore lattice exhibited frustration, as explored by Anderson. The pyrochlore lattice will be the focus of our interest.

1.2 Magnetic pyrochlore oxides

The magnetic pyrochlore oxide family achieves the corner-sharing tetrahedra class of triangular geometry desired for frustrated interactions. As a result of this inherent potential

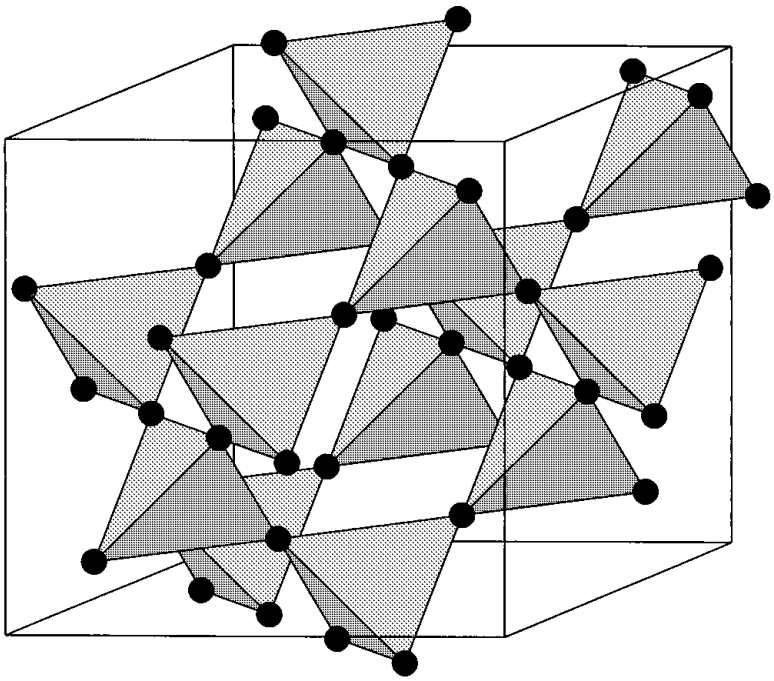

Figure 1.2: The rare earth ion sites for one unit cell of the cubic pyrochlore lattice, comprised of corner-sharing tetrahedra. From Ref. [25].

to exhibit frustration, the magnetic pyrochlore oxides have been a rich field of study for decades. A recent review by Gardner *et al.* provides an extensive overview of many of the pyrochlore oxides, and the menagerie of physical properties seen in this family of materials [14]. The namesake of the pyrochlore oxides is the material $NaCaNb_2O_6F$, which burns green, giving the name "green fire" [14]. The pyrochlores studied here are of the chemical formula $A_2B_2O_7$, where A is a trivalent rare earth, and B is generally a tetravalent transition metal. This material crystallizes into face-centred cubic space group $Fd\bar{3}m$. The A^{3+} and B^{4+} ions each sit on lattices of corner-sharing tetrahedra, as can be seen for the A-site in Fig. 1.2, where the tetrahedra are centred on sites of the diamond lattice. These two sublattices are interleaved with one another.

There is a large variety of choices on the A^{3+} and B^{4+} sites, as one or the other can be magnetic, or both, or none. The pyrochlores studied in this work all have magnetic A^{3+} ions and non-magnetic B^{4+} ions. The largest term of the Hamiltonian for these materials is the crystalline electric field, which determines the $|J, m_j\rangle$ states. The crystalline electric field has significant implications for the rare earth ions in the material and generally comprises

the largest term of the Hamiltonian describing the material. The rare earth ions have D_{3d} point symmetry. It can be represented most generally as

$$H_{\mathrm{CF}} = \sum_i \sum_{l,m} B_l^m O_l^m(J_i) \tag{1.2}$$

There, O_l^m are Stevens operator equivalents, J_i is the angular momentum operator, and B_l^m are the crystal field parameters [14]. The local electrostatic and chemical environment lifts the (2J + 1) degeneracy of energy levels of the A^{3+} free ion, splitting it into a collection of singlets and doublets, with the ground and first excited state often determining the low temperature behaviour of the spins. Kramers theorem states that rare-earth ions with an odd number of valence electrons must have energy levels split into at most, doublets, in zero field (Kramers ions). Ions with an even number of electrons, however, can split into a collection of doublets or singlets (non-Kramers ions). With the crystal field determining the available energy levels to the system, various types of exchange and dipolar interactions come into play.

The variety of materials and configurations also leads to all types of interactions in the Hamiltonian. After accounting for the crystal field, the interactions, H_{int}, then determine the nature of the system, whether it be long range order, glassiness, strongly correlated liquid-like behaviour, or total lack of order. As stated before, all are analogous to structural phases in materials. Some of the physics exhibited is briefly highlighted here, while spin ice will be discussed in more detail in the following section.

1.2.1 Paramagnet

Paramagnetism favours alignment of magnetic moments parallel to magnetic field. Insulating materials containing rare earth ions are very well characterized by a Curie law dependence of the susceptibility at high temperatures and low fields, where the moments do not really interact:

$$\chi = \frac{1}{3}\frac{N}{V}\frac{\mu_B^2 p^2}{k_B T}, \text{ for } k_b T >> g\mu_B H \tag{1.3}$$

Where p is the effective Bohr magneton number, μ_B is the Bohr magneton, and N/V is the ion density. This state where magnetic moments will follow any applied field is physically analogous to a gas, and is also characterized by a short correlation length. The accepted measured values for the magnetic moments of several rare earth ions are given Table 1.1, reproduced in part from Ref. [26]. With interacting magnetic moments in a ferromagnet,

however, the susceptiblity in the paramagnetic regime is described by a Curie-Weiss law:

$$\chi = \frac{C}{T - T_{\mathrm{c}}} \tag{1.4}$$

Where C is the Curie constant for a given material, and T_{c} is the transition temperature. This produces a diverging susceptibility as T approaches T_{c}.

Table 1.1: Ground state configurations and effective magneton numbers for select trivalent rare earth ions.

Element	Configuration	Ground state term	measured p
Pr	$4f^2$	$^3H_4$	3.5
Tb	$4f^8$	$^7F_6$	9.5
Dy	$4f^9$	$^6H_{15/2}$	10.6
Ho	$4f^{10}$	$^5I_8$	10.4
Yb	$4f^{13}$	$^2F_{7/2}$	4.5

1.2.2 Spin Liquid

A spin liquid is analogous to a normal liquid, exhibiting longer range correlations than a gaseous state (or paramagnetic state), but no long range magnetic order. True to this analogy, it is regularly referred to as a cooperative paramagnet. Generally, this state is typically a result of antiferromagnetic interactions, and frustration-favourable triangle-based geometry. There is an excellent review article on the recent state of the spin liquid search by Balents [27]. The pyrochlore family contains several excellent candidates. $Tb_2Ti_2O_7$ and $Yb_2Ti_2O_7$ elude showing long range order under a barrage of experimental techniques. Specific heat and ac susceptibility of $Tb_2Ti_2O_7$ is shown in Fig. 1.3, where we can see Hamaguchi *et al.* did not find long range magnetic order in susceptibility, in spite of a second order transition in the specific heat.

It is actually under this broad heading where the topic of this thesis, spin ice, fits. Spin ice displays the hallmarks of spin liquid behaviour: absence of order, and short range correlations. This will be discussed in further detail later.

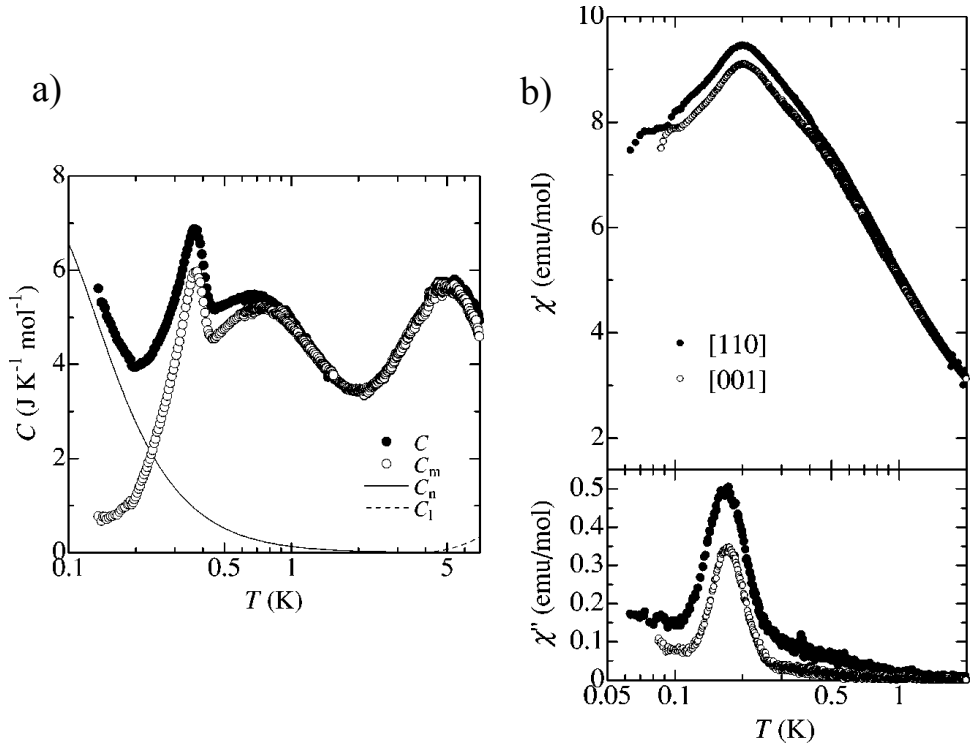

Figure 1.3: The specific heat and ac susceptibility of spin liquid candidate $Tb_2Ti_2O_7$. A signature of magnetic ordering is not present. From Ref. [28].

1.2.3 Spin Glass

The spin glass state is generally characterized by a freezing of the magnetic moments at some finite temperature T_f. This is traditionally achieved through a combination of geometric frustration and randomness, achieved through substitution of non-magnetic ions. The spin glass state is established definitively through a diverging non-linear susceptibility, χ_3, but can also be experimentally identified by a frequency dependent dissipation in ac susceptibility, χ'', and linear dependence of low temperature heat capacity and muon spin resonance. One example of this state is $Y_2Mo_2O_7$ [14], shown in Fig. 1.4, where specific heat shows no ordering transition.

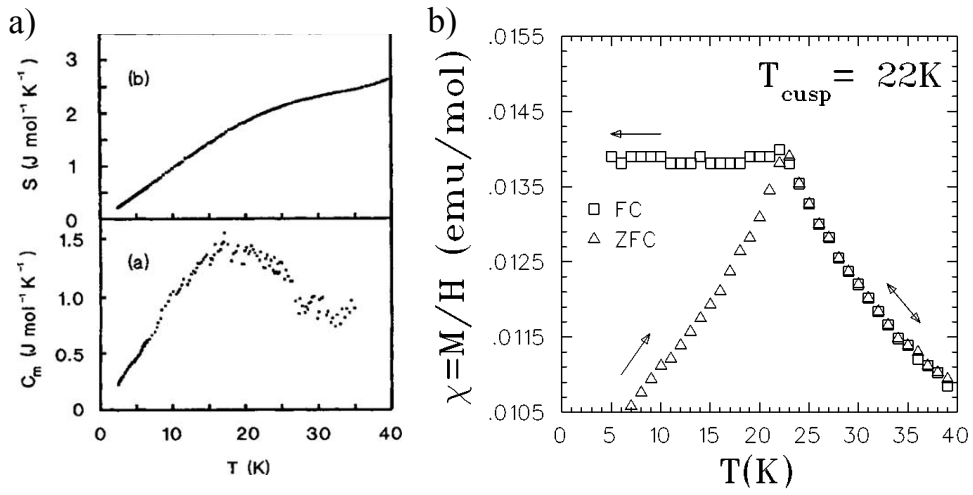

Figure 1.4: The specific heat (a) and susceptibility (b) of $Y_2Mo_2O_7$, a spin glass. Neither the specific heat or susceptibility exhibit a clear transition to long range order. From Refs. [29] and [30] respectively.

1.2.4 Long Range Order

There are a whole host of pyrochlores which display long range order. Systems such as $Gd_2Sn_2O_7$, $Er_2Ti_2O_7$, and $Tb_2Sn_2O_7$ are a few examples. With lowering temperatures, the absence of order can be a delicate state to maintain, and often some aspect of the system, such as further nearest neighbour interactions, single ion anisotropy, or anisotropic interactions, will allow order to become energetically favourable [14]. One of these long range ordered examples is shown in Fig. 1.5, $Gd_2Sn_2O_7$, with two thermodynamic signatures, specific heat and susceptibility.

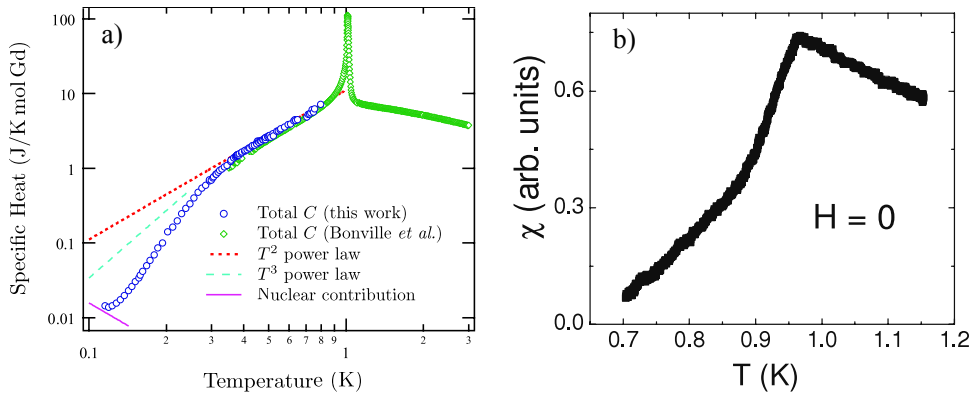

Figure 1.5: The specific heat (a) and susceptibility (b) of $Gd_2Sn_2O_7$. The ordering transition in specific heat corresponds well to the cusp in susceptibility. From Refs. [31] and [32].

Chapter 2

Spin Ice

2.1 Water Ice

Frustration (though not labelled as such at that point) was first identified in one of the most common chemicals on Earth, H_2O. Structurally, ice was determined to be composed of tetrahedrally coordinated molecules [33], with no sense of the position of the hydrogen atoms. Early calculations by Giauque and Ashley determined a residual measured entropy in water ice in 1933 [34], carefully verified by measurements by Giauque and Stout [35]. Bernal and Fowler had suggested the simplest possible structure of ice, mandating that water ice must order with two 'short' and two 'long' oxygen-hydrogen bonds [36]. In 1935, Pauling found that the residual entropy to be in agreement with these rules, having estimated the zero-point entropy to be $S_0 = (R/2)\ln(3/2)$. The ice-rules leave 6 possible arrangements per molecule, and lead to a highly (macroscopically) degenerate ground state.

Now, as mentioned previously, the analogy between the pyrochlore lattice and the tetrahedrally coordinated water ice had already been noted by Anderson in 1956 [23]. Very interestingly, it was found a few of the pyrochlore oxides actually displayed very similar physics. We will now discuss a magnetic system displaying analogous properties to water ice, spin ice.

2.2 Dipolar Spin Ice

Two particular pyrochlores, $Ho_2Ti_2O_7$ and $Dy_2Ti_2O_7$, are the protagonists in this story. Ho^{+3} ($J = 8$) is a non-Kramers ion while Dy^{+3} ($J = 15/2$) is a Kramers ion.

Very preliminary susceptibility measurements by Cashion *et al.* in 1968 found both $Ho_2Ti_2O_7$ and $Dy_2Ti_2O_7$ had significant magnetic moments at low temperatures, and likely antiferromagnetic interactions [37]. Heat capacity and susceptibility measurements of $Dy_2Ti_2O_7$ by Blöte *et al.* in 1969 found a broad maximum and suggested that not all the expected $S = R \ln 2$ entropy of a Kramers doublet ground state was being recovered, based on extrapolation to higher temperatures [38]. The dc susceptibility also hit a maximum at 0.9 K, then falling to nearly zero by 0.4 K, indicating a large anisotropy.

The spin ice phenomenology was initially recognized in 1997 by Harris *et al.* in $Ho_2Ti_2O_7$, a system which mapped to that of water ice [39]. The ferromagnetic effective exchange energy resulted in a highly degenerate ground state, just as in water ice, with six different configurations for each tetrahedra. The difference between this system and what Anderson studied was the local $\langle 111 \rangle$ axis, with spins at each vertex of a tetrahedron lying along an axis passing through the centre of the tetrahedron. With applied field, they were able to induce order. Muon spin resonance and diffuse neutron scattering verified the lack of order [40]. The ferromagnetic exchange was initally mystifying to the community studying this, as it was indeed thought that ferromagnetic exchange here should lead to long range order, which paradoxically this system avoided.

Specific heat measurements by Ramirez *et al.*, repeating the work of Blöte *et al.* over a larger temperature range in order to attempt to account for the missing entropy, again found that not all of the entropy expected for a Kramers doublet, $S = R \ln 2$, was recovered (Fig. 2.3). Once again, there was an absence of an ordering transition, with instead a broad

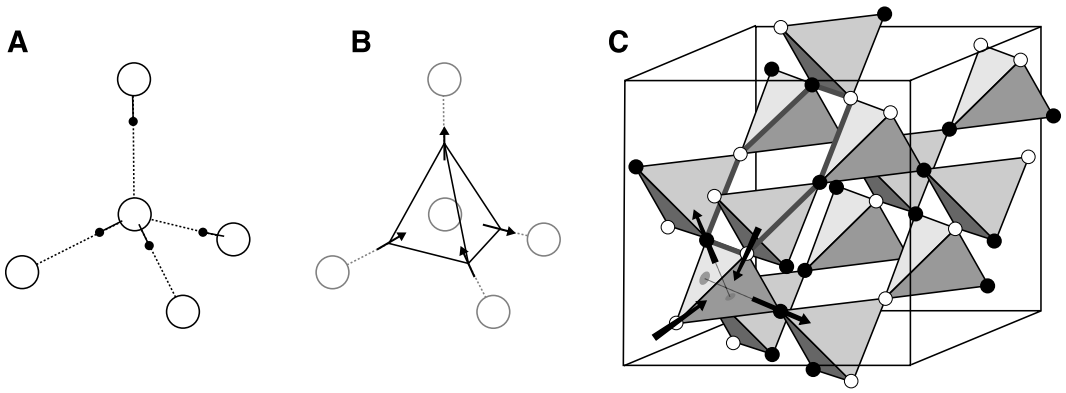

Figure 2.1: a) The coordination of oxygen atoms in ice showing the ice rules. b) how the ice rules map to a single tetrahedra. c) The cubic unit cell of the pyrochlore lattice. From Ref. [4].

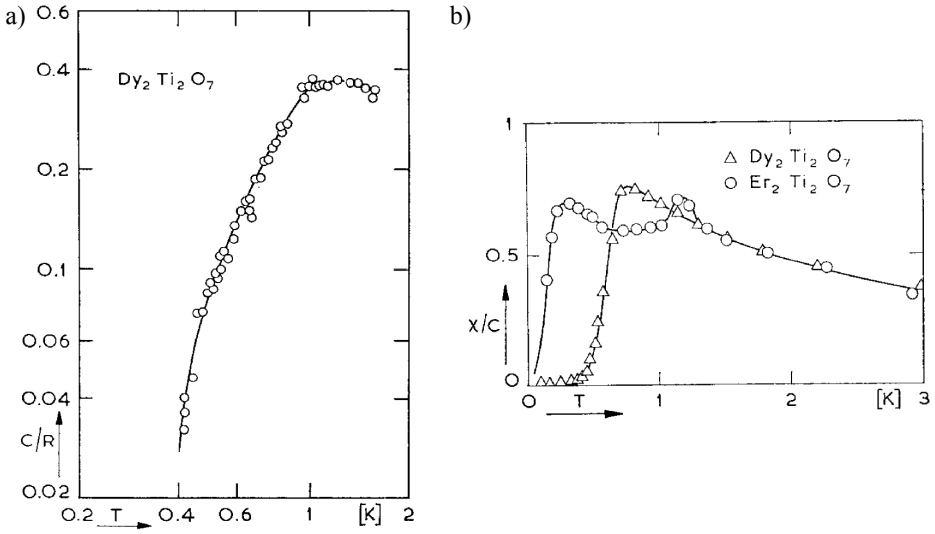

Figure 2.2: a) The specific heat of $Dy_2Ti_2O_7$, first measured by Blöte *et al.*, with no ordering signature. b) The dc susceptibility, showing a rapid drop in the susceptibility. From Ref. [38].

peak centred around ∼1.2 K. This agreed reasonably well with Monte Carlo simulations of the specific heat in zero field. The entropy $S_{\rm mag}(T)$ can be calculated through integration of the magnetic specific heat $C_{\rm mag}$,

$$S_{\rm mag}(T) = \int_1^2 \frac{C_{\rm mag}(T)}{T}\,{\rm d}T \tag{2.1}$$

which found the remaining entropy to be quite close to the Pauling $S_0 = (R/2)\ln(3/2)$ residual entropy of water ice, thus establishing this ice phenomenology could indeed describe $Dy_2Ti_2O_7$ [41]. In applied field, three distinct specific heat features were observed, but without orientation, it was not possible to narrow down the orientation-dependence of any features.

Monte Carlo simulations in tandem with specific heat measurements by Siddharthan *et al.* introduced dipole-dipole interactions into the system (up to fifth nearest neighbour), the first to suggest the importance of dipole-dipole interactions [42]. These simulations found $Dy_2Ti_2O_7$ to be commensurate with a spin ice state, but not $Ho_2Ti_2O_7$. Simulations

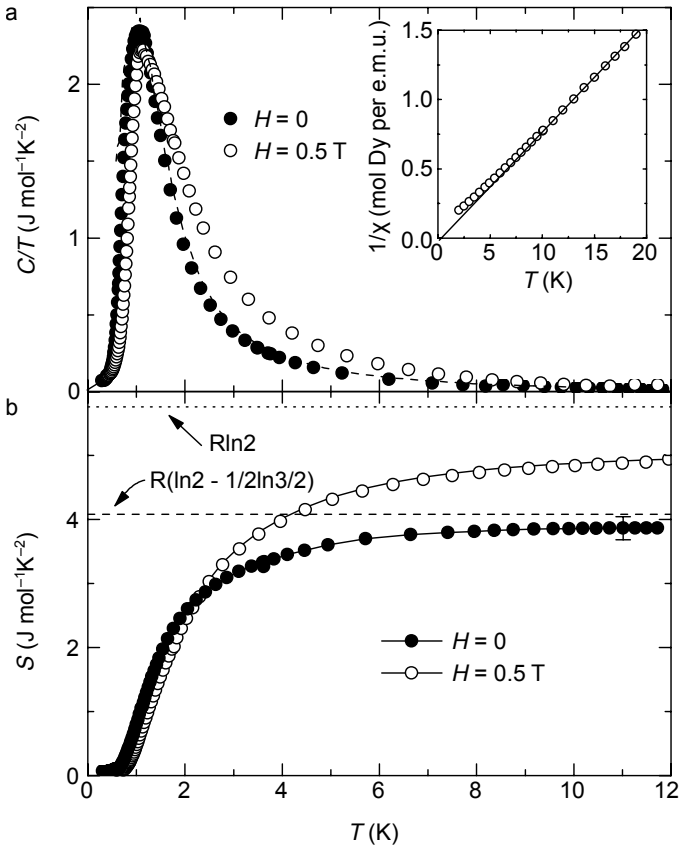

Figure 2.3: The specific heat measurement of $Dy_2Ti_2O_7$ by Ramirez *et al.*, and integrated entropy. The broad feature indicates no ordering, and the remaining entropy adds up to Pauling's residual entropy of ice with good agreement. From Ref. [41].

found an ordering transition, which agreed with an upturn in the measured specific heat, both shown in Fig. 2.4.

Jana and Ghosh calculated the crystal field parameters of $Ho_2Ti_2O_7$, and found the splitting between the ground state non-Kramers doublet and the next excited state of $\sim 150\text{cm}^{-1}$ (~ 215 K) [43]. With these crystal field parameters, calculated susceptibility was $\chi_{||}/\chi_{\perp} \sim 180$ at 10 K. This confirmed strong local $\langle 111 \rangle$ anisotropy in the low temperature spin state of the materials.

The ground state was verified to be a well-isolated doublet, $|J, m_J\rangle = |8, \pm 8\rangle$ with the next excited state 20.4 meV ($\sim$236 K) above by Rosenkranz *et al.* using neutron

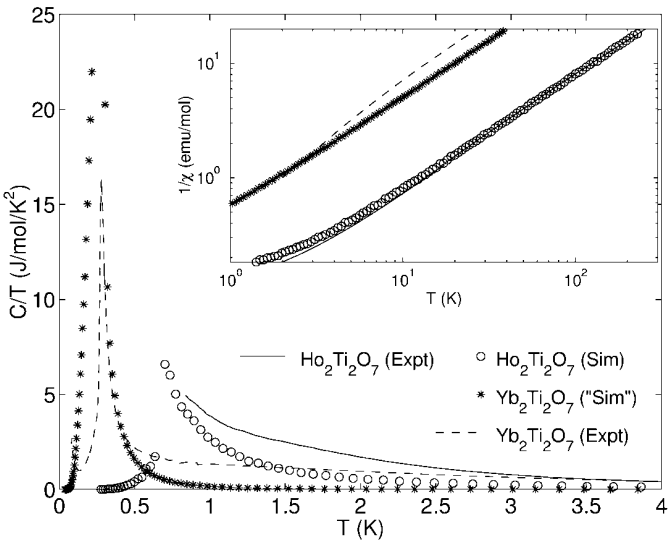

Figure 2.4: Simulations of $Ho_2Ti_2O_7$ specific heat by Siddharthan *et al.* considering dipole interactions up to 5^{th} nearest neighbours yield an ordering transition, and measured specific heat is consistent with this. From Ref. [42].

spectroscopy [44]. The susceptibility showed a significant easy axis anisotropy at 10 K, $\chi_z/\chi_\perp \sim 350$, which verified Ising spins along the local $\langle 111 \rangle$ axis for $Ho_2Ti_2O_7$. $Dy_2Ti_2O_7$ was estimated to exhibit much the same at 10 K, with ground state doublet $|J, m_J\rangle = |15/2, \pm 15/2\rangle$, a separation of ~ 30meV ($\sim$348 K) to the next excited state, and $\chi_z/\chi_\perp \sim 300$.

Theoretical work came through to explain the confusing set of experimental circumstances surrounding spin ice. The dipolar spin ice model was developed by den Hertog and Gingras, describing much of the spin ice phenomena very well [45]. The Hamiltonian,

$$H = -J \sum_{<ij>} S_i^{Z_i} \cdot S_j^{Z_j} + D r_{nn}^3 \sum_{j>i} \frac{S_i^{Z_i} \cdot S_j^{Z_j}}{|r_{ij}|^3} - \frac{3(S_i^{Z_i} \cdot r_{ij})(S_j^{Z_j} \cdot r_{ij})}{|r_{ij}|^5} \tag{2.2}$$

accounts for an exchange interactions J and a dipole-dipole coupling D. The dipole-dipole interaction is $D = (\mu_0/4\pi) g^2 \mu^2 / r_{\text{nn}}^3$, and at nearest neighbour distance, the dipolar interaction was $D_{\text{nn}} \equiv 5D/3$. At nearest neighbour, the exchange energy in Eq. 2.2 is defined as $J_{\text{nn}} \equiv J/3$. Testing the interplay between these two interactions using Monte Carlo simulations, they were able to map out a phase diagram (Fig. 2.5), demonstrating

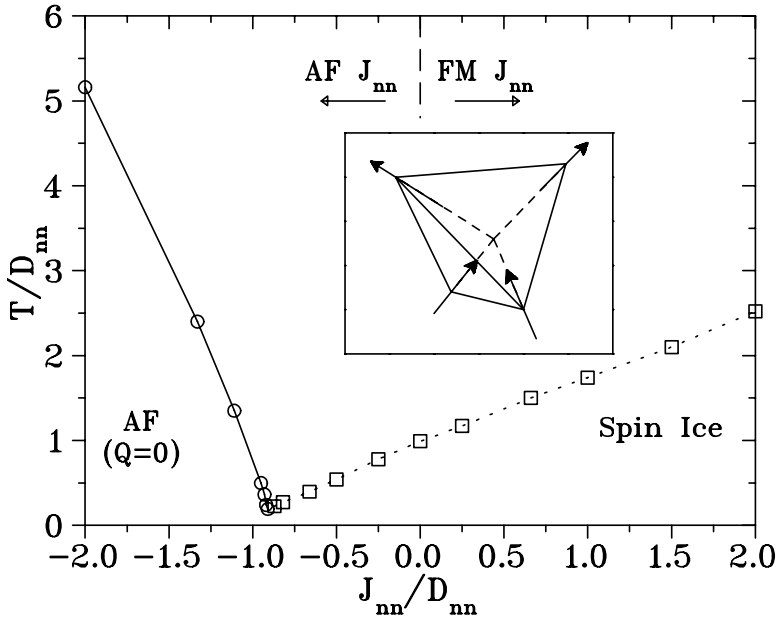

Figure 2.5: The dipolar spin ice phase diagram developed by den Hertog and Gingras. A ratio of 0.91 $J_{\rm nn}/D_{\rm nn}$ demarks the long-range ordered state and the spin ice state. From Ref. [45].

that while the spin ice materials show antiferromagnetic exchange interaction J, the large rare-earth moments lead to a substantial dipole-dipole interaction, which is ferromagnetic! In fact, they showed that up to a ratio of $J_{\rm nn}/D_{\rm nn} = -0.91$, the system remained a spin ice. Below this, they predicted that the system will undergo a second order transition to an anti-ferromagnetic state (four in, or four out). Dipole-dipole interactions were not truncated to fifth order as in previous work [42], which revealed that $Ho_2Ti_2O_7$ was indeed a spin ice when all long range interactions were considered using an Ewald summation [45].

A nearest neighbour description of the dipolar spin ice model, condensing the first terms into an effective exchange energy $J_{\rm eff} = J_{\rm nn} + D_{\rm nn}$, provides the physics seen in the nearest neighbour spin ice model. This yields a simpler Hamiltonian,

$$H = -\frac{(J-5D)}{3}\sum_{<ij>} S_i^{Z_i}\cdot S_j^{Z_j} = -J_{\rm eff}\sum_{<ij>} S_i^{Z_i}\cdot S_j^{Z_j} \tag{2.3}$$

Which explains the previous understanding based upon experimental evidence of a

ferromagnetic exchange energy [39].

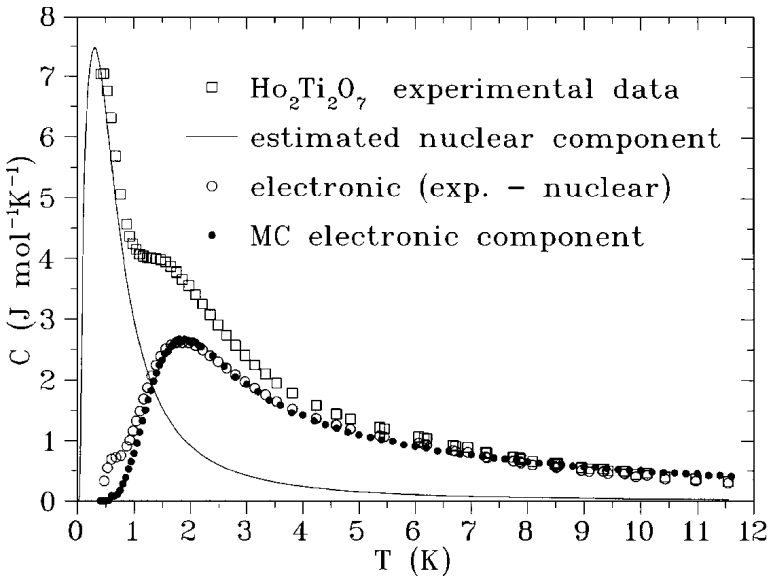

Figure 2.6: Specific heat of $Ho_2Ti_2O_7$ as measured by Bramwell *et al.* Subtraction of the nuclear hyperfine term reveals a specific heat very similar to that of DTO. From Ref. [46].

While $Ho_2Ti_2O_7$ was thought to have ordered due to an upturn in specific heat, Jana and Ghosh had shown that a feature due to the contribution of hyperfine interactions would be expected, peaking around 0.3 K [43]. The presence of this anomaly makes measuring the specific heat and accurately determining the residual entropy of $Ho_2Ti_2O_7$ more difficult, than say, $Dy_2Ti_2O_7$. Lower temperature specific heat measurements by Bramwell *et al.* verified the presence of this feature [46]. They were able to subtract this contribution and examine only the magnetic component, establishing that $Ho_2Ti_2O_7$ exhibits a broad anomaly much like that of $Dy_2Ti_2O_7$, shown in Fig. 2.6. They were able to fit the peak height to estimates of the exchange energy as based on Ref. [45], and determined a nearest neighbour exchange to be $J_{\rm nn} = -0.52$K. While showing that the specific heat anomaly was indeed characteristic of spin ice according to Monte Carlo work, they also found that $Ho_2Ti_2O_7$ is actually deeper in the spin ice regime, as shown by the phase diagram in Fig. 2.5. The entropy released from the system was calculated shortly after by Cornelius and Gardner [47] and it was found that it agreed quite nicely with the recovered entropy from Ref. [39]. They also reported χ for single crystalline $Ho_2Ti_2O_7$ for a single frequency, as well as magnetization along the numerous crystal axes, noting a plateau in the [111]

magnetization [47].

On the surface, it may seem that with substantial strength to nearest neighbours, dipole-dipole interactions should break the ground state degeneracy of the ice rules and cause long range order. Gingras and den Hertog used mean field theory to establish that the long range dipolar interactions are essential to the existence of the spin ice phenomena in these materials, dipolar spin ice. As found with Monte Carlo simulations [45], truncation of dipolar interactions leads to an ordering transition depending on the truncation point [48].

Along with the absence of any ordering seen in specific heat, other measurements of spin ice had found anomalous results. AC susceptibility measurements had observed unconventional freezing in dynamics at low temperatures. The earliest measurement, by Matsuhira *et al.*, was of polycrystalline $Ho_2Ti_2O_7$ and $Ho_2Sn_2O_7$, which found a frequency dependent freezing temperature for both materials (Fig. 2.7a). The relaxation, measured via temperature scans, was described by thermally activated Arrhenius behaviour over the temperature and frequency range studied, with barrier energies of 27.5 K and 19.6 K respectively [49].

This was followed by an intensive study of $Dy_2Ti_2O_7$ by Matsuhira and coworkers which included parametrization of the relaxation through scans in both temperature and frequency parameter space [50]. Temperature scans find two distinct thermally activated processes with two freezing temperatures, one feature at and above $\sim$10 K, and another at and below ~ 2 K, shown in Fig. 2.7b, c. Arrhenius behaviour described the high temperature freezing with a barrier energy of 220 K. At 10 K, frequency scans find the temperature dependence becomes very weak as the relaxation flattens into a plateau. The second thermally activated process at low temperatures was revealed with temperature scans, with a barrier energy of ~ 10 K. Both temperature and frequency scans are shown in Fig. 5.1. Detailed analysis of frequency scans concluded that a distribution of time scales were present at the higher temperatures (> 10 K), where relaxation fit a qualitative Davidson-Cole relaxation.

Published nearly coicidentally as Matsuhira *et al.*, Snyder *et al.* also explored the low temperature freezing in $Dy_2Ti_2O_7$ using ac susceptibility [51]. They also saw unconventional spin freezing into the spin ice state (Fig. 2.8a,b) and further characterized the unconventional aspect, by noting application of field enhanced the freezing temperature, and that spectral width of frequency scans are relatively narrow (~ 1.5 decades), with no distinguishable broadening. This was in contrast to the known freezing in spin glasses, where application of field suppresses freezing temperature and spectra are quite broad on the order of several decades, and continue to broaden as temperature is lowered [51]. The

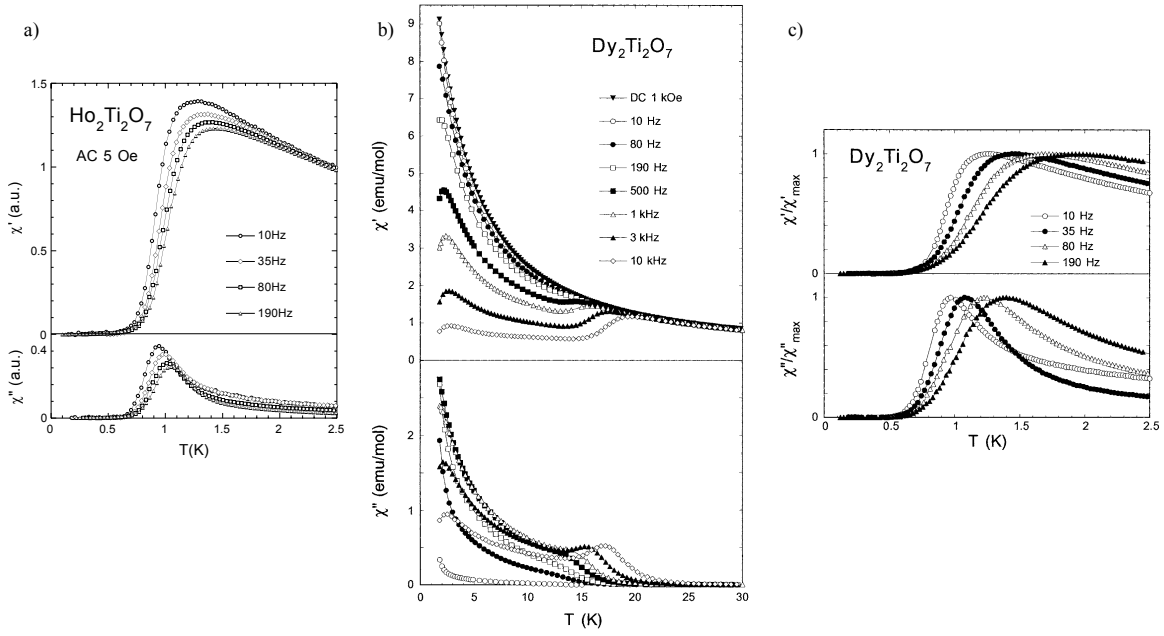

Figure 2.7: Real and imaginary components of ac susceptibility for $Ho_2Ti_2O_7$ and $Dy_2Ti_2O_7$ as measured by Matsuhira *et al.* a) From Ref. [49], exhibiting the frequency dependent freezing in $Ho_2Ti_2O_7$. b),c) $Dy_2Ti_2O_7$ showed very similar low temperature behaviour, as well as a high temperature freezing feature. From Ref. [50].

two relaxation modes are also seen in temperature scan data from that work. The low temperature freezing is predominately associated with a single relaxation mode, as judged by the spectral width (Fig. 2.8c) They also noted that single crystals displayed much the same behaviour, though this data was not presented.

Theoretical efforts by Melko *et al.* used a Monte Carlo loop algorithm to actually speed up the low temperature simulation dynamics and recover the missing entropy [52]. They predicted a long range ordered state distinguished by q = (0,0,2π/a) (and three other symmetry related wavevectors), with zero total magnetization, brought on by a first order transition at 0.18 K, while reproducing all previous high temperature behaviour. However, they had stated that dynamical equilibrium would be required to truly achieve that, which may not be experimentally attainable due to the large energy barriers separating states.

An excellent review of progress to this point was provided by Bramwell and Gingras [4]. Largely to this point, we have discussed development of the spin ice phenomenology and

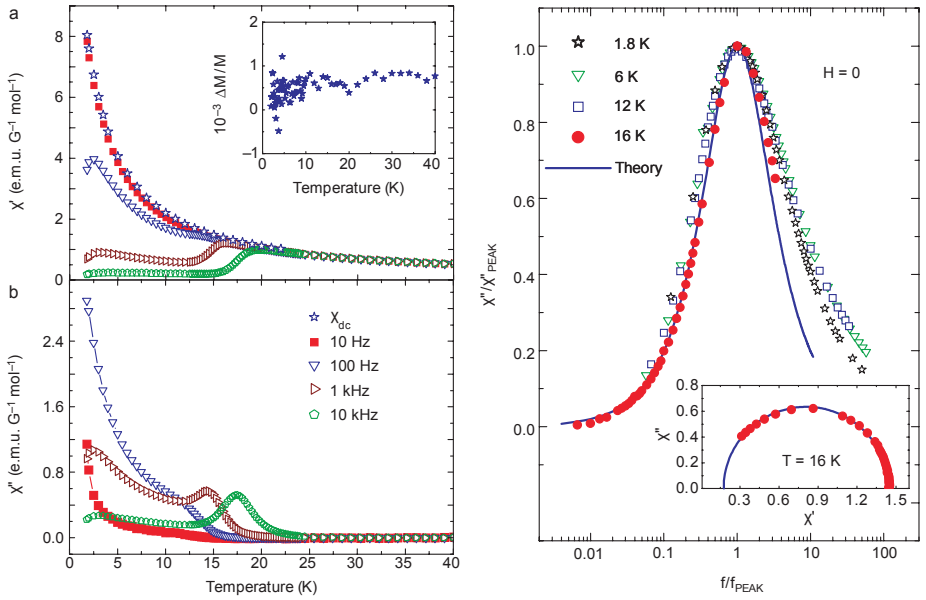

Figure 2.8: a) Real and b) imaginary components of ac susceptibility for $Dy_2Ti_2O_7$ as measured by Snyder *et al.*, with two temperature dependent freezing features. c) The normalized absorption spectra show a temperature dependence in the spectral width. From Ref. [51].

the verification that $Ho_2Ti_2O_7$ and $Dy_2Ti_2O_7$ indeed fit that description, primarily through specific heat. After this period, numerous experimental and theoretical works continued to study $Dy_2Ti_2O_7$ and $Ho_2Ti_2O_7$, some of which will be introduced now.

The crystal field parameters of $Dy_2Ti_2O_7$ were calculated by Jana *et al.* in 2002, finding a separation of $\sim$100 cm^{-1} ($\sim$144 K) from the Kramers ground state doublet to the next excited doublet. Ionic susceptibility calculations there with the calculated crystal field parameters gave $\chi_{||}/\chi_{\perp} \sim 180$ at 10 K, again, strongly confirming the local $\langle 111 \rangle$ anisotropy.

The nature of the high temperature relaxation feature in $Dy_2Ti_2O_7$ ac susceptibility was explored in measurements by Snyder *et al.* of $Dy_{2-x}Y_xTi_2O_7$, which discovered no change in the freezing temperature in changing frequency, T_f (Fig. 2.9) [53]. As the magnitude of the feature was diminished, Snyder *et al.* concluded the dilution merely impacted short range correlations.

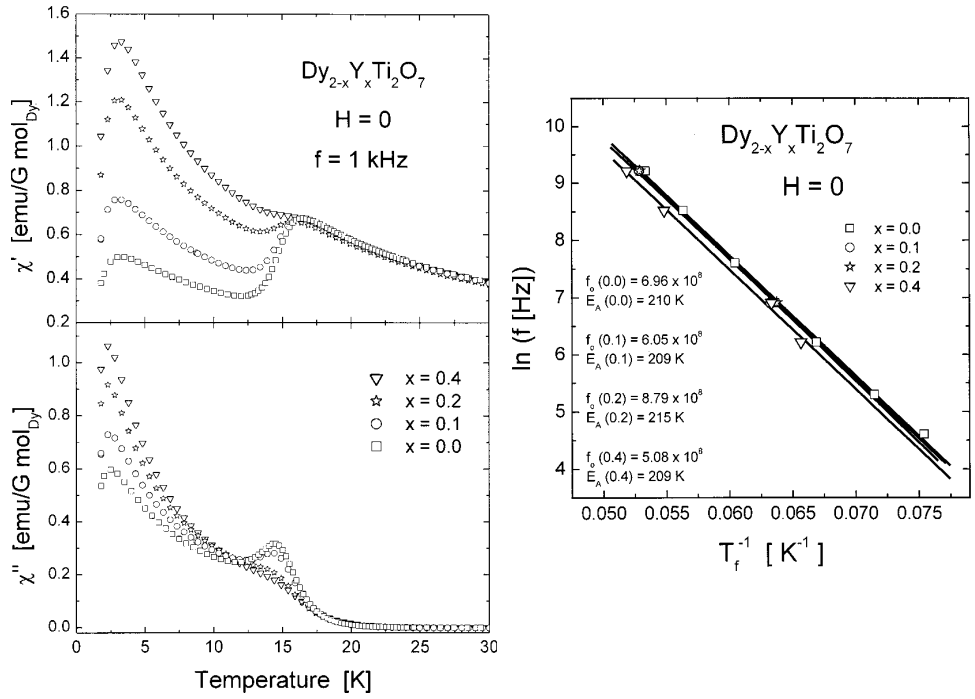

Figure 2.9: The effect of dilution on the high temperature ac susceptibility feature in $Dy_2Ti_2O_7$, and the shift in the freezing temperature. Snyder *et al.* used this result to show dilution only impacted short range correlations, and support that the relaxation was not a single ion effect. From Ref. [53].

Single crystal $Dy_2Ti_2O_7$ specific heat data was presented by Higashinaka *et al.* in 2002 [54], nearly coincident with work released by Matsuhira *et al.* on specific heat and magnetization [55]. The magnetization measurements showed a plateau developing $\sim$1 K, while specific heat showed evolution of two features, out of the initial broad zero-field feature. This was thought to be due to decoupling into kagome and triagular lattice planes along the [111] direction, inducing a reduced residual entropy phase coined "kagomé ice".

Sakakibara *et al.* observed what appeared to be a magnetic analogue to a liquid-gas transition with magnetization measurements along the [111] axis of $Dy_2Ti_2O_7$. A critical point was identified at $T_c = 0.36$K and $H_c = 0.93$ T. No current theory seemed to account for its presence.

This was followed shortly by measurements of the heat capacity in varying magnetic field under [100] and [111] directions by Hiroi *et al.* [56]. The [111] axis curiously exhibited

two peaks, with the lowest temperature peak seemingly changing to that of a first order transition at $T_c = 0.5$K and $H_c = 1$ T. This agreed qualitatively with the liquid gas transition measured by Sakakibara *et al.*, though without quantitative agreement on the critical point. They also were able to stabilize the kagome ice state between fields of 0.3 T and 0.6 T. While some measurement differences were noted in the size of the specific heat peak at low temperatures with Ramirez *et al.*, the residual entropy was recovered. Higashinaka *et al.* also published a magnetic field study very shortly after and found that there was a reduced residual entropy in the kagome ice state [57], similar to the result of Ref. [55].

The phenomena of the cross-over to a second thermally activated regime in $Dy_2Ti_2O_7$, seen by Matsuhira *et al.*, was further explored by Snyder *et al.* in 2003 [58]. They labelled it as a double cross-over phenomena, and were able to conduct frequency scans to lower temperatures and further observe the nature of the crossover. Several important conclusions on the nature of the relaxation were added. The first thermally activated regime is suggested to be governed by the barrier energy set by crystalline electric field levels. The quasi-temperature independent regime, beginning below $T_{\rm cross} \sim 13\,{\rm K}$ was determined to be quantum tunnelling dominated, which reverts to thermally activated behaviour below $T_{\rm ice} \sim 4\,{\rm K}$, as it freezes into the ice state [58].

Ehlers *et al.* used neutron spin echo and ac susceptibility to reveal the missing high temperature relaxation feature in $Ho_2Ti_2O_7$ [59, 60], which had been found in $Dy_2Ti_2O_7$ [50, 51]. While initially the high temperature thermally activated feature was thought to be absent in $Ho_2Ti_2O_7$, they were able to observe it with neutron spin echo, and extrapolate the relaxation into the ac susceptibility time window. Application of fields up to 1 T was used to enhance the ∼15 K feature. The feature was determined to be of single ion origin, due to the Q-independence of the scattering, and an Arrhenius activation energy (293 K), very near that of first excited crystal field state. The 1 K freezing feature was also observed here, with a barrier energy of ∼20 K, also finding that this relaxation must become unimportant above 4 K [59]. Strangely, doping with 5% La at the Ho sites yields the same barrier height, but roughly a 10^2 increase in relaxation frequency. They also guess that $Dy_2Ti_2O_7$ might possess a lower energy scale for freezing, along with the slower intrinsic dynamics seen there. They suggest that it is the slower $Dy_2Ti_2O_7$ dynamics that allows it to be better distinguished from the low temperature process. Further work by Ehlers *et al.* in 2004, again utilizing neutron spin echo and ac susceptibility, verified their work from 2003. As well, application of a 10 kOe field finds a barrier energy of 24 K for the low temperature process [60].

Further work by Snyder and coworkers added several more susceptibility measurements and added magnetization measurements which found a splitting in FC and ZFC at 650

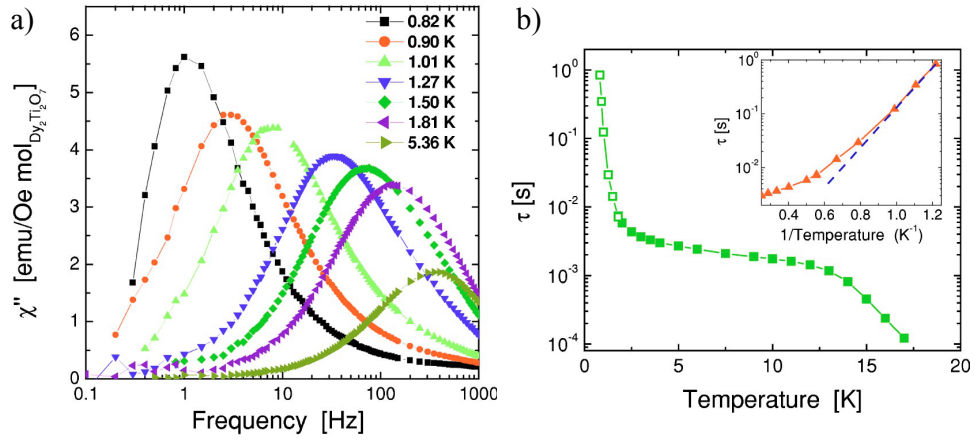

Figure 2.10: a) The χ'' frequency spectra of $Dy_2Ti_2O_7$ by Snyder *et al.* b) The relaxation time of $Dy_2Ti_2O_7$ as determined by ac susceptibility, which clearly indicated the three relaxaion regimes seen in spin ice. From Ref. [61].

mK [61]. Several low temperature χ'' spectra are shown in Fig. 2.10a. The relaxation time, demonstrating three different regimes of relaxation is shown in Fig. 2.10b. The relaxation determined by frequency scans appeared to be trending to Arrhenius type, but there was insufficient data to make this conclusion.

Loop flip dynamics were further investigated as part of simulation work in 2004 where Melko and Gingras undertook a comparison of single spin flip dynamics and loop-flip dynamics [62]. Among many other things, they found the freezing in simulation for single spin dynamics was much like that found in experiment. Interestingly, they found that a Volger-Fulcher form could be used to describe the acceptance rate ($A(T)$) of spin flips, the percentage of successful Monte Carlo flips.

$$A(T) \propto \exp\left(\Delta/T - T_{\mathrm{f}}\right) \tag{2.4}$$

The dynamical freezing is ascribed to the large energy barriers separating nearly degenerate ground states, which are out of reach at the low temperatures of this system. With loop moves allowed, as the system freezes in to the two-in two-out state and single spin flip moves become less and less available, loop moves become accessible as a method for the system to release trapped entropy. The specific heat and entropy for $Dy_2Ti_2O_7$ calculated by this loop flip algorithm are shown in Fig. 2.11.

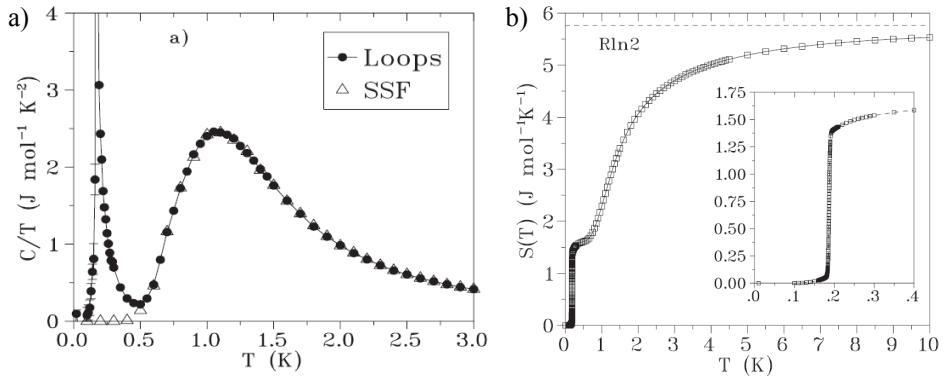

Figure 2.11: The specific heat and entropy simulated by Melko and Gingras utilizing a loop flip algorithm, where spin ice finds a non-degenerate ground state at ~ 0.18 K and recovers the $R \ln 2$ entropy. From Ref. [62].

Shi *et al.* measured ac susceptibility in an orientation study of $Dy_2Ti_2O_7$ from 2 to 40 K in 2007, [63]. This was the first $Dy_2Ti_2O_7$ single crystal ac susceptibility data published. Along the [001] and [111] directions, they observed some field dependence of the relaxation. As only χ' was reported, it is difficult to compare to other works, since they use an unconventional definition of the freezing temperature, where T_f is taken to be at the maximum of χ'. Typically, the maximum of χ'' is utilized. Regardless, they report 200 K and 186 K as Arrhenius barrier heights for the high temperature feature, for the [001] and [111] directions respectively. The low temperature feature was also present in both orientations, and they qualitatively saw enhanced freezing temperature with applied field, as in Ref. [51]. It is not stated if a demagnetization correction was implemented.

Muon spin resonance work by Lago *et al.* found Arrhenius dependence to high temperature relaxation, with a barrier energy of 210 K, and a plateau in the temperature dependence at lower temperatures. Curiously, spin fluctuations on the order of $\tau \sim 10^{-6}$s were seen down to 20 mK, which was ascribed to nuclear spin interactions between ^{161}Dy and ^{163}Dy.

Magnetocaloric measurements by Orendáč *et al.* used adiabatic demagnetization of DTO to determine relaxation times from 0.3 K to 0.4 K [64]. They note a loss of equilibrium between the spins and the lattice at ~ 0.4 K, as well as the onset of a sharp increase in relaxation time at 0.3 K as previously seen in neutron scattering experiments [65]. The relaxation follows a Raman or Orbach-like spin lattice relaxation process, but can also be fit to an Arrhenius process with barrier energy 3.6 K, shown in Fig. [64]. They note

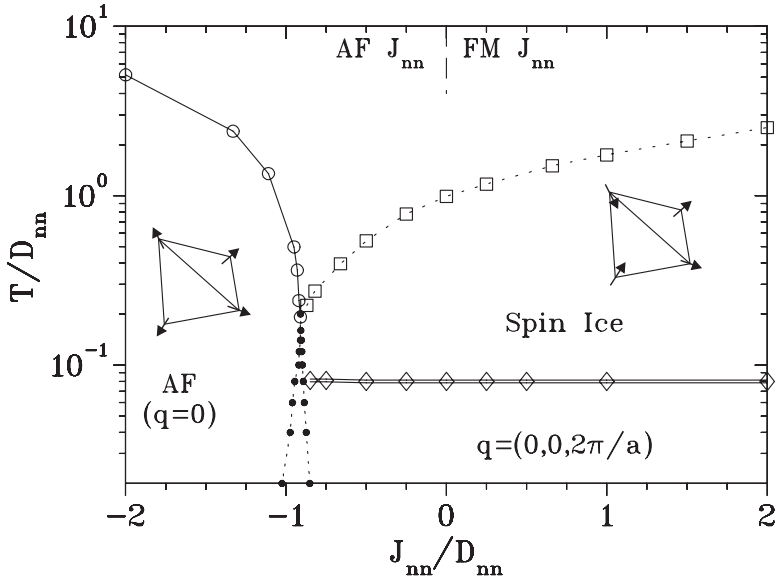

Figure 2.12: The spin ice phase diagram including ordered state as determined by Melko and Gingras. Use of a loop flip algorithm determined the ordered state should exist for spin ice. From Ref. [62].

that this work will not necessarily quantitatively extend ac susceptibility works to lower temperatures due to changing temperature in order to measure this effect, but should provide qualitative extension of the dynamics observed in Ref. [61].

Interestingly, three different regimes are consistently seen amongst several different measurement techniques, including ac susceptibility [50, 58], neutron scattering [66], neutron spin echo (NSE) [59, 60], forward nuclear scattering [67], and longitudinal field muon spin resonance (μSR) [68]. All of these measurements probe different time scales, but similar temperature dependence is seen in all three. The first, high temperature, characteristic generally seen is Arrhenius behaviour, seen in ac susceptibility (220 K for $Dy_2Ti_2O_7$ [50], and 210 K for $Dy_2Ti_2O_7$ [51]), neutron spin echo (293 K for $Ho_2Ti_2O_7$ [59]), μSR (210 K for $Dy_2Ti_2O_7$ [68]), and forward nuclear scattering (272 K for $Dy_2Ti_2O_7$ [67]). As the temperature lowers, the excited crystal field states can no longer act as a relaxation channel. The system is left to rely on the next fastest mode of relaxation, quantum tunnelling of spin states within the ground state doublet. This appears as a quasi-temperature independent plateau observed in relaxation, with a relatively shallow barrier energy. Here, the system becomes Ising. For $Dy_2Ti_2O_7$, this occurs at timescales of $\sim$3 ms in ac susceptibility [61],

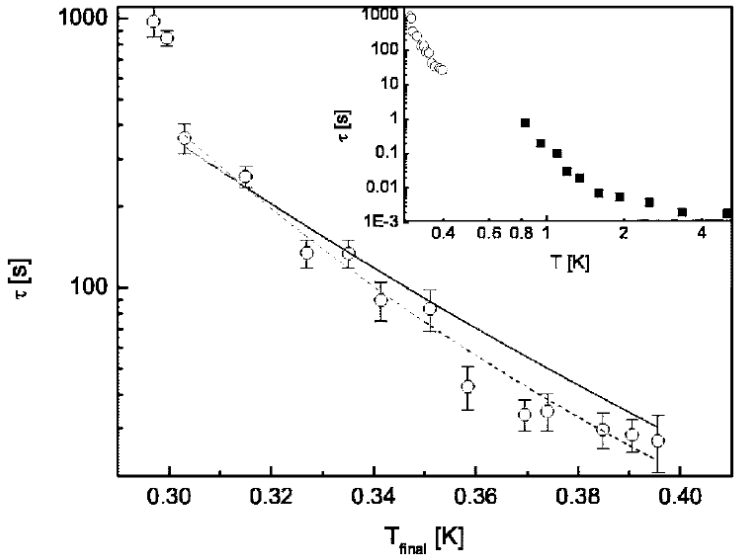

Figure 2.13: The relaxation time of $Dy_2Ti_2O_7$ as determined by Orendáč *et al.*, where the solid line represents a T^{-9} Raman process, and the dashed represents an Arrhenius relation. From Ref. [64].

$\sim$0.5 μs in μSR [68], and for $Ho_2Ti_2O_7$ $\sim$10 ns in neutron scattering [66]. Lastly, quantum tunnelling between spin states is no longer an option for the Ising spins. At temperatures on the order of the effective exchange J_{eff}, $\sim$1 K, the system begins to freeze into the two-in, two-out ground state. This freezing is also observed as the equilibration timescale becomes longer than the characteristic timescales of magnetization measurements, for instance [61]. Temperature scans in ac susceptibility find it to be Arrhenius in nature, as described previously here.

Work by Yavorksk'ii *et al.* was the first to introduce exchange interactions beyond nearest neighbour; up to 3rd nearest neighbour were considered in order to achieve better agreement between the dipolar spin ice model and experiment [69]. This was referred to as the general dipolar spin ice model, while the dipolar spin ice model only considering nearest neighbour exhange was referred to as the standard dipolar spin ice model. Neutron scattering work was successfully reproduced, and improved agreement with specific heat results [57] was also found utilizing this new model.

The volume of work on these two canonical spin ices is vast, and cannot be discussed in its entirety here. Rather, we have highlighted some of the key results, and also discussed

any results which will have impact on the results presented here, specifically the dynamics measurements of $Dy_2Ti_2O_7$ and $Ho_2Ti_2O_7$.

2.3 Other spin ice materials

The spin ice family is not limited to the two canonical spin ice materials, $Dy_2Ti_2O_7$ and $Ho_2Ti_2O_7$. To this point, several other pyrochlores have shown evidence of being candidates as well. $Ho_2Sn_2O_7$ exhibited a freezing in polycrystalline ac susceptibility extremely similar to $Ho_2Ti_2O_7$, and was studied in the same initial work [49]. This conclusion was reinforced in polycrystalline neutron scattering works by Kadowaki *et al.*, who determined $Ho_2Sn_2O_7$ displayed dipolar spin ice behaviour [70]. Like $Ho_2Sn_2O_7$, $Dy_2Sn_2O_7$ was intially suggested to be a spin ice by Matsuhira *et al.* in an ac susceptibility study of pyrochlore stannates, based upon similar frequency dependent freezing to $Dy_2Ti_2O_7$ [71]. $Pr_2Sn_2O_7$ was suggested to be a spin ice as part of the same study, based on ac susceptibility measurements. $Pr_2Sn_2O_7$ has been labelled a dynamic spin ice by Zhou *et al.*, where even less of the total $R \ln 2$ entropy is recovered at the lowest temperatures studied, and the rapid freezing out of dynamics is not yet seen in neutron scattering [72].

2.4 Summary

This is by no means a complete review of the spin ice phenomenology up to this point, but instead gives a series of snapshots of the experimental and theoretical determinations of its characteristics. Dipolar spin ice possesses corner-sharing tetrahedral lattice geometry, and requires that the spins residing on that lattice be good realizations of Ising spins. The crystalline electric field in $Ho_2Ti_2O_7$ and $Dy_2Ti_2O_7$, with well isolated ground state doublets for Ho^{3+} and Dy^{3+} respectively[43, 73], mean that this condition is met. Two early phenomenological signs of the spin ice state were the residual Pauling entropy [41] and the rapid freezing of dynamics in the spin ice state [51]. The dipolar spin ice model was developed to describe the specific heat, which agreed well with thermodynamic determinations of the specific heat and by extension entropy [45]. The next chapter will describe a fascinating twist to the already substantial volume of work on dipolar spin ice: the fractionalization of magnetic dipoles into monopole excitations.

Chapter 3

Magnetic Monopole Excitations in Spin Ice

3.1 History

Monopoles have been pursued by physicists since the presentation of Maxwell's equations, which would be beautifully symmetric if discrete magnetic charges existed. Milton provides a summary of the recent status of the field [74]. In 1931, Dirac showed that magnetic charges, g, were allowed in the formalism of quantum mechanics, under the quantization condition $eg = m'\hbar c$, where m' is an integer or integer plus 1/2 [75]. Various other methods were used to express this quantization condition. One variety, termed non-Abelian monopoles, were found theoretically using non-Abelian gauge theories. Non-Abelian theories predict huge mass for these monopoles, and even the smallest mass is on the order of 10 TeV, out ot the range of current particle accelerator technology. Searches can be labelled as direct measurements, looking for free monopoles, or indirect measurements, which rely on observing effects that should be attributable to the existence of free monopoles. The direct measurements included detecting trapped monopoles by examining particle accelerator detector elements (which have a 100% probability of being able to trap a monopole). Other experimental work was largely focused on limiting the possible values of mass and charge of the monopole, and so to-date, monopoles have not been directly observed, but rather limits on where they still may lie, have been established [74]. There have been no confirmed observations of monopoles to date.

3.2 Recognition

As it happens, the Dirac or non-Abelian monopole is not the only type available for study. Recently, the realization that a fractionalized excitation which behaved like a magnetic monopole could exist in spin ice was made, and has had groundbreaking impact. The topic has already been the subject of a review [76]. In the popular literature, Castelnovo *et al.* first observed in 2008 that the excitations out of the spin ice ground state could be described as magnetic monopoles [5]. However, in the relatively obscure Russian literature in 2005, Ryzhkin actually intially proposed that defects in the ice rules ground state of spin ice (three-in, one-out or one-in, three-out) are in fact localized magnetic point charges. They carried a charge $m = \pm 2\mu/a$, because of the non-vanishing divergence of the magnetization [77], where a is the dual lattice spacing, while μ is magnetic moment. The comparison to defects in water ice was pointed out, stating that these magnetic defect quasiparticles play analogous roles to ionic defects in water ice. Ryzhkin also derived expressions for the frequency dependent susceptibility $\chi(\omega)$ coming out of this model:

$$\chi(\omega) = \frac{m^2/\Phi}{1 - i\omega\tau} \tag{3.1}$$

Where ω is the frequency, H_ω is applied ac magnetic field, $\Phi = (8/\sqrt{3})ak_{\mathrm{B}}T$, τ is the characteristic time scale defined by

$$\tau^{-1} = (\mu_1 n_1 + \mu_2 n_2)\Phi \tag{3.2}$$

Where μ is the mobility, while n is defect density. This was a largely theoretical work lacking quantification, all within the framework of the nearest-neighbour model, for non-interacting quasi-particles assumed to be in the dilute limit. However, he initially proposed the idea of magnetic point defects acting as effective monopole charges, and also very importantly, the analogy of the defects in spin ice playing the same role as ionic defects in water ice.

In 2008, as stated previously, Castelnovo *et al.* independently published a fundamentally similar result, proposing the existence of fractionalized dipoles in spin ice behaving as magnetic monopoles. They mapped the two-in, two-out ice rules ground state to a divergenceless vacuum, excitations out of which would cause a spin flip generate a magnetic dipole with charges at the centre of each tetrahedron. The dipole created by the spin flip can then be separated, by subsequent spin flips (which restore the ice rules to the intermediate tetrahedra) in an applied field, interacting via a Coulomb force $-\mu_0 q_{\mathrm{m}}^2/(4\pi r)$. What allows deconfinement and consideration of these excitations as independent monopoles is

the fact that the energy cost of a dipole pair does not diverge with the number of spin flips along the dipole string (Fig. 3.1). The charge carried by these monopoles is $q_{\mathrm{m}} = \pm 2\mu/a_{\mathrm{d}}$, and after separation, they are subject to a Coulomb interaction. These monopoles required no modification of Maxwell's equations, nor did they relate to the quantisation condition introduced by Dirac.

Simulations as part of this work searched for a first-order liquid-gas transition which should be present for a Coulombic lattice gas, along the [111] direction. The [111] direction favours creation of monopoles, and acts as a tunable chemical potential. This would be a transition between a low density kagome ice state, and a high density ordered state, or equivalently, a monopole gas to monopole liquid state. Indeed, this first order transition had been seen in field in the work by Sakakibara *et al.*, which experimentally seemed to be a magnetic analogue to a liquid-gas transition [78]. Theoretical simulations did in fact find very good qualitative agreement with the transition seen by Sakakibara *et al.*, giving weight to the monopole interpretation of spin ice, as no previous mechanism had accounted for its presence. This was a strong early confirmation of the monopole picture, and naturally, many other works quickly followed.

3.3 Initial Observation and Characterization

Castelnovo *et al.* sparked a fire in the spin ice community which then set to work to experimentally observe and characterize these monopoles, making 2009 an eventful year for spin ice monopole publications. Here, we highlight the important results presented on spin ice in the aftermath, though not all of them explicitly hunting for monopoles.

Clancy *et al.* were not explicitly searching for monopoles, but rather focusing on neutron scattering measurements of $Ho_2Ti_2O_7$ [66]. Zone boundary scattering at 0.2 K was found to be very similar to scattering in $Dy_2Ti_2O_7$. The expectation of the dipolar spin ice model of diffuse scattering disappearing at $|\mathrm{Q}| = 0$ was shown. Field applied along the α-chains was able to decompose the system into ordered [110] and $[1\bar{1}0]$ chains. Very high resolution inelastic neutron scattering found, on the order of 10^{-9} seconds, $Ho_2Ti_2O_7$ spins were static below ~ 2 K. Curiously the relaxation regimes were very similar to those seen in $Dy_2Ti_2O_7$.

Theoretical simulations by Jaubert and Holdsworth used previous $Dy_2Ti_2O_7$ ac susceptibility work as evidence of monopole dynamics [6]. They created a Coulomb gas in the spin ice framework, by placing monopole charges on diamond lattice sites, and used Monte Carlo simulations to extract characteristic timescales of relaxation. The timescale used to compare to ac susceptibility measurements actually came from the dynamics of the

Dirac strings of flipped dipoles, rather than the monopoles themselves, and the simulation probed the monopole dynamics through the string timescales. These revealed dynamics which were quite comparable to $Dy_2Ti_2O_7$ ac susceptibility observing the unconventional

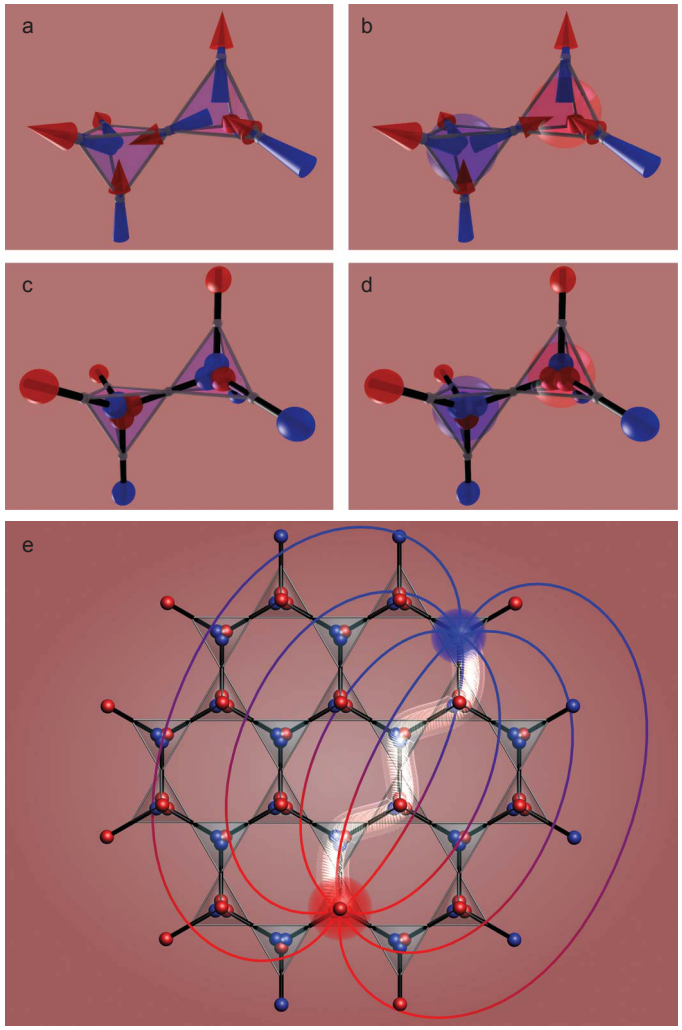

Figure 3.1: The dumbbell model demonstrating how a single spin flip leads to two effective monopole charges at the centre of each tetrahedra. a) Two-in, two-out ice rules state. b) Spin flip leads to magnetic dipole. c, d) The dumbbell equivalents. e) The motion of a defect via a dipole string through the lattice, moving away and becoming effective monopoles. From Ref. [5].

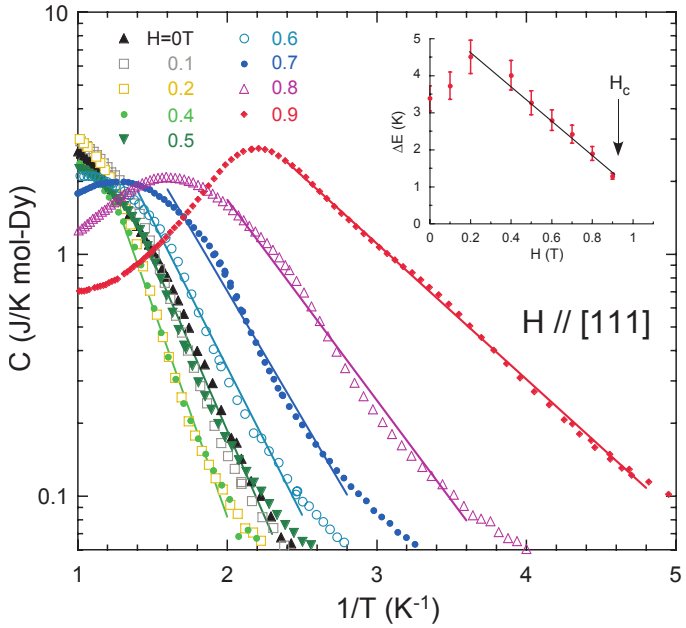

Figure 3.2: Specific heat of $Dy_2Ti_2O_7$ in a [111] magnetic field. Inset: Arrhenius barrier energy as a function of field. This measurement was used to support the existence of monopoles. From Ref. [8].

crossover in spin ice [58, 61], and so were presented as another experimental signature of magnetic monopoles. The agreement was not perfect, however, the development of a higher temperature high density state to a low temperature freezing into the ice-rules degenerate ground state was well described to 1 K, as can be seen in Fig. 5.13. It is also important to note that the possibility of sustained monopole current was not considered likely.

Kadowaki *et al.* used neutron scattering and specific heat measurements of $Dy_2Ti_2O_7$ under application of a [111] magnetic field to report the observation of magnetic monopoles in spin ice [8]. A study of low temperature specific heat, fitted to $C(T) \propto \exp(\Delta E(H)/k_BT)$, found an Arrhenius activation energy under applied field H. The fit described the intermediate field range reasonably well, as can be seen in Fig. 3.2. Creation energy in zero field was approximately 3.5 K, based upon the specific heat. They attribute this law to the changing density of monopoles, as should occur along the [111] axis [5]. In the same work, they use neutron scattering near the critical point of the liquid-gas transition to observe if there are any critical fluctuations between high- and low-density states. Experimental neutron scattering and Monte Carlo simulations of the dipolar spin ice model first used

the kagome ice state as a check, and then did indeed find a weakened kagome ice pattern, as well as a buildup of diffuse scattering around Bragg points corresponding to the high density state near the critical point (T_c = 0.05 K, H_c). There were some quantitative discrepancies between the Monte Carlo scattering pattern and the experiment. However, this work showed both that monopole creation could be controlled with a field-generated Arrhenius type creation energy, and reinforced the picture of the liquid gas transition which they find reinforcement of the first order liquid-gas transition.

Muon spin resonance (μSR) experiments by Bramwell *et al.* then presented a measure of the charge and current of magnetic monopoles in $Dy_2Ti_2O_7$. Here, Onsager's theory of Coulombic liquids was applied to monopole charges in spin ice (behaving as a magnetic Coulomb fluid). Comparable to the ionization of water ice, represented as $2H_2O = [H_3O^+OH^-] = H_3O^+ + OH^-$, where the brackets indicate a bound ion pair, this paints the monopoles as interacting as bound pairs, and unbound free charges. Onsager's theory allows determination of the elementary charge, which of course for this magnetic analogue would be the elementary magnetic charge of the real material in question. The fundamental result os this is the dissociation constant as a function of applied field $K(B)$,

$$K(B) = K(0)(1 + b + \frac{b^2}{3})... \tag{3.3}$$

where b is the renormalized magnetic field,

$$b = \frac{\mu_0 Q^3 B}{8\pi k^2 T^2} \tag{3.4}$$

In order to verify this theory, Bramwell *et al.* used transverse field μSR to probe the spin fluctuation rate of $Dy_2Ti_2O_7$ and from the rate of decay for muon precession (Fig. 3.3, extract the monopole charge, $\sim 5\mu_B\mathring{A}$. The realm of applicability of the theory for this technique is found to be between 0.07 K and 0.3 K, where the effective charge is found to be temperature independent. This was billed as showing perfect duality for electricity and magnetism in Onsager's equations, as well as being the first three dimensional realization of fractionalization. They do point out that the existence of a network of Dirac strings would stifle a magnetic current [11] but propose that perhaps that the dilute monopole regime has sufficiently few strings present.

Morris *et al.* reported evidence of monopole observation through specific heat and neutron scattering measurements on $Dy_2Ti_2O_7$. The specific heat evidence relied on the Debye-Hückel theory of dilute Coulomb gases in order to describe the specific heat of $Dy_2Ti_2O_7$ below 1 K, where defect density is small. This provided a reasonably good fit

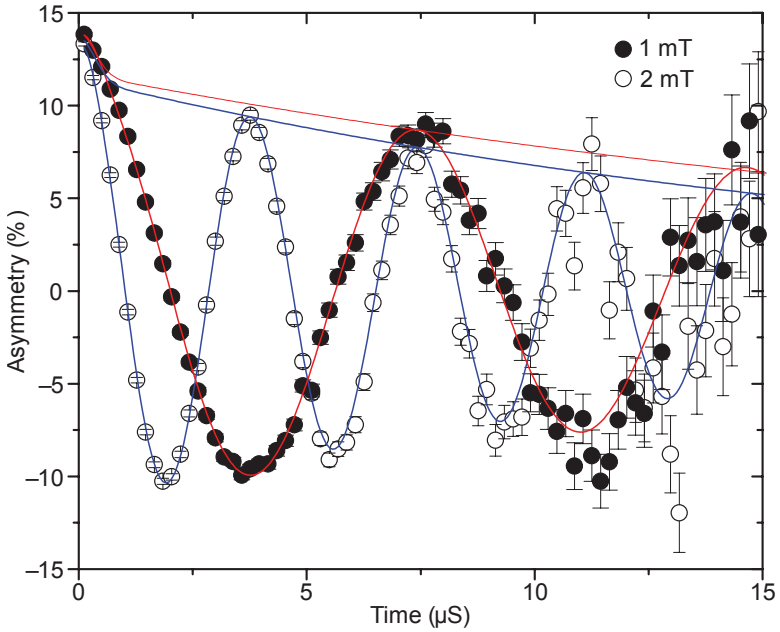

Figure 3.3: The muon precession used by Bramwell *et al.* to determine the monopole charge in $Dy_2Ti_2O_7$ and put forward the magnetricity theory of spin ice. From Ref. [7].

to the specific heat of $Dy_2Ti_2O_7$ from 1 K to 0.4 K. As part of the same work, neutron scattering was used to observe the dipole Dirac strings, tuning the density and orientation of the strings with a magnetic field along the [001] axis, orienting all the spins into an ice rules state, and allowing thermal excitations to develop out of this state, separating and forming dipoles. Simulations of the dynamics of the strings were very similar to measured results, able to reproduce a cone of scattering determined to be a signature of these strings [9]. Not only did this result show monopoles, but also observed the Dirac dipole strings.

Fennell *et al.* have been the only group thus far to support the existence of monopoles in a spin ice other than $Dy_2Ti_2O_7$; polarized neutron scattering measurements were used to experimentally verify the Coulomb phase at low temperatures and further validate the monopole interpretation in $Ho_2Ti_2O_7$. Spin flip and non-spin flip correlations were separated via polarization analysis, the only way to visualize pinch points in the neutron scattering. Pinch points, seen to be a clear reciprocal space signature of the long range dipolar-origin Coulomb force, were seen in both experimental neutron scattering and Monte Carlo simulations, with good agreement between the two. These pinch points had also been seen nearly simultaneously in another polarized neutron scattering work on $Ho_2Ti_2O_7$ by

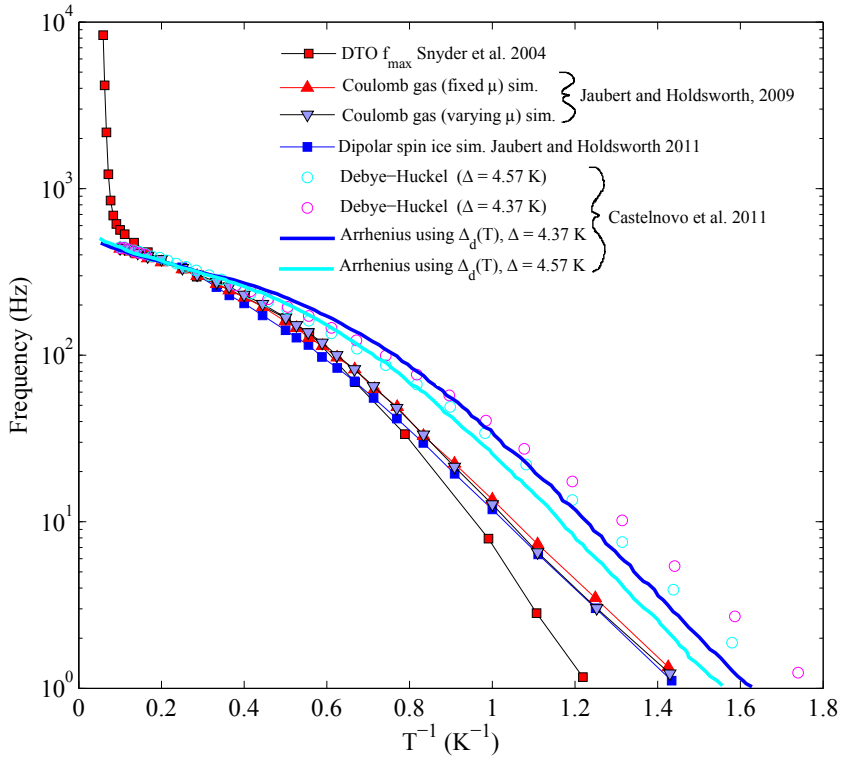

Figure 3.4: Compilation of theoretical studies of relaxation based on $Dy_2Ti_2O_7$.

Chang *et al.* [79]. The scattering patterns were also interpreted to posit that bound dominate at high temperatures, and free dominate at low temperatures.

3.4 Onward

The pace of the literature did not slow down much after that initial burst, as the search for more experimental confirmations continued. Castelnovo *et al.* proposed another experiment as a means of observing magnetic monopoles, this time through non-equilibrium phenomena [80]. Simulated thermal quenches were used to observe the diffusion and annihilation of monopoles. Surprisingly, when quenched to $T > 0.4$ K, the equilibrium value was attained quickly, but when quenched to below that, there was significant deviation from

power law decay of the density. Some defects freeze in non-contractible monopole pairs, which were unable to completely resolve themselves (recombine) at very low temperature [80]. They proposed using zero field nuclear magnetic resonance (NMR) or neutron scattering to observe the time dependence of non-contractible monopole pairs. However, quench speeds which would be required to achieve this are not necessarily experimentally attainable; they suggest on the order of 10-100 ms to induce large number of non-contractible pairs.

Slobinsky *et al.* observed very curious non-equilibrium phenomena corresponding to magnetic deflagration in a detailed magnetization measurement study along the [111] axis [81]. Magnetization sweeps in varying temperature showed equilibration generally occurring without difficulty above T_{equil} =600 mK, but below this temperature, magnetization sluggishly lags the equilibrium curve, until suddenly, it jumps up to the equilibrium magnetization curve value for $T \sim T_{\text{equil}}$. Varying sweep speed below T_{equil} found that above a particular ramp rate, magnetization jumps occurred as well. This was attributed Zeeman energy released via spin flips in increasing field increases the energy available to spins in the sytem, which are able to draw upon that for subsequent spin flips, which releases more energy, and so on. This avalanche effect below T_{equil} seems to be the result of a thermal runaway process, where the spins are unable to dump energy to the phonons, and instead the energy is channeled largely into the rest of the spins, verified by measurements of sample temperature. While not clear proof of monopole excitations, they do consider it in the context of monopole excitations [81]. This perhaps could be an interesting way to achieve high monopole densities at low temperatures.

In 2011 Jaubert and Holdsworth expanded substantially upon their 2009 work [6], which added, among other things, a direct simulation of the dipolar spin ice model and the relaxation seen there [11]. This agreed reasonably well with the Coulomb gas simulation, confirming that the Coulomb gas was a physically plausible interpretation of the lattice. Further work also simulated simply the relaxation of the dipolar spin ice, which also agreed for the most part with the experimental data and Coulomb gas simulation, further validating the Coulomb model [11]. In the instances of both work, however, there was a noticeable disagreement below 1 K between the simulations and the actual experimental work by Snyder *et al.* It was suggested that extending to further nearest neighbours might account for this difference, as it previously had with matching simulations to neutron scattering data in spin ice [69].

Klemke *et al.* used various thermal relaxation and transport measurements of single crystal $Dy_2Ti_2O_7$ in a [110] field and development of a thermodynamic field theory to support the presence of thermally activated monopole and anti-monopole defects [82]. As the temperature of $Dy_2Ti_2O_7$ in a quasi-adiabatic heat capacity measurement relaxes, various

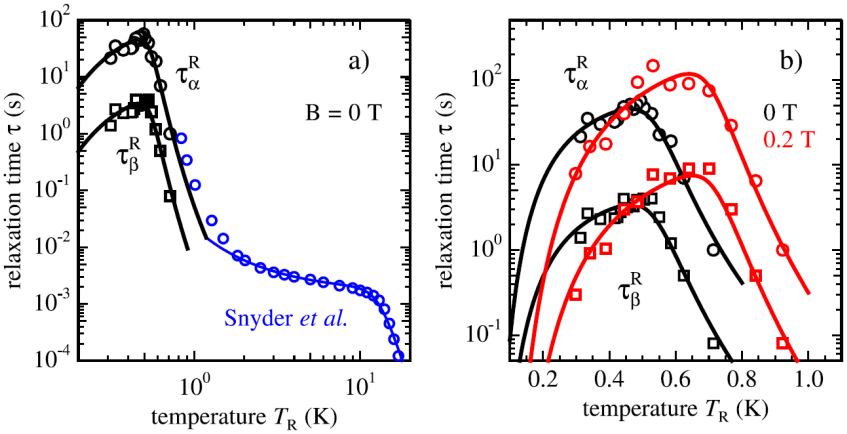

Figure 3.5: The relaxation time of $Dy_2Ti_2O_7$ extracted from thermal relaxation measurements. From Ref. [82].

time constants of relaxation were extracted, most importantly two timescales distinguishable below 1.1 K, τ_α and τ_β. Above 1.3 K, an Orbach type process is found to describe the relaxation, which also agrees with that of Snyder *et al.*. Conversely, Orendac *et al.* used an Orbach process to describe their low temperature data, below 0.4 K [64]. At $\sim$500 mK they observe a crossover in the relaxation rate to a plateau regime in relaxation time (Fig. 3.5). Below 1.1 K, a modelling of an attempt frequency as a function of temperature, $b_\nu(T_R)$, is used (Eq. 3.5) to describe the crossover to re-emergent faster dynamics, which they attribute to a gradual loss of screening.

$$b_\nu(T_R) = \bar{b}_\nu + d_\nu T_R \exp \frac{E_\nu + \epsilon_\nu}{k_B T_R} \tag{3.5}$$

The barrier energy to relaxation for both α and β processes is $E_\alpha/k_B = E_\beta/k_B = 8.3$K, with a screening potential of $\epsilon_\nu/k_B \sim 1$K. $\bar{b}_\nu$ accounts for strong screening, while d_ν is a fit coefficient. Application of field increases relaxation times, with an appreciably larger barrier of 15 K and screening potential of 2 K. A relaxation time τ_γ was also taken from thermal conductivity measurements. They put forward the temperature and field dependence of these measurements, in the context of their theory, as proof that the magnetic excitations in spin ice are indeed monopole defects.

Magnetization decay work by Giblin *et al.* has furthered the Onsager theory in spin ice and christened it a 'magnetolyte' [13]. The purpose of this work was to indeed show that

spin ice could behave as an ionic solution in chemical equilibrium, much like an electrolyte, via an equilibrium of quantities of so-called bound n_{b} and free n_{f} monopoles.

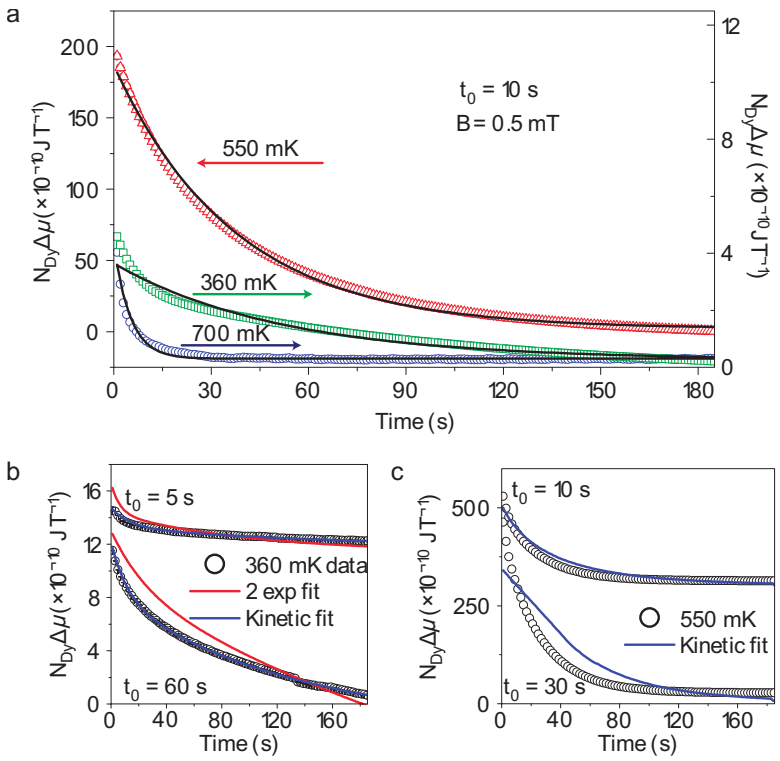

Figure 3.6: The work of Giblin *et al.*, showing the success of the kinetic Onsager-Wien-type model and failure of the exponential relaxation model at low temperatures. This reinforced the magnetricity work of Bramwell *et al.* From Ref. [13].

This principle behind this work was to 'charge' $Dy_2Ti_2O_7$ in the same manner as one would a capacitor, simply using a magnetic field instead of an electric field. This application of field only affects the forward reaction, and thus generates free charges. By varying initial charging conditions, specifically charging time and applied field, the decay of the magnetization (free charges becoming bound, and bound charges recombining) was observed using a SQUID magnetometer along the [100] direction. For one of the temperatures studied, 360 mK, it was found that the two timescales of relaxation which seemed present in the magnetization data could not be resolved by a simple two exponential fit. Instead, the kinetic chemical equilibrium model that they put forward fit quite nicely across the range of applied fields B and charging times t_0 employed. At the centre of this kinetic

model are the linearized rate equations 3.6 and 3.7. The solution to these provides the fit to the magnetization decay for the varying field strengths and charging times. Here, K is the equilibrium constant of dissociation and recombination, k_{Or} is the rate constant of dipole ordering in field, and k_{D} is the rate constant of dissociation of bound pairs.

$$\frac{\mathrm{d}\Delta n_{\mathrm{f}}(t)}{\mathrm{d}t} = k_{\mathrm{D}}\Delta\tilde{n}_{\mathrm{b}}(t) - 2K^{-1}k_{\mathrm{D}}n_{\mathrm{f}}^{\mathrm{eq}}\Delta n_{\mathrm{f}}(t) \tag{3.6}$$

$$\frac{\mathrm{d}\Delta\tilde{n}_{\mathrm{b}}(t)}{\mathrm{d}t} = -(k_{\mathrm{Or}} + k_{\mathrm{D}})\Delta\tilde{n}_{\mathrm{b}}(t) + 2K^{-1}k_{\mathrm{D}}n_{\mathrm{f}}^{\mathrm{eq}}\Delta n_{\mathrm{f}}(t) \tag{3.7}$$

This work was extremely important for validation of the Wien effect as observed by μSR [7], as the dynamics measured here (in the range of field and temperature studied) further confirmed the relation to Onsager's electrolyte work. Very good agreement was achieved between this and their experimental data. The ability of spin ice to act as a magnetic capacitor was heralded as paving the way for magnetronic circuitry.

Castelnovo *et al.* had previously used Debye-Hückel theory, which describes the interactions of a dilute Coulomb gas, to interpret specific heat data with some success as part of work with collaborators [9]. They later applied it to interpret dynamics of monopoles in spin ice, as probed by ac susceptibility. They attempt a couple approaches, loosely based on this. The first considers $\tau \propto 1/\rho$ in the manner of Ryzhkin [77] where ρ is the defect density calculated based on the Debye-Hückel picture. They also attempt to use an Arrhenius expression with a 'dressed' barrier energy, that is, a barrier energy that is temperature dependent, rooted in the change of the Debye charge screening length. The success of these approaches was limited, and provided no quantitative improvement over the agreement of the simulation work in comparison to experimental data. However, the scope of this approach is limited to the dilute limit, and the authors outline several options to improve this approach. Castelnovo *et al.* outline several approaches to improving agreement, including introducing interactions between bound pairs of monopoles, and interactions between bound pairs and single charges. This initial work shows no improvement over the work of Jaubert and Holdsworth (Fig. 3.4), but the corrections suggested here may be able to rectify that difference.

The work of Ref. [7] was outright refuted with other μSR results which showed that transverse field μSR is unable to resolve these monopoles, but instead the exponential decay previously seen was in fact purely an artifact of the sample holder [83]. Here, Dunsiger *et al.* showed that transverse field μSR was not sensitive enough to observe an Onsager effect in spin ice. Monte Carlo work showed that the local field at the muon sites was large (0.3

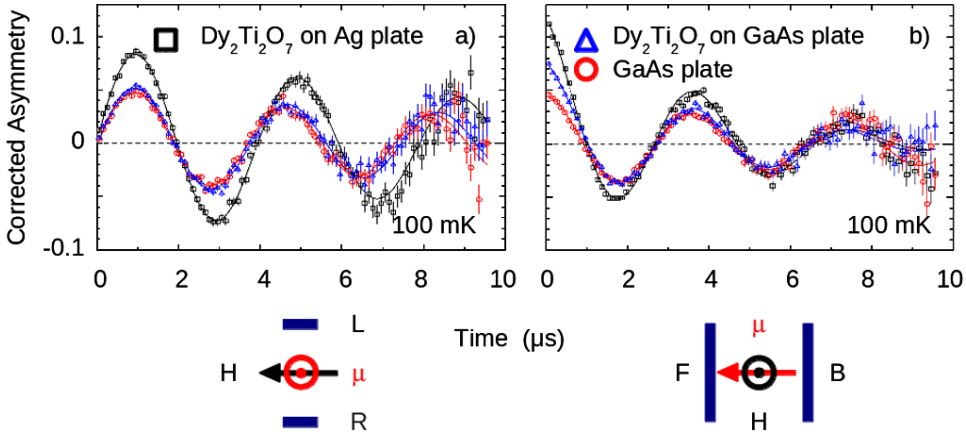

Figure 3.7: The muon precession used to determine the monopole charge, repeated by Dunsiger *et al.* This determined the experiment used by Bramwell *et al.* to prove the existence of monopole currents did not have the sensitivity to actually do so. From Ref. [83].

T) and would overwhelm any monopole signature, which was using fields on the order of 1 mT. Key measurements using a silver sample versus a GaAs sample holder, as had been used in Ref. [7], showed that the muon precession rate was largely a result of the GaAs signal (Fig. 3.7). Dunsiger *et al.*, with careful zero-field μSR configurations, were able to determine that there is a substantial temperature independent muon relaxation rate below 5 K, exhibiting persistent spin dynamics (PSD), not unlike several other pyrochlore family members. However, this result is somewhat mysterious in terms of the results seen in many other techiques, concluding low temperature thermally activated spin dynamics.

3.4.1 Other spin ice

Zhou *et al.* created two entirely new pyrochlore spin ices, $Dy_2Ge_2O_7$ and $Ho_2Ge_2O_7$, as evidenced by specific heat measurements, which allowed for calculations showing Pauling's residual entropy at the lowest temperatures studied [84]. $Ho_2Ge_2O_7$ was akin to $Ho_2Ti_2O_7$ and $Dy_2Ti_2O_7$, while $Dy_2Ge_2O_7$ was out in a new region of phase space. Within the nearest neighbour model, $Dy_2Ge_2O_7$ gave $J_{\rm eff} = 0.62$ K. $Dy_2Ge_2O_7$ was found to match nicely with predictions based upon a Debye-Hückel theory, with Bjerrum corrections included as well, accounting for interactions between bound dipole pairs. The primary importance of this is having a material with a different monopole 'chemical potential', enabling

exploration of other phenomena which are normally exhibited in electrolyte Coulomb lattice gases, and reproducing this physics in magnetolytes.

The question remains where these monopole excitations stand in the historical sense; that is, of the monopoles discussed briefly in the first section of this chapter. Costa-Quintana and López-Aguilar undertook comprehensive electrodynamics calculations in order to reconcile the existence of monopole charges, interacting via a Coulomb law, but without requiring any changes to Maxwell's equations [85]. They determined that while the spin ice defects emulate monopoles in the generation of microscopic and molecular fields, the macroscopic averaged field still satisfies $\nabla \cdot \langle B \rangle = 0$.

3.4.2 Monopoles in Artificial Spin Ice

The observation of magnetic monopoles was not merely limited to the pyrochlore oxides. Artifical geometrically frustrated systems, composed of patterned 2D lattices of magnetic moments, have also been used to observe ice properties. Square and honeycomb lattices have demonstrated ice rule behaviour, but now monopole behaviour has been observed as well [86].

3.5 Summary

It is here where we will recap the introduction and explain how the thesis will proceed. Dipolar spin ice was already the focus of a large community within condensed matter, prior to any mention of fractionalized magnetic excitation which behaves as a monopole. This novel way of examining the canonical dipolar spin ice materials sparked experimental and theoretical efforts to further understand this phenomenon. Evidence of monopole excitations, based on the existing dipolar spin ice formulation, has been interpreted from neutron scattering [8, 10, 9], specific heat [8, 9, 82], ac susceptiblity [6], and magnetization [13] measurements, though refuted in μSR [7, 83]. The particular focus of this thesis will be the ac susceptibility measurements of spin ice. The monopole interpretation appears to diverge from describing existing ac susceptibility data at low temperatures.

We set out with two primary goals in mind. The first is to explore spin ice parameter space through the two canonical spin ice, $Ho_2Ti_2O_7$ and$Dy_2Ti_2O_7$. The large majority of work has focused on $Dy_2Ti_2O_7$, but there is much to be gained from examining $Ho_2Ti_2O_7$, with a variation in exchange energy. Second, we wish to explore the discrepancy between low temperature Coulomb gas simulations [6] and measured ac susceptibility [61], in order

to verify if Coulomb dynamics do describe low temperature ac susceptibility. Failing this, we can at least determine how the relaxation timescales do diverge from the simulated predictions.

Chapter 4

Experimental Details

4.1 Samples

Single crystal $Ho_2Ti_2O_7$, prepared by H. A. Dabkowska, and $Dy_2Ti_2O_7$, prepared by K. A. Ross and H. Noad, were synthesized at McMaster University, using a two-mirror floating zone image furnace and growth procedure similar to those described in Ref. [87]. The floating zone method of crystal growth begins with a stoichiometric polycrystalline feed rod of the desired material, for example, $Ho_2Ti_2O_7$. The polycrystalline material is created via standard solid-state reaction, firing stoichiometric amounts of constituent oxides over the period of several days, with intermediate grindings. The starting material for the growth was created by mixing stoichiometric amounts of oxides Ho_2O_3 and TiO_2 for $Ho_2Ti_2O_7$, and Dy_2O_3 and TiO_2 for $Dy_2Ti_2O_7$.

A schematic of the furnace is shown in Fig. 4.1. An infrared molten zone is maintained between the single crystal seed and polycrystalline feed rods, with the rods counter-rotating on the order of 10 rpm. The rods are slowly fed downwards, often in an overpressure of oxygen or argon gas. The $Dy_2Ti_2O_7$ was grown in 3 atm of oxygen gas, at a growth rate of 6 mm/h.

4.2 ^{3}He/^{4}He Dilution Refrigerator

Nature has allowed several clever tricks to get experimentalists to access temperatures generally quite unnatural here on Earth. The experimental stage is thermally isolated, as

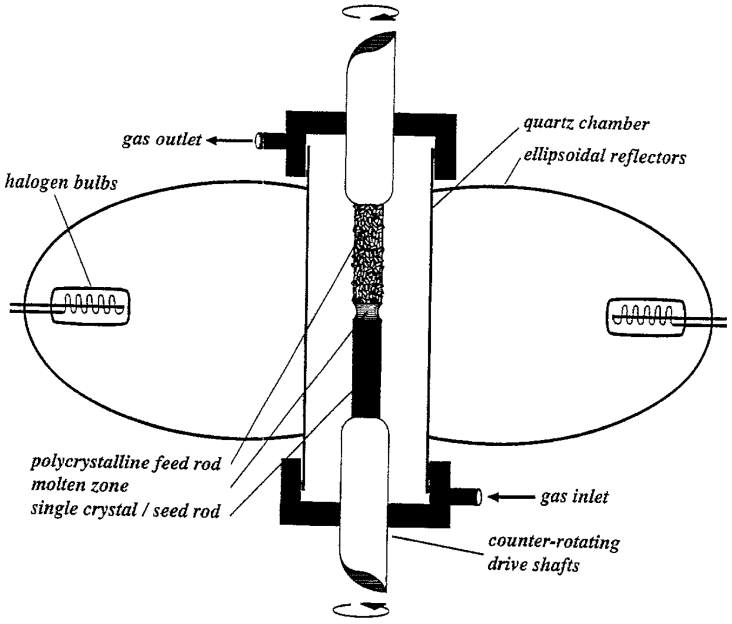

Figure 4.1: Schematic of a floating zone image furnace, from Ref. [87], like the one used to grow the samples for this work.

best as possible, from its surrounding environment. This is done via vacuum and materials choices, attempting to reduce potential heat tranfer to the cold stages of the fridge as much as possible. The experimental stage is contained in a vacuum canister, which is contained within a double-walled dewar with a vacuum space between.

The first stage of cooling is accomplished by immersing the vacuum can into liquid nitrogen (with boiling temperature 77 K), introducing an exchange gas into the vacuum space (neon), and allowing the system to cool to 77 K. After this, helium is used for further refrigeration. Liquid helium boils at 4.2 K, and filling the bath space with helium allows the system to cool (slowly) to 4.2 K. The next stage of cooling is achieved through evaporative cooling of liquid helium, which is drawn from the bath space into the 1 K pot through an impedance, controlling the flow. Pumping on the liquid helium in the 1 K pot with a mechanical pump allows continuous evaporative cooling down to $\sim$1 K. This is quite straightforward, however, and temperatures of this scale have been available to scientists for over a century.

The theory and operation of a dilution refrigerator is described thoroughly in Pobell [89]

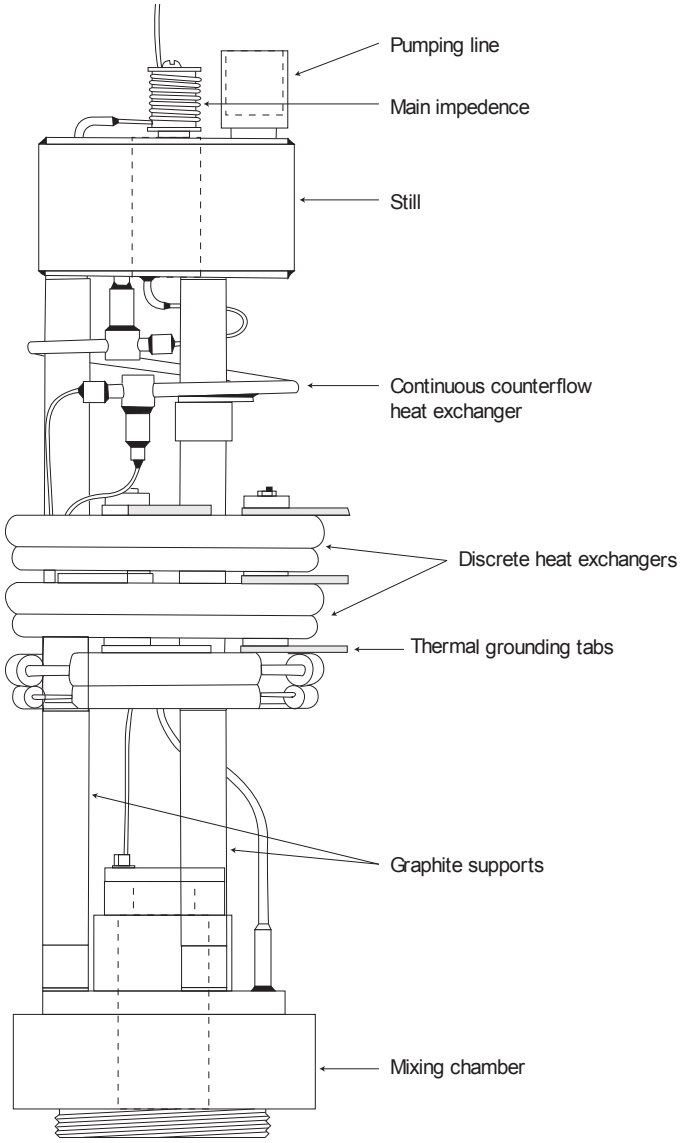

Figure 4.2: The S.H.E. dilution refrigerator, Model DRP-36, used in this work, reproduced from Ref. [88].

and Richardson and Smith [90]. A dilution refrigerator operates using the heat of solution in liquids between liquid ^{3}He and ^{4}He to cool to temperatures on the order of mK. Above a content of 6.6% ^{3}He, a phase separation into a light ^{3}He-rich and dense ^{4}He-rich phases

is possible below the λ-transition line. Wih decreasing temperature, the concentration of ^{3}He in the ^{4}He-rich phase approaches 6.6% rather than 0%, an essential physical feature required to run a dilution fridge. By preferentially removing ^{3}He atoms from the ^{4}He rich phase, ^{3}He atoms will need to move across the phase boundary to maintain equilibrium of solution between the two phases, which will result in a cooling based upon the enthalpy difference between the two [89].

The dilution refrigerator is implemented as follows. The mixture of ^{3}He and ^{4}He gas, referred to as the mix, is condensed by thermal contact with the 1 K pot, into the mixing chamber (Fig. 4.2). For a concentration of ^{3}He greater that 6% in solution with ^{4}He, the system will phase separate into a dense ^{3}He poor (^{4}He rich) and a lighter ^{3}He rich (^{4}He poor) phase (or, concentrated and dilute). A pipe to the still, allows the dilute phase to fill the still via pressure difference, as a mix circulation pump keeps the still at low pressure. The still is kept at a temperature $\sim$0.7 K, where the vapour pressure of ^{3}He is much larger than that of ^{4}He, meaning ^{3}He gets preferentially pumped away. As ^{3}He is removed from the still, ^{3}He atoms will preferentially migrate across the phase boundary, continually cooling the mixing chamber via the latent heat of mixing. The fridge is operated in continuous cycle mode, where the evaporated ^{3}He is returned from the mix circulation pump to recondense in the mixing chamber, and continue the cycle of circulating ^{3}He across the phase boundary. As a result, the fridge is able to cool to temperatures on the order of $\sim$1 mK, and remain cold for months.

The low temperature measurements conducted in this work were done on a S.H.E. Corporation ^{3}He/^{4}He Dilution Refrigerator DRP-36, represented schematically in Fig. 4.2. The base temperature in its current configuration is $\sim$15 mK.

The most important piece of equipment besides the refrigerator itselt is the thermometry, as the large share of low temperature experiments are extremely temperature dependent. The secondary thermometer is a calibrated germanium resistance thermometer (GRT) from *Lakeshore Cryotronics*. This calibration was verified using the overlap between the temperature dependence of a paramagnetic salt CMN down to 50 mK, and beyond 50 mK, to base temperature, using nuclear orientation thermometry [91].

There are several nested layers of shielding providing a favourable noise environment at the experimental stage. The 1K shield, a blackbody radiation shield heat-sunk to the 1 K pot, is lead-coated. This is surrounded by a cryogenic μ-metal shield in the bath space, and an external room temperature μ-metal shield. It is a necessity to screen out as much field as possible, as we are operating with fields much smaller than Earth's field. The residual field is estimated to be $<$ 1mOe.

4.3 AC Susceptibility Measurement

AC susceptibility measurements were made using a second order superconducting quantum interference device (SQUID) axial gradiometer[1] used and described in previous work [92, 91, 93, 94], schematically represented in Fig. 4.3. The design of the magnetometer is described J. A. Quilliam's thesis, Ref. [91]. The SQUID has a fundamental advantage when used as part of a gradiometer configuration. The pickup coil of conventional ac magnetometers rely on the induced voltage that is proportional to frequency. This makes low frequencies prohibitive, as the signal-to-noise ratio decreases significantly. The SQUID, however, is an extremely sensitive magnetic flux-to-voltage converter, where there is no proportionality to frequency. The operation of a SQUID will not be discussed here, the interested reader is pointed towards two excellent books, [95] and [96].

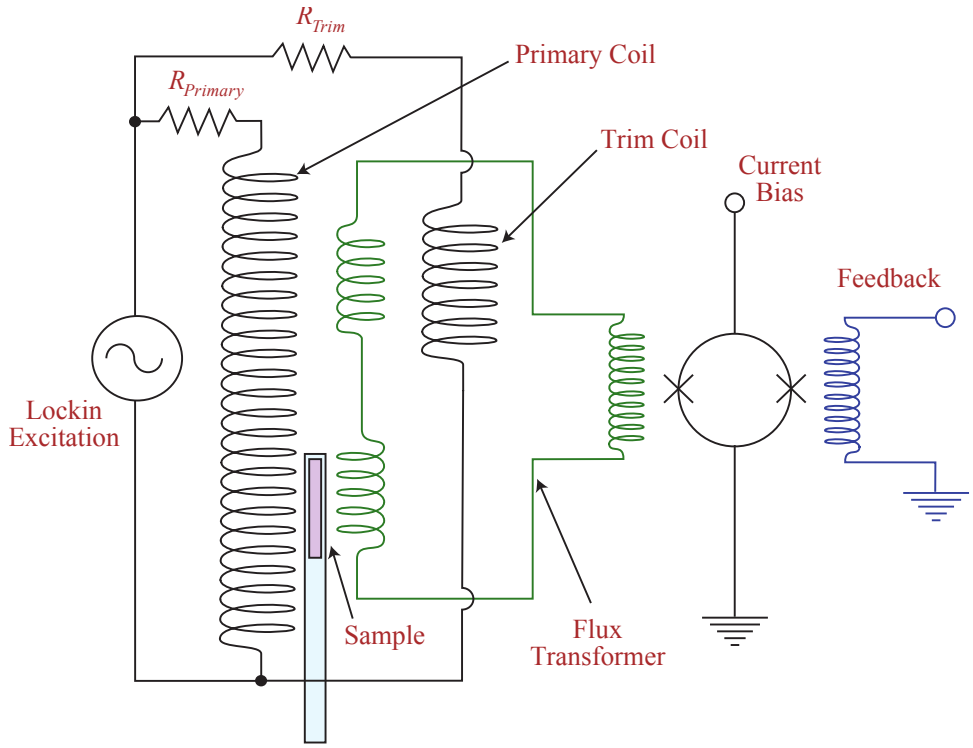

Figure 4.3: Magnetometer used in this work, reproduced from Ref. [91].

The SQUID magnetometer used here is comprised of three coils of NbTi wire on a

[1]Constructed by Jeffrey Quilliam

phenolic form as the sensing coils, which are coupled to a dc SQUID through a superconducting flux transformer. The three coils are the counterwound loops of a second order gradiometer, the sensing coil. The sensing coil form is contained in the bore of a second phenolic form, the excitation coil, wound with 375 turns of NbTi wire. Balance of the gradiometer is achieved through positioning in the gradiometer and tuned with a trim coil coupled to one of the gradiometer coils, in parallel with the primary coil. The innermost shielding layer is a lead shield surrounding the SQUID, isolating it from the excitation field and the entire magnetometer is further shielded by another lead shield. Both the dc SQUID and 100 kHz SQUID controller were obtained from the company *ezSQUID*. The ac excitation source used was a *Stanford Research* SR830 lock-in amplifier, which also read the signal from the SQUID operated in feedback. The output of the feedback loop is a voltage proportional to χ, and a calibration remains to be performed. The samples were contained within one branch of the gradiometer, mounted on a sapphire rod with *General Electric 7301* varnish. The sapphire rod was clamped to a copper base, which was heat sunk to the rest of the magnetometer, and to the mixing chamber of a dilution refrigerator. The long axis of the sample being studied was mounted to the sapphire sample holder with an orientation accuracy of ± 2 degrees.

Temperature scans for base temperatures of the fridge are acquired with every run. Rather than removing the sample, the offset due to misbalance is measured each cooldown by doing a frequency scan at the base temperature, where all physics is frozen out. That is, any response is at far lower frequencies, far beyond the reach of our frequency range. The magnetometer signal has a slight frequency dependence, though miniscule in comparison to an actual signal. The misbalance can be corrected for mechanically (physically shifting in the z-direction the location of the sensing coil in the bore of the excitation coil) or magnetically, by changing the trim coil current.

Data was typically acquired by remaining at a single temperature and varying frequency, scanning from high frequency to low. Some scans were taken to be certain that there was no hysteresis in this measurement, by scanning from low to high frequency. On occasion, successive scans were taken at the same temperature in order to be sure no further relaxation had occurred. Some temperature scans were acquired for $Ho_2Ti_2O_7$, sitting at one frequency and varying temperature from low to high, with appropriate wait times to ensure thermal equilibration.

While the SQUID gradiometer is far superior to a conventional gradiometer at low frequencies, high frequency performance is limiting. Currently, frequencies of up to 1 kHz can be measured confidently. However, there are several limiting factors in the setup, including low-pass filters, twisted NbTi pairs, and the bandwidth of the SQUID controller as set up. The bias current, open loop gain, closed loop gain, and modulation can all be

adjusted to get the best frequency range possible.

4.4 Calibration and Correcting for Demagnetizing Effects

4.4.1 Susceptibility and Demagnetizing Fields

The response of a magnetic system gauged by the change in magnetization in response to an applied field is known as the ac susceptibility $\chi(\omega) = \frac{\mathrm{d}M(\omega)}{\mathrm{d}H(\omega)}$. The susceptibility is complex, and contains in- and out-of-phase components χ' and χ'' respectively,

$$\chi(\omega) = \chi'(\omega) - i\chi''(\omega) \tag{4.1}$$

However, the measurement of the true, bulk susceptibility χ is complicated by demagnetising fields gauged by demagnetising factor N, which hide the true magnitude of of the susceptibility and give a measured value of χ_A:

$$\frac{1}{\chi} = \frac{1}{\chi_A} - 4\pi N \tag{4.2}$$

This can be expanded into both the real (4.3) and imaginary (4.4) components, following Ref. [50] and Ref. [93].

$$\chi' = \frac{\chi'_A - 4\pi N(\chi'^2_A + \chi''^2_A)}{(1 - 4\pi N\chi'_A)^2 + (4\pi N\chi''_A)^2} \tag{4.3}$$

$$\chi'' = \frac{\chi''_A}{(1 - 4\pi N\chi'_A)^2 + (4\pi N\chi''_A)^2} \tag{4.4}$$

The demagnetizing field of the sample can be quite large with the rare earth ions dealt with here, as both the Dy and Ho magnetic moments are $\sim$10 μ_B. This makes it crucial in the accurate determination of the true susceptibility, $\chi(\omega)$, along with correct calibration of the output voltage of the SQUID feedback loop. This can be accounted for by calculating the sample geometry dependent demagnetizing factor N. The demagnetising factor for rectangular prisms was determined by Aharoni [97], through some unwieldly

algebra, producing a large expression, reliant only on the dimensions of the prism, widths a and b, and length c.

Samples are generally easiest prepared as rectangular prisms, using either a wire saw or low revolution diamond saw to prepare samples. Favourable sample dimensions can be used to reduce the demagnetisation factor. Generally, a rectangular prism of length c, where c a,b, where a and b are the other side lengths, is to be strived for, with the desired crystal axis of study along the long axis.

4.4.2 Calibration

The method for correction will follow that described in Ref. [93]. While we are able to calculate the demagnetisation factor, the feedback of the SQUID controller is only converting the flux to a voltage. This needs to be normalized to units of susceptibility. One method of doing this is using a superconducting sample of lead, perfectly diamagnetic and with has a susceptibility of -1. The voltage output of the SQUID feedback loop can then be converted to units of susceptibility.

Alternatively, another method of calibration conceived by J. A. Quilliam, utilizes instead two rectangular prism-shaped samples with different aspect ratios. These samples have respective demagnetisation corrections N_1 and N_2. A parameter space of calibration factors C_1 and C_2, is then generated. For each permutation of C_1 and C_2 scaling the apparent susceptibility (Eq. 4.5), the demagnetisation correction for each sample is applied using 4.2. Calibration factors from parameter spaces C_1 and C_2 were applied to the raw feedback data from the SQUID controller for the two samples involved in any given measurement pair.

$$\chi_{\mathrm{A}_1} = C_1 V_1 \text{ and } \chi_{\mathrm{A}_2} = C_2 V_2 \tag{4.5}$$

The overlap is then calculated for all permutations using 4.6, attempting to minimize this quantity and maximize the overlap between the two curves. The combination of calibration factors C_1 and C_2 which correspond to the maximized overlap are then used in tandem with their geometry-dependent demagnetisation factors in the remainder of the analysis.

$$\sum (\chi_1'' - \chi_2'')^2 / ((\chi_1'')^2 + (\chi_2'')^2) \tag{4.6}$$

The magnetometer was calibrated using frequency scans of samples measured at 600, 700, and 800 mK. A single calibration factor for a particular sample applies to frequencies

from 1 mHz to 100 Hz, and all temperatures for a single sample. The agreement between the measurements of the two different samples is quite good, and reinforces the accuracy of the demagnetisation correction.

One restriction of the method is that it assumes the true, bulk susceptibility of a material is not geometry-dependent. This is extremely likely to be a safe assumption with the sample geometries studied, as we are dealing with a macroscopic quantity of material. Perhaps in the presence of some confined geometry, such as a thin film or wire, the susceptibility differs, but here we can expect bulk behaviour.

Chapter 5

AC susceptibility of $Ho_2Ti_2O_7$ and $Dy_2Ti_2O_7$

5.1 Motivation

In this chapter, we will present measurements of the ac susceptibility of dipolar spin ice. As discussed extensively in the Introduction, numerous ac susceptibility studies of dipolar spin ice are present in the literature, summarized in Fig. 5.1. However, there are substantial absences in this map of parameter space. No frequency scans of $Ho_2Ti_2O_7$ were undertaken, and no measurements below 10 Hz presented. Previous theoretical determinations of the relaxation time of $Dy_2Ti_2O_7$ had a clear descrepancy below 1 K with low temperature susceptibility data, as can be seen when the data is plotted in the axes natural to exponential freezing behaviour, $\log f$ vs $1/T$.

The relaxation timescales at low temperatures are crucial to the development of the theory of monopole excitations in dipolar spin ice. The low defect density limit provides an excellent stress test of the theory in the dilute, low temperature regime. The energy scales associated with the frequency dependent relaxation are an insight into the long range dipole interactions in the classic dipolar spin ice model, as well as the long range interactions of a Coulomb monopole gas. Initially, the spin ice community also found a huge disparity between relaxation times of $Ho_2Ti_2O_7$ and $Dy_2Ti_2O_7$ using different techniques [14], leaving room to probe why they are different through a direct comparison within one experimental technique. These absences are critical gaps in the understanding of how the system behaves. As the magnetometer used in this work is capable of measuring to 1 mHz, substantial gains are to be made in the data available to the spin ice community.

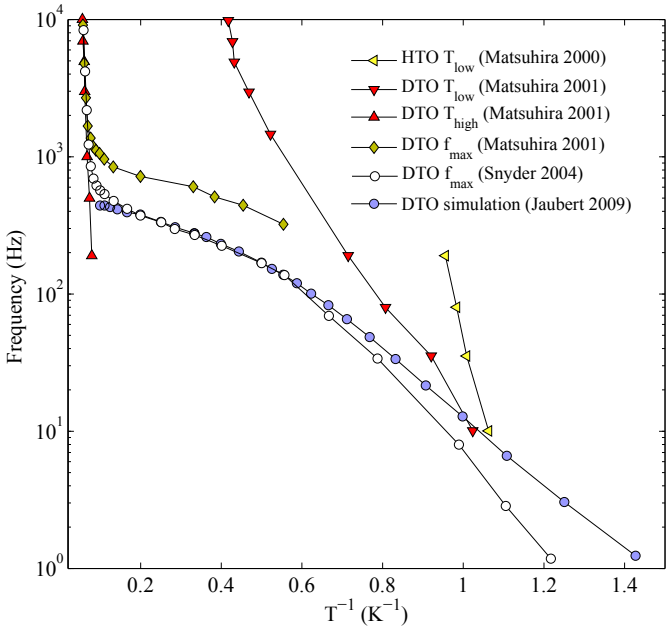

Figure 5.1: Compilation of prior AC susceptibility work on $Ho_2Ti_2O_7$ and $Dy_2Ti_2O_7$.

The first test of this was undertaken in studying $Ho_2Ti_2O_7$ [93], the less-favoured spin ice for study of monopole defects, as evidenced by the preference of the literature. The second result comes from a study of $Dy_2Ti_2O_7$ [94] in response to the surprising result of $Ho_2Ti_2O_7$, both of which will be described here.

5.2 Experimental Results

The dimensions and demagnetisation factors of the studied samples are in Table 5.1. Both $Ho_2Ti_2O_7$ and $Dy_2Ti_2O_7$ were measured using the magnetometer discussed in the preceeding chapter. The frequency range dictated the temperatures which were measured: $Ho_2Ti_2O_7$ was measured in the temperature range 600 mK to 1300 mK, while $Dy_2Ti_2O_7$ was limited to 500 mK to 1500 mK. The frequency range for the $Ho_2Ti_2O_7$ study was 1 mHz to 500 Hz, as a result of bandwidth limiting by the SQUID set-up. For the $Dy_2Ti_2O_7$ study, the frequency range was 1 mHz to 1 kHz. Fields of up to 15 mOe ac were applied to the $Ho_2Ti_2O_7$ samples, and up to 6 mOe for $Dy_2Ti_2O_7$ samples, both along the [110] crys-

talline direction. All data presented has been corrected for the demagnetizing field, unless otherwise stated.

Table 5.1: Sample dimensions of $Ho_2Ti_2O_7$ and $Dy_2Ti_2O_7$.

Sample	Dimensions (a×b×c)	Demagnetisation Factor N
HTO-A	$1.1 \times 1.1 \times 2.6$ mm^3	0.1538
HTO-B	$0.6 \times 0.6 \times 3$ mm^3	0.0846
DTO-A	$1.0 \times 1.0 \times 3.9$ mm^3	0.1126
DTO-B	$0.4 \times 0.4 \times 3.8$ mm^3	0.0533

The in-phase (χ') and out-of-phase (χ'') components of ac susceptibility are plotted in Fig. 5.2(a,b) for $Ho_2Ti_2O_7$ and Fig. 5.2(c,d) for $Dy_2Ti_2O_7$. There is clear frequency-dependent freezing. Below 600 mK or 500 mK, for $Ho_2Ti_2O_7$ and $Dy_2Ti_2O_7$ respectively, we were no longer able to observe the peak of the absorption spectra χ'', which had shifted below our frequency window. In order to verify the freezing in $Dy_2Ti_2O_7$, frequency scans at both 350 and 450 mK were acquired, finding no relaxation modes between 1 mHz and 1 kHz. A surface plot of the parameter space for the compiled spectra for each, $Ho_2Ti_2O_7$ (Fig. 5.3) and $Dy_2Ti_2O_7$ (Fig. 5.3), also gives an excellent picture of the overall character of the parameter space, as well as the difference between temperature and frequency scans.

Some temperature scans of $Ho_2Ti_2O_7$ are presented in Fig. 5.4. Here, a characteristic freezing temperature $T_f(f)$ is determined by extracting $\chi'' = \chi''_{\max}(T_f)$.

Superimposed normalized χ'' spectra, plotted as $\chi''/\chi''_{\max}$ versus $f/f_{\max}$, are shown in Figs. 5.5a and 5.5b. The difference in the spectral width is clearly apparent in $Ho_2Ti_2O_7$, where we see a shift of width from the low- to high-frequency side of the spectra. The $Dy_2Ti_2O_7$ spectra width does not change significantly over the temperature range studied.

The data can also be represented in an Argand-type plot, χ'' versus χ' in Fig. 5.6a and Fig. 5.6b for $Ho_2Ti_2O_7$ and $Dy_2Ti_2O_7$ respectively. This is a typical method of examining dielectric frequency spectra. The characteristic is not quite Debye-type, which would be represented by a symmetric semi-circle. Instead, we see something more of the empirical Davidson-Cole type, where the plots make a less than perpendicular intersection with the x-axis. Curiously, it cannot be fit by a single Davidson-Cole-type mode of relaxation. Other empirical susceptibility relations, such as Cole-Cole and Havriliak-Negami do not capture the character of the plot either. This is the case for both $Ho_2Ti_2O_7$ and $Dy_2Ti_2O_7$. Some indications as to why this is appears further on in the discussion.

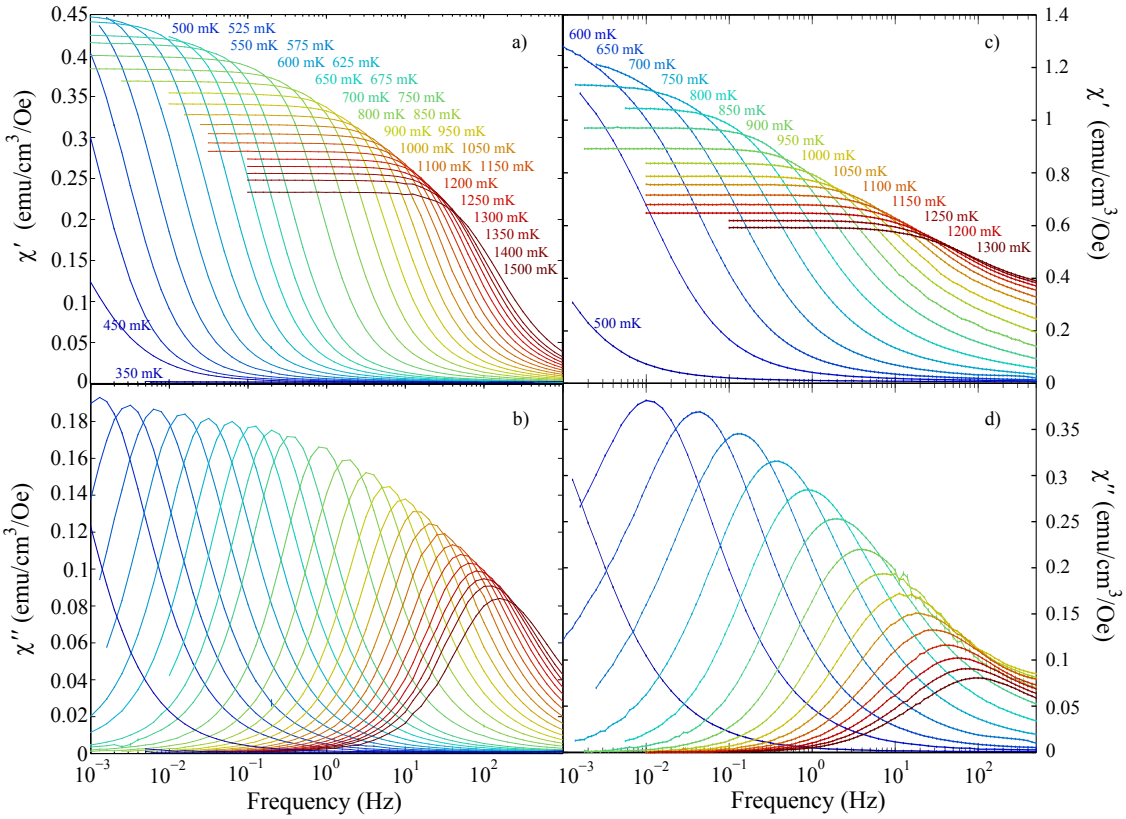

Figure 5.2: AC susceptibility frequency scans of $Ho_2Ti_2O_7$: a) χ' and b) χ'', and $Dy_2Ti_2O_7$: c) χ' and d) χ''. Both materials show a strong signature of frequency dependent spin freezing.

Due to the relatively narrow spectra, the relaxation can be well characterized by extracting the frequency at which χ'' is maximized, $f_{\max}$. The plots of $f_{\max}(T^{-1})$ and $f(T^{-1}_{\max})$ are shown in Fig. 5.7. In the low temperature limit, both $Ho_2Ti_2O_7$ and $Dy_2Ti_2O_7$ are observed to trend to an Arrhenius law, $f_{\max} = f_0 \exp(-E_A/T)$. Fitting from 1 K to 600 mK for the $Ho_2Ti_2O_7$ relaxation, we are able to extract a barrier energy of 10.71 K for the frequency scans, with $f_0 = 5.91 \times 10^5$ Hz. Fitting an Arrhenius relation to the temperature scans, we find a barrier energy of 13.08 K, with $f_0 = 2.14 \times 10^7$ Hz. For $Dy_2Ti_2O_7$, we are able to fit from 850 mK to 500 mK with a barrier energy of 9.79 K and $f_0 = 3.92 \times 10^5$ Hz. This is all shown in Fig. 5.7. We have attempted fits to energy barriers of 2 J_{eff} and

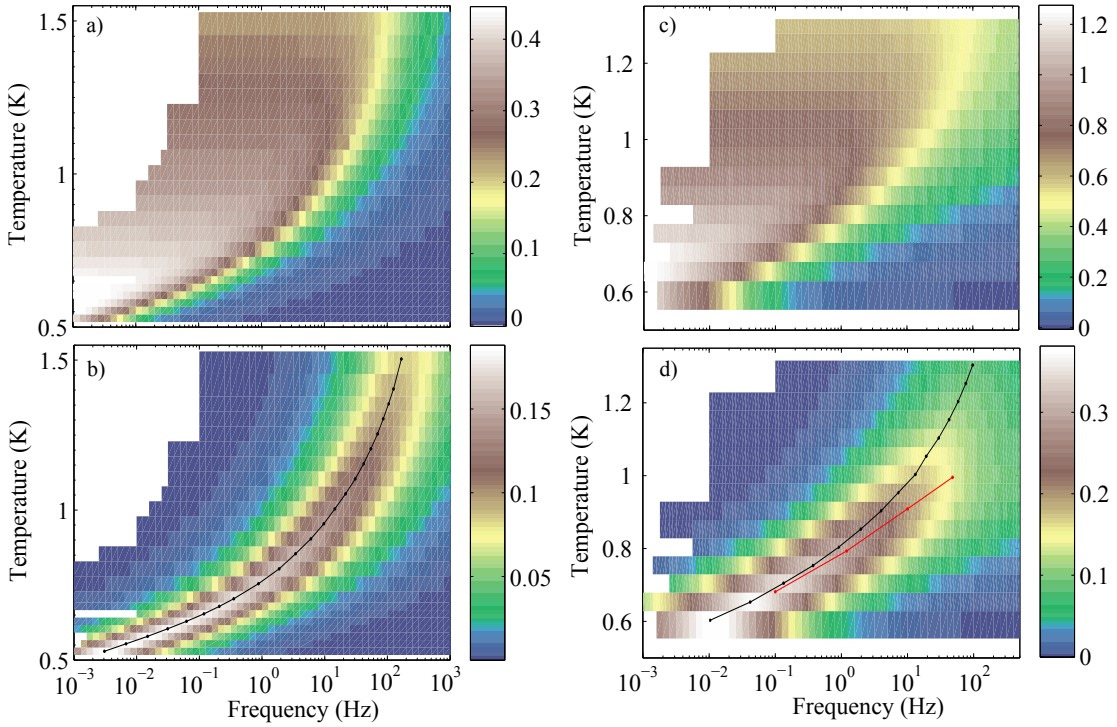

Figure 5.3: Surface plot of $\chi'(f,T)$ and $\chi''(f,T)$ for a,b) $Ho_2Ti_2O_7$ and c,d) $Dy_2Ti_2O_7$. The difference in the spectra as they evolve in temperature is very apparent.

$6J_{\text{eff}}$, which also appear in Fig. 5.7.

The importance of a demagnetization correction is expressed in Fig. 5.8, using $Ho_2Ti_2O_7$ as an example. This shows how sample geometry-dependent the correction is, and that the correction does not merely comprise a shift in the log y-axis, but is also includes temperature dependent shift.

The differences in the width of the absorption spectra are quantified by measuring the half-width at half-maximum on the high- and low-frequency sides of the spectra, abbreviated as HWHM+ and HWHM- respectively. This is plotted in Fig. 5.9. Here, it is clear that $Ho_2Ti_2O_7$ is quite different than $Dy_2Ti_2O_7$. The spectral width gives insight into the number of relaxation modes involved, and we can infer that $Ho_2Ti_2O_7$ has a slightly broader distribution of relaxation times compared to $Dy_2Ti_2O_7$.

We have used the low frequency data to acquire or extrapolate to a value for the dc limit of χ, by simply extrapolating in the Argand diagrams to the low frequency $\omega \to 0$

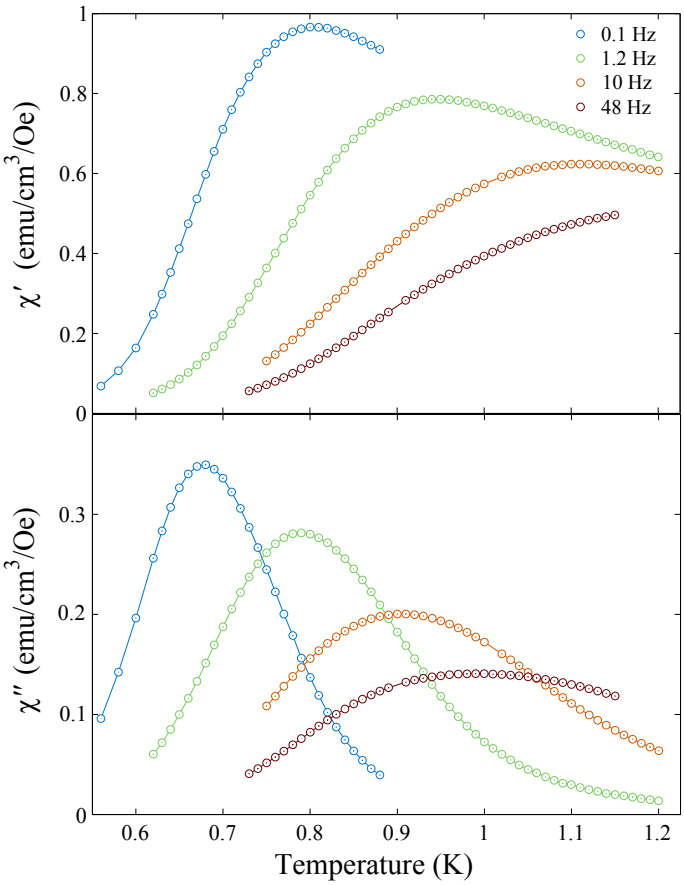

Figure 5.4: χ' and χ'' for temperature scans of $Ho_2Ti_2O_7$ at fixed frequencies, used as an alternate parametrization of ac susceptibility.

limit. This is shown in Fig. 5.10. We see that this extrapolation does not yield a linear dependence on inverse temperature.

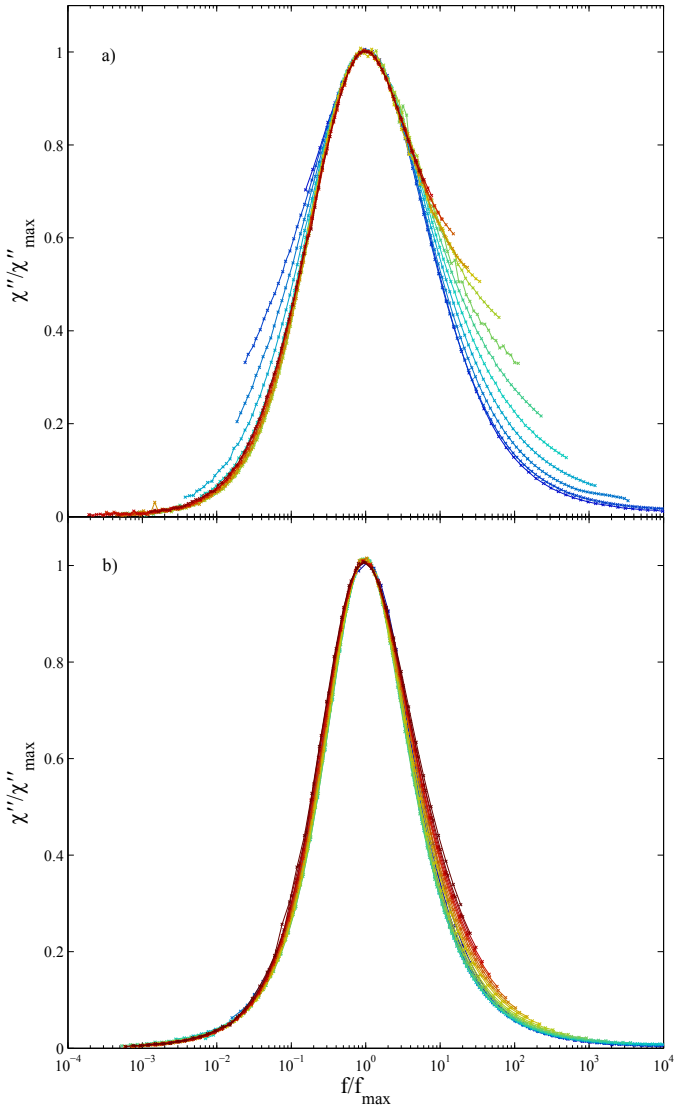

Figure 5.5: Superimposed χ'' absorption spectra for a) $Ho_2Ti_2O_7$ and b) $Dy_2Ti_2O_7$. The width of the $Dy_2Ti_2O_7$ spectra is much more symmetric in temperature.

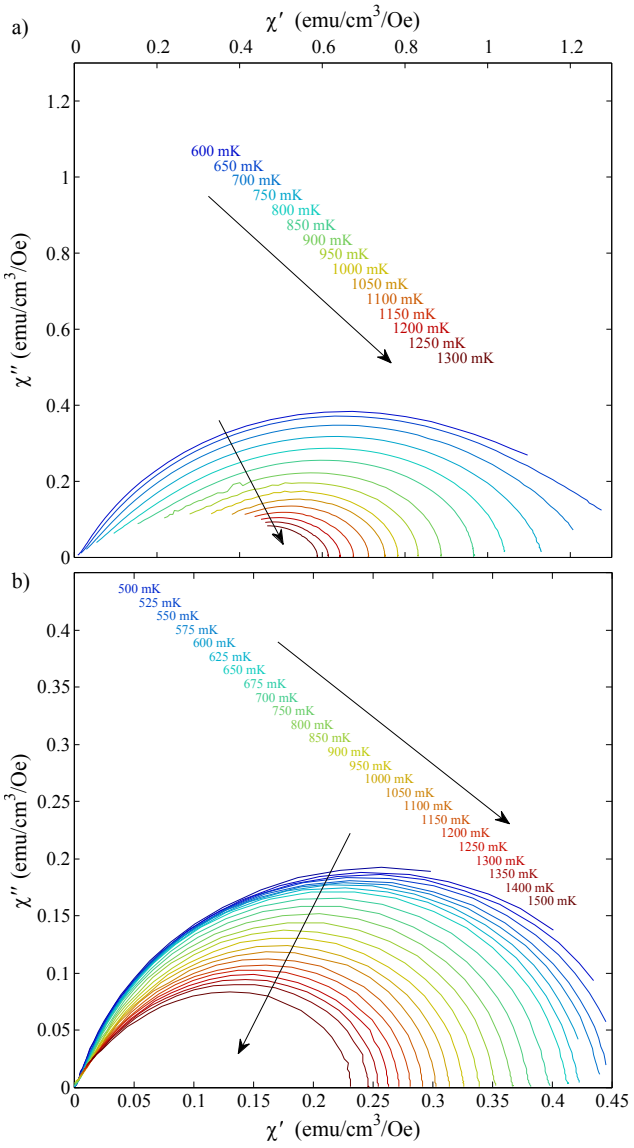

Figure 5.6: Argand plot of the imaginary, χ'', versus the real, χ', components of the ac susceptibility for a) $Ho_2Ti_2O_7$ and b) $Dy_2Ti_2O_7$. The shape of the spectra does not correspond to a typical Debye-type.

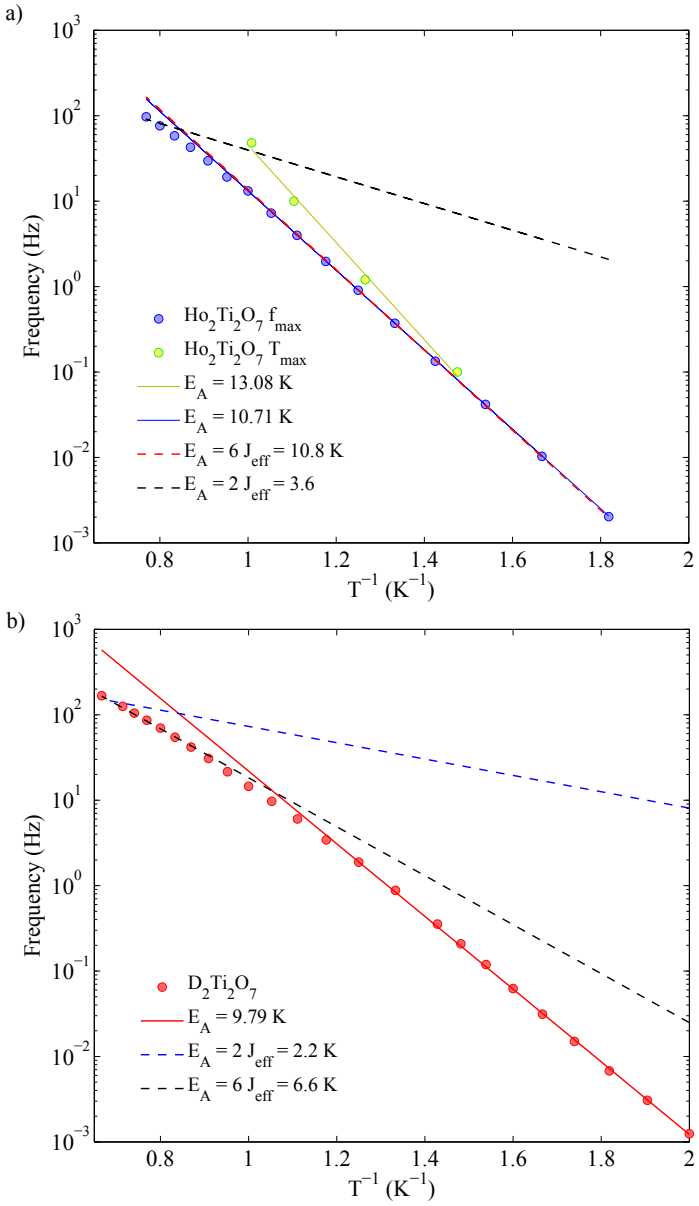

Figure 5.7: Arrhenius fits of different barrier energies for $Ho_2Ti_2O_7$ and $Dy_2Ti_2O_7$. While $E_A = 6\ J_{\text{eff}}$ works very well for $Ho_2Ti_2O_7$, it clearly does not describe the $Dy_2Ti_2O_7$ data.

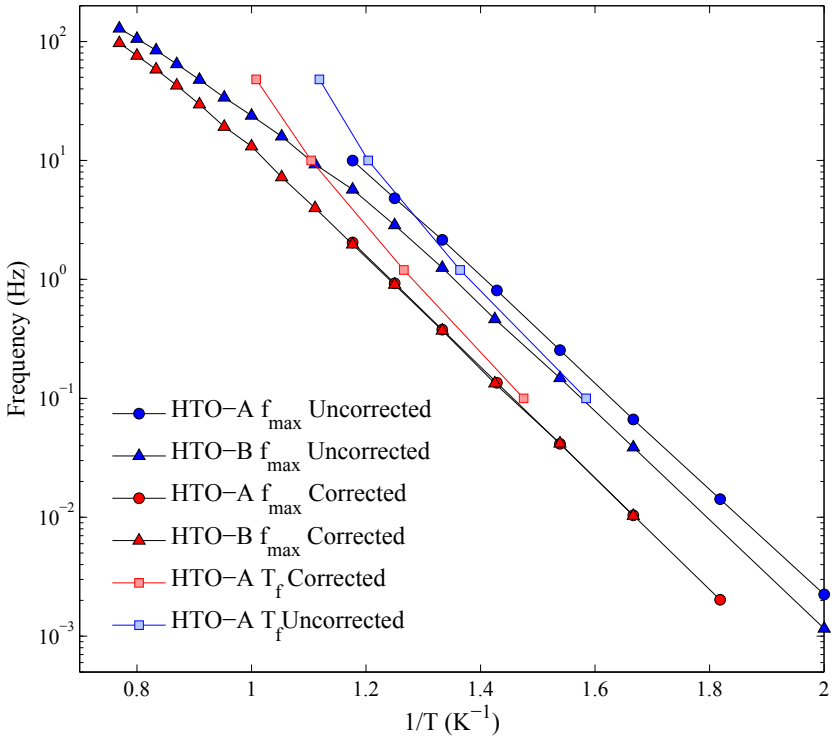

Figure 5.8: The peak relaxation frequencies $f_{\max}$ for both $Ho_2Ti_2O_7$ sample A and sample B are shown, prior to and after demagnetization correction. The impact the correction has on the relaxation frequency is not merely a constant frequency shift, but is also temperature dependent.

5.3 Comparison and Discussion

There are a few key differences to be considered when comparing ac susceptibility data. Firstly, there are two different ways to parametrize a freezing temperature and characteristic frequency, which is measured either by varying temperature at a given frequency, or varying frequency at a given temperature. In the case of temperature scans, a freezing temperature where $\chi''(T_{\rm f}) = \chi''_{\max}(T)$ is extracted for a given frequency, while in the case of frequency scans, by extracting $\chi''(f) = \chi''_{\max}(f)$ for a given temperature. These parametrizations do not agree over all parameter space, as can be seen in Ref. [50, 93],

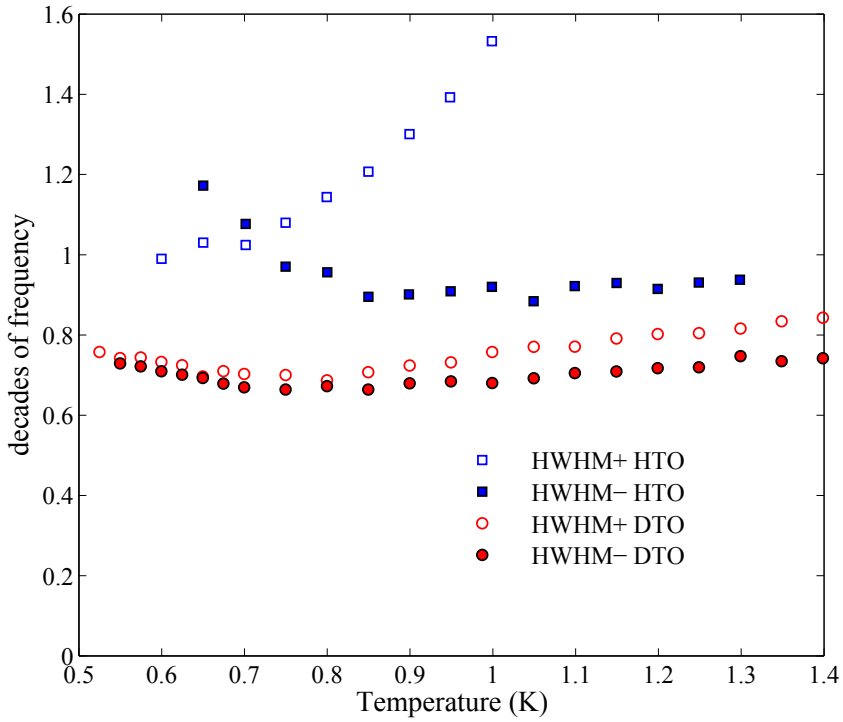

Figure 5.9: Spectra half-width at half-max for $Ho_2Ti_2O_7$ and $Dy_2Ti_2O_7$. The difference in spectra width between the two materials indicates $Ho_2Ti_2O_7$ has a larger distribution of relaxation times.

and can be seen from a surface plot of parameter space, $\chi'(f,T)$ and $\chi''(f,T)$, in Fig. 5.3a and 5.3b. Here we see this in the difference in barrier energy for HTO between temperature scans and frequency scans: 13.08 K and 10.7 K. Ideally, a set of temperature scans would contain all of the information needed to reconstruct isotherms through varying frequency, and then extract the characteristic frequency as done here. Scans in frequency space are a natural way in which to view dissipation in χ'', which is usually comprised of relatively symmetric distribution in frequency. Hastily measured temperature scans may have some thermal equilibration issues, especially in appreciably slow systems such as the spin ice materials studied here. The actual spin temperature of a slow system may lag the recorded experimental stage temperature.

As outlined here and elsewhere [50, 93], implementation of the demagnetization cor-

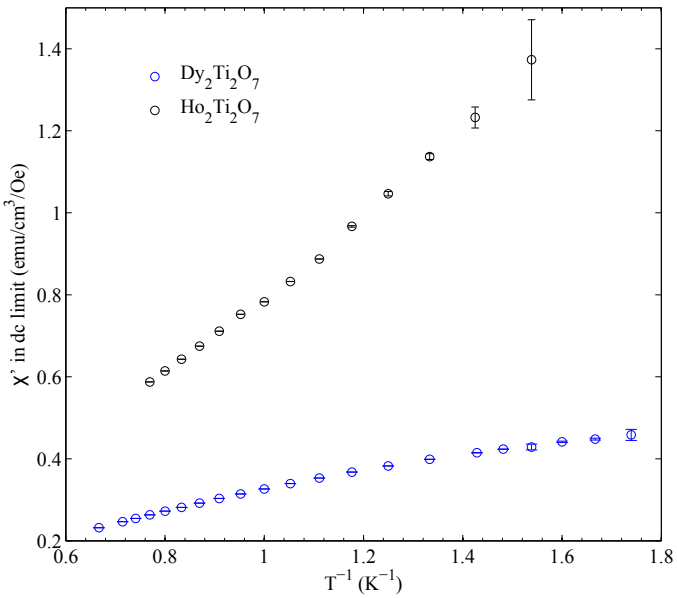

Figure 5.10: $\chi'(\omega \to 0)$ for $Ho_2Ti_2O_7$ and $Dy_2Ti_2O_7$, for comparison to DC limit predictions. The susceptibility magnitude of $Ho_2Ti_2O_7$ is growing significantly faster in temperature than $Dy_2Ti_2O_7$. Neither follows a Curie law over the entire temperature range.

rection is also crucial to a correct parametrization of freezing. Many results do not state exactly their treatment of this issue [51, 58, 61, 63], which becomes especially important at low temperatures with the substantial moments of these rare-earth ions. Because not all results have treated this on the same footing, it can be very important to note in comparison to other results.

The difference between polycrystalline materials and single crystalline materials can also have some impact. Averaging over all orientations as polycrystalline measurements do, may convolute any possible orientation dependence into a single barrier energy, or an averaged magnitude of χ , for example. However, it is not clear that this should be an issue in this system in the zero field limit. Along the [110] and [1$\bar{1}$0] directions, the spins which see the field are along the so called α- and β-chains respectively [98]. Two spins of each tetrahedron see the field, two spins are orthogonal to the field. When field is applied along the x-axis, this ordering is still commensurate with a two-in two-out ground state,[99] as it has been found experimentally [65, 66]. In the [100] direction, all spins see a

component of the field, and field applied along this orientation will only reinforce the two-in two-out state [99]. For a large enough field applied along the [111] direction, one spin per tetrahedron is parallel to the field, while the other three see only a small component of it. This orientation is the only one which does not yield a two-in two-out ground state in the magnetized limit. Measurements have observed a plateau in magnetization [47, 100, 101], and this is the orientation which yields the liquid-gas type transition seen in experiment [78] and attributed to a condensing of monopoles [5].

We are exclusively operating in the low field limit, which means that we are definitely in the spin ice regime at our lower temperatures. We do not approach the field required to reorient the spins into α- or β-chains, as we can see in Ref. [98] thus we are only probing thermal excitations. It is not clear that orientation should have any effect on time scale or barrier energy at these field levels.

5.3.1 $Ho_2Ti_2O_7$ versus $Dy_2Ti_2O_7$

$Dy_2Ti_2O_7$ and $Ho_2Ti_2O_7$ share some surprising similarities, beyond qualitatively both displaying the same changing barrier height developing into a thermally activated freezing, characterized by a crossover from a plateau regime to one of steep temperature dependence. First, the microscopic tunnelling scale used to define the plateau can be inferred to be very similar, based on examining the timescales of the relaxation for a given temperature. Pevious conclusions had been made otherwise [11], but it seems that microscopic timescale which would define quantum tunnelling of spin states prior to the spin ice freezing must be quite similar. The huge difference in timescales according to technique is quite common in spin ice and will be discussed later on. Second, the crossover to the Arrhenius nature occurs at slightly higher temperature for $Ho_2Ti_2O_7$. This is based upon the temperature ranges which were suitably fit by an Arrhenius expression, and that $Ho_2Ti_2O_7$ commences freezing (i.e. has a lower characteristic frequency of relaxation) at a higher temperature than $Dy_2Ti_2O_7$. This agrees with phase diagrams based on the nearest neighbour exchange energy and dipole-dipole coupling (Fig. 2.12), as presented in Ref. [62]. Third and most importantly, the energy barrier is remarkably similar, 10.7 K for $Ho_2Ti_2O_7$ and 9.79 K for $Dy_2Ti_2O_7$. Previous analysis had guessed at an involvement of $6J_{\text{eff}}$ [11], which was validated by our measurement of $Ho_2Ti_2O_7$ which finds $6J_{\text{eff}}$ as well. Our measurement of $Dy_2Ti_2O_7$ finds a significantly different scaling of $\sim 9J_{\text{eff}}$. We have shown that this energy scale is not universal to the freezing of spin ice, and that it agrees with $6J_{\text{eff}}$ is purely coincidental.

We turn to why this may be. The dipole-dipole interaction energy is the same for both $Ho_2Ti_2O_7$ and $Dy_2Ti_2O_7$, with D = 1.41 K [11]. However, it is the exchange energy scale

that varies between the two materials, with J^{HTO} = -1.65 K, and J^{DTO} = -3.72 K, the source of the difference in the effective exchange energy. The antiferromagnetic exchange, however, which varies roughly by double, seems to have little impact on the barrier. As might be expected, in the dilute limit, relaxation is likely dominated by the cost of long range interactions which originate in the dipolar interaction energy. So, as we vary the nearest neighbour exchange, the small response confirms the dipole energy scale plays the largest role in the energy barrier at low temperatures.

There are two distinctive features in the absorption spectra of the two spin ice, shown in Fig. 5.5, to remark upon. The first is the overall spectral width, which is indicative of the distribution of relaxation timescales. $Dy_2Ti_2O_7$ has a width of ∼1.4-1.6 decades, and $Ho_2Ti_2O_7$ has a width of ∼2-2.5 decades. When compared to the theoretical width of 1.14 decades [51], it is apparent that there may be more than one timescale associated with the relaxation observed here. The second is the lack of symmetry of the spectra. While $Dy_2Ti_2O_7$ displays some slight assymetry appearing at higher temperatures, it is different and more evident in $Ho_2Ti_2O_7$, which quickly diverges to the point where we can no longer measure the HWHM within our frequency range. HWHM+ also remains quite stable for $Ho_2Ti_2O_7$. At the lowest temperatures, the low frequency side of the $Ho_2Ti_2O_7$ spectra displays some broadening. $Dy_2Ti_2O_7$ also exhibits some slight broadening at low temperatures.

The very apparent differences between these spin ices beg the question: what are the well-known physical differences between the two? One notorious difference is a large spin-orbit interaction. The nuclear hyperfine component is very apparent in the large Schottky anomaly in $Ho_2Ti_2O_7$ specific heat. As discussed above, this has plagued specific heat measurements of $Ho_2Ti_2O_7$ and made it somewhat difficult, at first, to tell if the requisite residual entropy was present in spin ice [46]. Could this interaction provide a relaxation channel for the spins? The interaction peaks at 0.3 K and may be related to the rise of HWHM-.

The lack of apparent 15 K freezing signature in zero dc field $Ho_2Ti_2O_7$ ac susceptibility measurements is another significant difference which may affect higher frequency processes (HWHM+). Ehlers *et al.* have determined that it was mostly overwhelmed by the low temperature mode in $Ho_2Ti_2O_7$, which was considered relatively faster than $Dy_2Ti_2O_7$ [60]. This faster lower temperature process then concealed the 15 K feature, but application of dc field to polycrystalline $Ho_2Ti_2O_7$ was able to enhance the freezing temperature and expose the 15 K feature. This effect, of an applied field enchancing the freezing temperature of the high temperature process, is also seen in $Dy_2Ti_2O_7$ [51]. Faster probably is not the best way to describe it. As mentioned above, we find instead that $Ho_2Ti_2O_7$ freezes out faster than $Dy_2Ti_2O_7$. Perhaps more likely is that the high temperature process does not

freeze out as quick - that is, it has a shallower barrier energy than that of $Dy_2Ti_2O_7$. $Ho_2Ti_2O_7$ may also have a slightly weaker Ising anisotropy as well, with some mixture of other states in the ground state [102]. If this is the case, there may be other contributions to relaxation pathways at lower temperatures, effectively shorting the quantum tunnelling plateau. There is some argument for why this may not be an appropriate explanation, which lies in calculated crystal field parameters. Jana and Ghosh found that the splitting of the ground state doublet and first excited doublet should be smaller in $Dy_2Ti_2O_7$.

Dy^{3+} is also a Kramers ion, which Ho^{3+} is not. This probably has minor impact, as the singlet state which may exist if Jahn-Teller distortion destroyed the non Kramers doublet of Ho would probably preclude dipolar spin ice behaviour. So much of the spin ice phenomenology is well defined, it seems unlikely that the ground state doublet of Ho could be compromised and still show such similar phenomenology.

Lastly, Ho possesses one stable isotope, while Dy has multiple. Lago *et al.* tentatively used interactions between ^{161}Dy and ^{163}Dy as the explanation for a background fluctuation rate in μSR at 20 mK [68]. It is not apparent what impact this might have on our measurement, as we did not measure an isotopically enriched sample of $Dy_2Ti_2O_7$.

5.3.2 Previous Experimental Results

There are a limited number of studies of low temperature $Ho_2Ti_2O_7$ ac susceptibility to compare to. Any available works for comparison are presented in Fig. 5.11. Matsuhira *et al.* found Arrhenius relaxation with an energy barrier of 27.5 K at low temperatures [49]. We see nothing near this energy barrier in both frequency scans and temperature scans, but this could be attributed to the difference between polycrystalline and single crystal samples, differences in the implementation of demagnetization correction, and finally differences between temperature and frequency scans. The barrier energy found by Ehlers *et al.* for zero dc field at the 1 K feature are somewhere between the result of Ref. [49] and our 13.08 K, there, 20 K was reported as a barrier energy[59]. We plot their doped spin ice and applied field results in Fig. 5.11 for contrast. Doping at these levels seems to have no impact on energy barrier, but speeds up relaxation, possibly by confounding the ice rules [59], while field serves to increase freezing temperature [60]. The other work on $Ho_2Ti_2O_7$ ac susceptibility [47] does not offer any points of comparison as they are in the higher temperature frequency range. Interestingly, there is no work in the literature studying frequency scans of $Ho_2Ti_2O_7$ at higher temperatures demonstrating the crossover in the same manner as $Dy_2Ti_2O_7$, verifying if $Ho_2Ti_2O_7$ obeys the plateau $2J_{\text{eff}}$ Arrhenius relaxation. It was not stated if demagnetisation corrections were not employed in the work

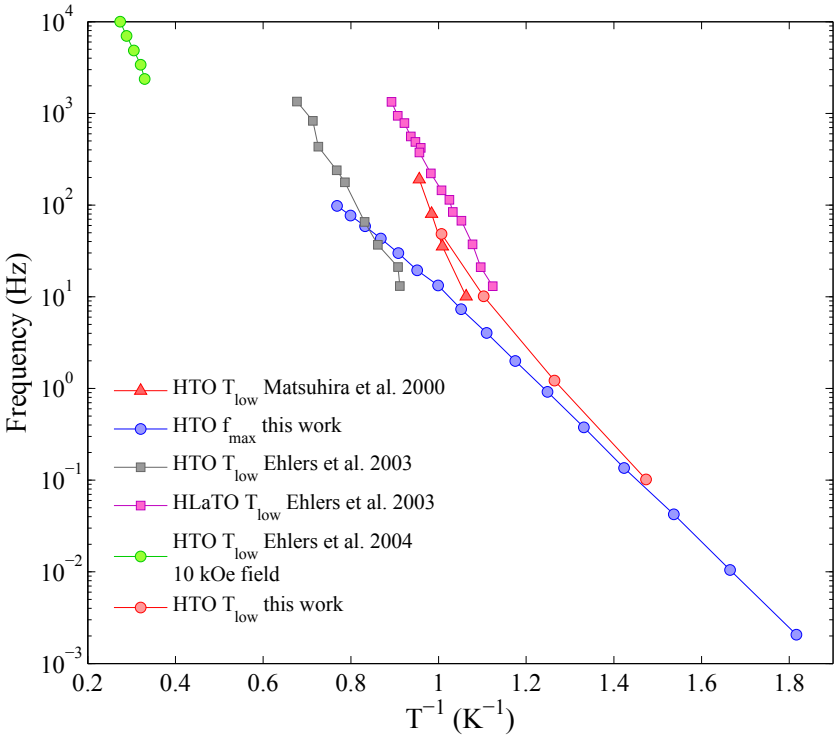

Figure 5.11: Compilation of ac susceptibility works measuring $Ho_2Ti_2O_7$, including this work. Temperature scans do not adequately determine the barrier energy found by frequency scans.

of Ehlers *et al.*, in which case we may be able to anticipate some shifting of the freezing to lower temperatures.

There are several relevant works to compare to for $Dy_2Ti_2O_7$. While our work did not extend up to the temperatures covered by the work of Matsuhira *et al.*, Fig. 5.11 shows our work is consistent with their characteristic frequency for the results of Matsuhira *et al.* An energy barrier of 10 K for the low temperature ac susceptibility feature was determined from temperature scans, which agrees quite nicely with our work. However, this could not be confidently inferred from this work (based on the differences found in $Ho_2Ti_2O_7$ temperature and frequency scans). Their analysis of the Argand diagrams in the context of Davidson-Cole relaxation qualitatively agrees with what we see here at our highest temperatures. A demagnetisation correction was used here.

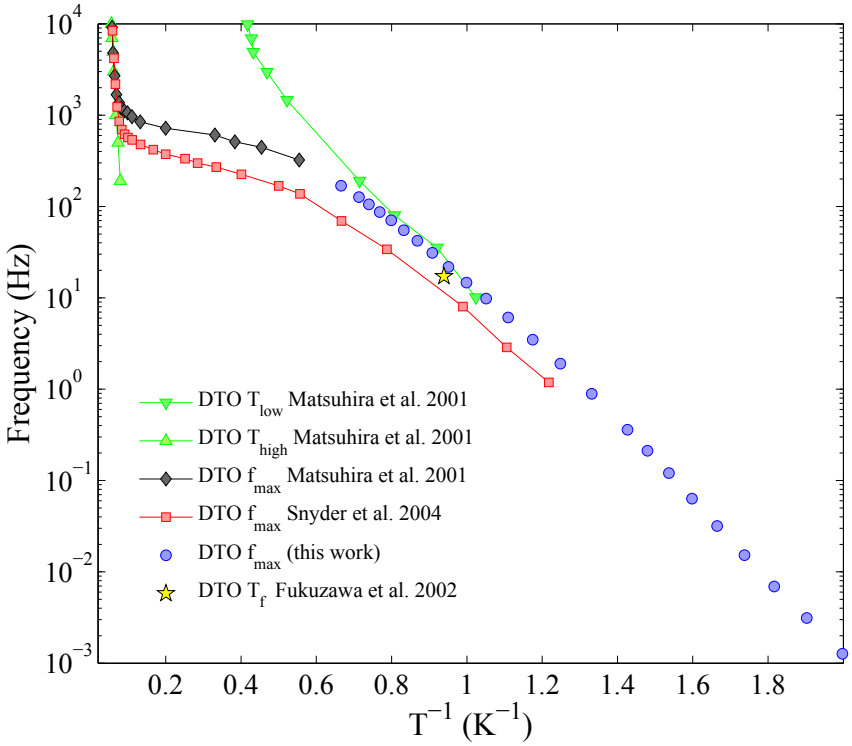

Figure 5.12: Compilation of ac susceptibility works measuring $Dy_2Ti_2O_7$, compared to the result presented here. There is good qualitative agreement with other $Dy_2Ti_2O_7$ work.

The singular point determined by Fukazawa *et al.* [100] also sits right in the thick of things, and is consistent with our measurement (Fig. 5.12). The results of Snyder *et al.* are qualitatively consistent with our work down to 800 mK. Quantitatively, there is an offset in our results and theirs, as can be seen in Fig. 5.12. The origin of this offset is not clear, although it may be due to an error in calculation. Snyder *et al.* state they are using a definition of $\tau_{\max} = 1/f_{\max}$ [61], and so we have recovered $f_{\max}$ accordingly. Snyder *et al.* were not able to measure the behaviour of the relaxation below 800 mK due to practical limitations [61], and so we are unable to compare barrier energies. While it is not clear if or how a demagnetisation was applied, it could be expected to shift the peak to a lower frequency.

The phenomenon of narrowing absorption spectra observed by Snyder *et al.* [61] is not seen in these measurements. Snyder *et al.* suggested that it exhibited some resemblance

to the anti-glass phenomenon in $Li_{1-x}Ho_xYF_4$, of which a signature was proposed to be narrowing frequency spectra, as opposed to broadening as a spin glass usually does. Measurements since then [92] have shown this is not the case in that system though, and any resemblance is possibly due to demagnetization effects [93].

5.3.3 Previous Theoretical Results

An attempt was made to fit our results over the range studied with a Volger-Fulcher type equation with a finite freezing temperature, Eq. 2.4, which is does not describe the relation well. This was a check to see if the dynamics were perhaps similar to freezing of the single spin flip acceptance rate as found in Melko *et al.* in Ref. [62]. However, this does not capture the experimental relaxation. We also see no possible onset of loop move dynamics, which makes sense, as we have no mechanism to implement the experimental equivalent.

Comparing to the initial theory of Ryzhkin, we see something more complex than anticipated in the zero frequency limit of susceptibility. While he predicted a simple linear dependence in inverse temperature in Eq. 5.1, we see in Fig. 5.10 that $Dy_2Ti_2O_7$ is not linear, while $Ho_2Ti_2O_7$ appears to be. The error bars on the last few $Ho_2Ti_2O_7$ data points are large, so this affords a qualitative comparison more than anything. However, it is another discerning point between $Ho_2Ti_2O_7$ and $Dy_2Ti_2O_7$, as well as between the magnitude of the two susceptibilities.

$$\chi(0) = (3/2)(\mu^2/a^3)/kT \tag{5.1}$$

A comparison to his prediction for τ will come up later in discussion of the Debye-Hückel theory.

The simulations of Jaubert and Holdsworth do not agree with our $Dy_2Ti_2O_7$ characteristic frequencies, as shown in Fig. 5.13. As it should be noted, Monte Carlo simulations do not have an intrinsic time scale, and so they had to scale their results to those of Snyder *et al.*, normalizing the Monte Carlo timescales to the experimental relaxation at 4 K. Thus, their offset from our data can be neglected, as a scaling factor only produces an offset on a log-y graph. This cannot explain a difference in slope, which is clearly apparent in the figure.

As well, we see that their data does not agree very well with Snyder below 1 K. The magnitude of this difference is not apparent when plotted as τ versus T, but when plotted as either τ or $f_{\max}$ versus $1/T$, it becomes very clear that a significant slope difference means the experimental relaxation is freezing out much faster than the Coulomb gas or

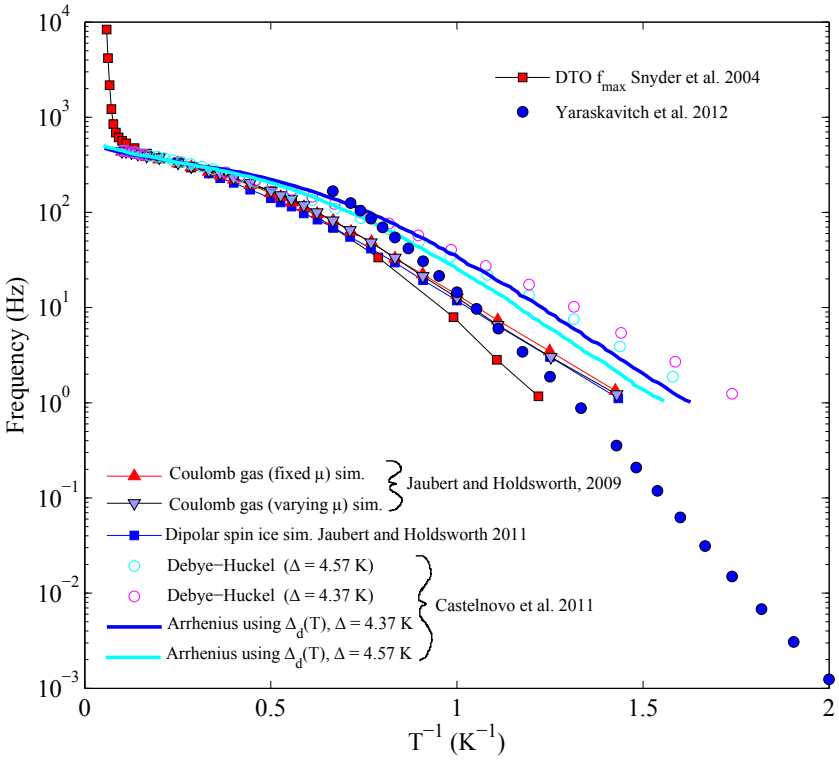

Figure 5.13: Compilation of theoretical works comparing to $Dy_2Ti_2O_7$ ac susceptibility, including $Dy_2Ti_2O_7$ result presented here. Neither the Debye-Hückel theory or Coulomb gas simulations capture the barrier energy as we measure it.

dipolar spin ice simulations predicted. Plotting as a function of inverse temperature is the more natural way to view any system in which Arrhenius behaviour might be expected. The clear disagreement been our measurement of $Dy_2Ti_2O_7$ and the simulations of Jaubert and Holdsworth is in how 'quickly' the dynamics freeze. At 0.6 K, where they report their last data point, we see that the disagreement between ours and their work has opened up to nearly a decade gap. They report a barrier of near 6 K at the lowest temperatures studied there [11], but predict a continuously changing barrier energy. We still qualitatively agree with their prediction of continuous, thermally activated dynamics, but disagree on barrier energy.

Their work studying monopole density brings up some interesting points as well. While

we see Arrhenius behaviour over a very large frequency range (10^0-10^3 Hz), it is over a relatively very small range in actual temperature (1-0.6 K in $Ho_2Ti_2O_7$, 0.85-0.5 K in $Dy_2Ti_2O_7$). When we examine the work by Jaubert and Holdsworth predicting monopole density, we see that monopole density has in actuality changed by a very small amount over these temperature ranges [11]. Thus, while we see Arrhenius behaviour, over this small temperature range, it still might be getting continually slightly steeper, until it approaches some kind of low density limit once screening has disappeared. Even so, at this temperature, the density may be small enough that we have already reached the energy cost plateau, as it were.

It is not clear why the dipolar spin ice model is able to reproduce specific heat so correctly, but not the low temperature freezing of dynamics. However, Yavorsk'ii *et al.* found simulations utilizing second and third nearest neighbour exchanges were required for improved reproduction of neutron scattering data, and provided improved agreement with specific heat.

Looking at the calculations by Castelnovo *et al.* in Ref. [12], we see poor agreement with our $Dy_2Ti_2O_7$ relaxation (Fig. 5.13). The Debye-Hückel theory does not agree with experimental ac susceptibility, and finds far too shallow an energy dependence, in its presented form. Attempts to describe the relaxation using a temperature dependent barrier height $\Delta_d(T)$ also fall short, and do not show fast enough freezing in temperature. They do anticipate Arrhenius behaviour at low enough temperatures, as screening length diverges and monopole cost approaches a constant value in temperature. They made no reference to work on $Ho_2Ti_2O_7$ displaying Arrhenius behaviour at low temperatures [93]. As with the work in Refs. [6, 11], the qualitative aspect of the freezing is captured, but the quantitative aspect is left wanting.

As it turns out, their work looks more flattering in Ref. [12] than it actually is because they seem to have mis-plotted the data of Snyder *et al.* Also as a result, the phenomenological fits they attempt are also not actually in agreement with experimental data. It remains to be seen if the authors suggestions of accounting for interactions of bound pairs following Bjerrum, and introducing interactions between bound pairs and free monopoles, referred to as dipole-ionic corrections, have any effect on this disagreement. Hard-core effects were also listed as a possible correction.

Physically, the interpretation of a temperature-varying barrier energy which increases as screening falls off, makes sense. The application of this theory should be an excellent proof if indeed the excitations within are behaving as a good Coulomb gas ought to. However, while Debye-Hückel theory seemed to have reasonable success describing specific heat in Refs. [9, 12], in that same form it is unable to describe ac susceptibility. The

further corrections need to be implemented in order to judge if this method could aptly describe experimental work. The limiting test will be if these corrections still allow correct description of experimental and simulated specfic heat.

5.3.4 Other Dynamics Results

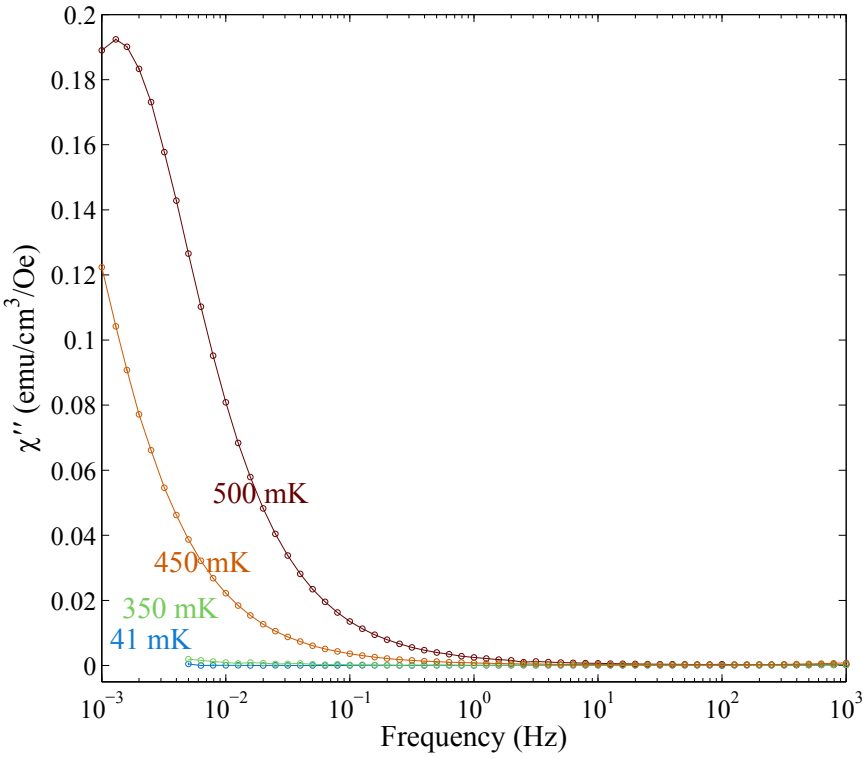

Figure 5.14: χ'' for 41 mK, 350 mK, and 450 mK scans of $Dy_2Ti_2O_7$, showing no spin relaxation modes at these temperatures, within this frequency range.

The determination of three different relaxation regimes within spin ice was introduced when discussing previous results. It seems highly unusual for such similar behaviour in temperature to be observed by so many different measurements at such different time scales, especially since some measurements associate the relaxation with only one timescale [60, 61]. This has been commented upon in several places [68, 102, 14, 93]. This difference

in time scales is currently not understood in the literature, nor do we suggest to have solved anything with this work. As said above, some measurements attribute this relaxation to a single process (neutron spin echo and ac susceptibility), but yet, it can be observed in very disparate time scale windows. Different techniques have different timescales, and probe different aspects of the system. AC susceptibility is a bulk, Q = 0 probe. μSR, however, is a local probe which averages over Q [68]. Neutron scattering can be used to explore Q. This may account for some of the differences, but it remains mysterious that similar temperature dependence is observed in most measurement types. However, as above, agreement generally falls on a high and low thermally activated regime, separated by a quantum tunnelling regime. Recent measurements of zero-field μSR by Dunsiger *et al.* which found persistent spin dynamics in $Dy_2Ti_2O_7$ [83], further confuse the matter. It seems very strange that no temperature dependence in the muon fluctuation rate is present below ∼5 K, as strong temperature dependence is seen in so many measurements. However, as stated above, this may be related its nature as a local probe.

Other methods relying on thermal excitations have been used to extract spin relaxation times: magnetocaloric measurements [64], and thermal relaxation measurements [82]. We compare to these results in Figure 5.15. Orendac *et al.* is a qualitative comparison, rather than quantitative. This is cautioned in that work, due to the use of magnetic field and change in temperature, but it is still put forward as a possible extension of ac susceptibility relaxation. A loss of equilibrium is noted at ∼400 mK. The loss of equilibrium indicates introduction of another time scale, that between the spins and lattice, which convolutes the relaxation time of the spins. Indeed, we see that their barrier energy (slope on Fig. 5.15) is significantly smaller than would be expected from our work, and exhibits significantly faster dynamics. We find that this result does not provide a qualitative extension of the timescales determined by ac susceptibility, other than to show some form of freezing.

The relaxation methods employed by Klemke *et al.* are also compared to ac susceptibility in that work [82]. The observation of two timescales is intriguing, as based upon our spectral width we observe more than one time scale as well. It is interesting that inherent to Jaubert and Holdsworth's dipolar spin ice simulation are two timescales which they average to determine the reported τ [11]. They also attempt a comparison to Ref. [61], but in fact our measurements show there are no modes of spin relaxation in the temperature range they observed (Fig. 5.14). Klemke *et al.* also are probably experiencing the loss of spin-lattice equilibrium, but much easier to see than in Ref. [64]. Fig. 5.15 shows, at roughly 500 mK, where the temperature dependence of the relaxation time has a clear change in temperature dependence and approaches a plateau. This is likely just a loss of equilibrium, though there it is explained as a loss of charge screening in the spin system.

Re-entrant spin dynamics, as that measurement implies, do not make any sense in

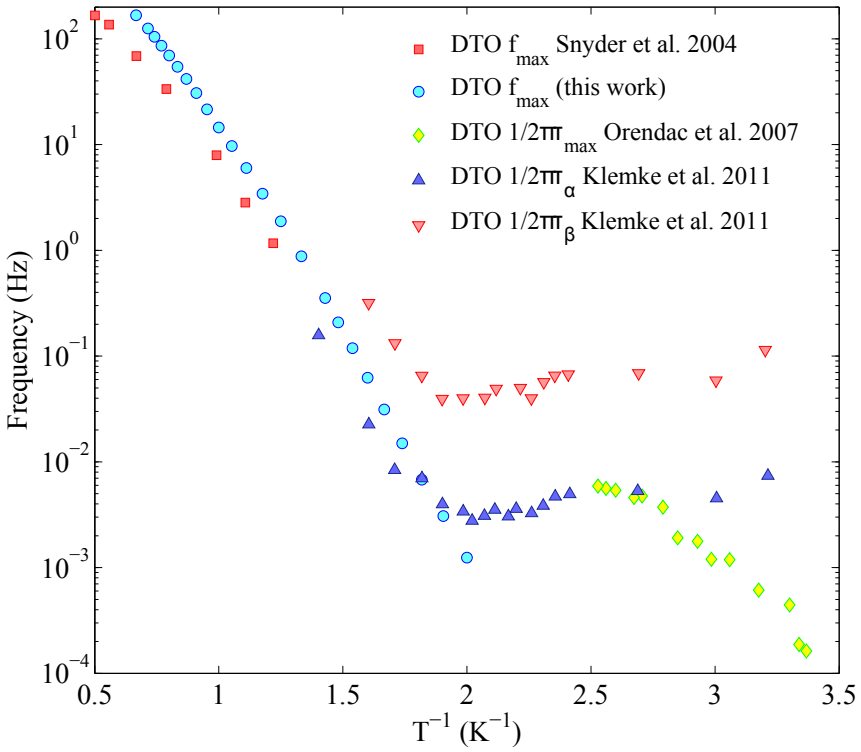

Figure 5.15: Comparison of $Dy_2Ti_2O_7$ relaxation time to that determined by thermal methods.

the context of the system. The measurements we present here as well as most of the experimental and theoretical literature [60, 68, 66, 6, 11, 12] agrees with freezing spin dynamics, roughly thermally activated. This type of freezing is extremely unlikely to plateau at these temperatures, as the material freezes solid into the two-in two-out time scale. Instead, the measurement of Ref. [82] is likely experiencing some loss of equilibrium, where the spin-lattice relaxation timescale becomes on the order of (or longer than) the timescale of the measurement, and giving a misleading plateau in relaxation.

The low temperature ac susceptibility scans of $Dy_2Ti_2O_7$, while basically featureless, are extremely significant because of that absence, indicating $Dy_2Ti_2O_7$ is quite frozen. While we cannot comment on whether to change in slowing down of dynamics at 300 mK [65, 64] does occur, we can say at 350 and 450 mK there is definitely no relaxation modes in

ac susceptibility which would correspond to the timescales presented as part of the thermal measurements. The thermally based measurements are ineffective probes of relaxation of the spin sub-system of spin ice at low temperatures.

This apparent loss of spin-lattice equilibrium has been observed in several works. Measurements of magnetization have found a freezing at approximately $T_f \sim$600 mK [61, 81]. Not coincidentally, this also seems to be that below this temperature the above-mentioned thermally-derived relaxation works [64, 82] deviate significantly from ac susceptibility results. The true spin temperature in these measurements may in fact be much hotter (thus indicating faster dynamics) than the lattice temperature would indicate. This would agree with what had been seen above, where the spins are unable to cool on the timescale of the measurement to the lattice temperature. In order for these measurements to truly compare to ac susceptibility results, the spin lattice coupling must be considered. Right now, the spin-lattice coupling has been introduced somewhat as an unknown into the equation, albeit a fast unknown which was expected to not complicate spin measurements. Thus, an accurate comparison is impossible.

The non-equilibrium works by Slobinsky *et al.* [81] are quite interesting, as it is very revealing about what kind of time scales might be required in order for the spin and lattice within spin ice to come into a thermal equilibrium. With the exponentially slowing spins and a decoupling of the spins and lattice, long timescales are required in order to be sure the system is at the expected temperatures. These measurements incorporate spin and lattice phenomena. However, loss of equilibrium has also been seen in experiments purely focusing on spin dynamics. For example, the single flip dynamics work by Melko and Gingras found that $Dy_2Ti_2O_7$ and $Ho_2Ti_2O_7$ fell out of equilibrium at freezing temperatures 0.4 K and 0.6 K respectively [62]. Dynamical arrest observed by Castelnovo *et al.* in simulated quenching experiments indicated that quenching the monopole system below 0.4 K can introduce non-contractible monopole pairs which take the system away from equilibrium monopole density for the system [80].

Time-domain measurements of magnetic relaxation by Giblin *et al.*, supporting the monopole picture as mentioned in Chapter 2, also bear some relation to our measurement. Applying a field for a given time and measuring the resultant decay of magnetization is also an excellent way to probe relaxation timescales in a material. This work found that a simple two exponential fit cannot describe the decay, and instead find that the magnetolyte description of spin ice provides an excellent fit of the experimental data at one temperature, 360 mK. However, the characteristic timescales are roughly on the order of 10^1 and 10^2s respectively [13]. Our measurement is in thermal equilibrium and dynamical equilibrium, for each individual measurement in frequency and temperature. However, probing a wide spectrum of frequencies allows us to determine where a system falls out

of equilibrium, or, where the magnetization can no longer track the oscillating field. Our measurement makes it clear that spin ice is quite frozen on the time scale of Giblin *et al.*, in the low field limit, at these temperatures. Fig. 5.14 shows no evidence of any relaxation at frequencies corresponding to those timescales, on the order of 100 mHz and 10 mHz. The measurements they make are at a temperature where our measurements would indicate a relaxation timescale of order 10^4s would be observed, if the same barrier energy was maintained. The time over which the data is reported (180 seconds) is not even an entire time constant at these timescales.

Here we should point out the difference in field magnitude as well as orientation. Giblin *et al.* use fields on the order of 1 Oe, while our $Dy_2Ti_2O_7$ ac susceptibility measurement relies on fields of 6 mOe at most. As well, they were studying the [100] orientation, as opposed to the [110] orientation studied here.

Regarding the field magnitude, while three orders of magnitude is quite substantial even by astronomical standards, it is not clear that this will fundamentally change anything about the system. Numerous phase diagrams seem to suggest that, under any orientation, substantial field (5-10 kOe) is required to induce any order. However, it seems unlikely that there would be any substantial difference in relaxation, as we are just probing spin flips. As discussed earlier, both [110] and [100] are commensurate with the two-in two-out ground state, though in [110] perhaps there is another energy scale associated with the α- and β-chains. There is nothing orientation-specific in observing the Wien effect in spin ice, according to the theory of Giblin *et al.* We may anticipate that there could be some dependence of the diffusion coefficients as a result of being able to probe only two of four spins. Regarding the field magnitude, the theory is derived on the assumption that any field perturbation is sufficiently small to treat the system with chemical thermodynamics. Indeed, examining b and the plot of the free charge conductivity $\kappa(B)/\kappa(0)$ provided in that work (Fig. 5.16), we see by extrapolating even with a field three orders of magnitude smaller (and b three orders of magnitude smaller), the difference in $\kappa(B)/\kappa(0)$ will be minor. So, their non-equilibrium dynamics should be observable within our experimental window of frequency, temperature, and field.

One possible explanation for this, as pointed out earlier with respect to the ac susceptibility measurements, is there was no mention made if or how a demagnetising field was accounted for in this result. We have shown here the demagnetising field makes a substantial contribution at the low temperatures to masking the apparent low temperature dynamics. Surely, if it impacts upon the characteristic relaxation timescale a frequency shift on the order of a decade at low temperatures, it must have some bearing on the time domain magnetization. This may be convoluted with any expression of dynamics purely due to free and bound currents. In a low field limit, the magnetisation can be given by:

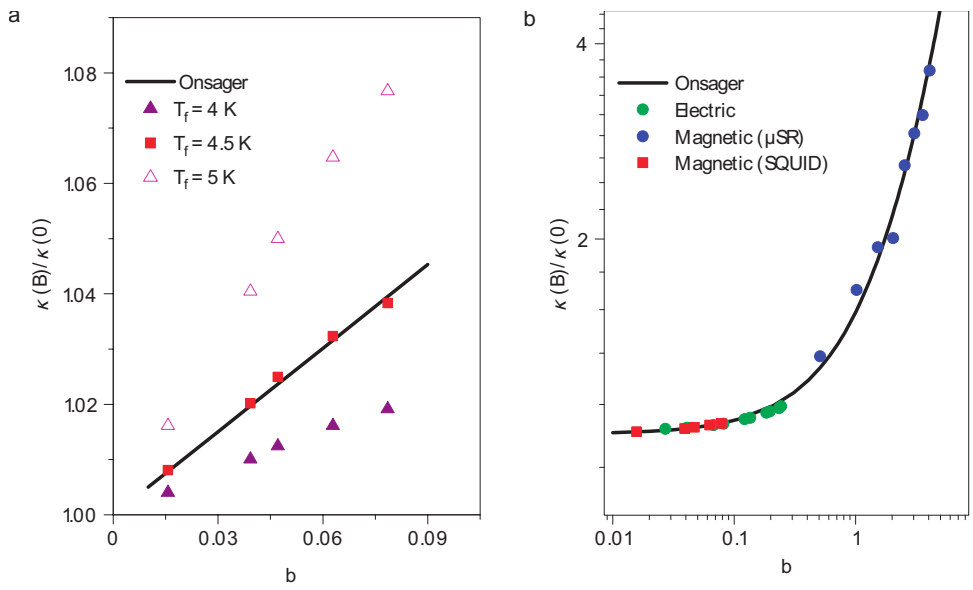

Figure 5.16: $Dy_2Ti_2O_7$ magnetolyte theory is shown to describe the time domain magnetization results of Giblin *et al.*. We are operating in a similar b regime as this experiment. From Ref. [13].

$$M = \chi(B_{\text{applied}} + B_{\text{demag}}), B_{\text{demag}} = -4\pi NM \tag{5.2}$$

Starting from a non-equilibrium value depending on applied field, as B_{applied} is removed, the system begins to relax, via decay of the magnetization. While this is occurring, the demagnetising field is evolving with the changing magnetization, thus changing the apparent magnetization as measured by a magnetometer. In fact, this may be responsible for the failure of a two exponential fit in Ref. [13]: the convolution of the bound and free monopole pair timescales with the decay of the demagnetising field.

A second consideration is thermal equilibrium of that experiment. In the most mundane circumstances, the thermometry may have been incorrect, or there was insufficient time given for the measurement apparatus in Ref. [13] to properly thermalize. When brought up in the context of the earlier discussion of the loss of spin-lattice equilibrium, this becomes a very possible reality. The loss of spin lattice equilibrium means the loss of the cooling mechanism for the spins. An appropriate wait time to ensure the spins are at the same temperature of the lattice will become essential below ∼600 mK. In order to make measurements at 360 mK, this may mean waiting for a length of time on the order of several

time constants, which we show to be at least over 1000 s below 500 mK for $Dy_2Ti_2O_7$. To be safe, something on the order of 12-24 hours may be more appropriate for thermalization of the spin sub-system.

One or both potential explanations may realize why the theoretical and experimental relaxation as determined by Giblin *et al.* does not appear in our measurement. The conclusive test would be to reproduce this experiment, along the [100] axis and with a large field. One risk of a larger ac field is heating in the sample via released Zeeman energy, which may pose a problem if poor thermal equilibrium exists with the lattice. It is possible that the [100] orientation induces some odd dynamics, and the difference in field means we do not have substantial signal to observe the phenomenon at hand. If a loss of equilibrium is responsible, this may have far-reaching implications for many other measurement techniques below ∼600 mK, and should serve as a cautionary tale.

5.3.5 The existence of monopoles

By no means do these measurements of the spin dynamics of $Ho_2Ti_2O_7$ and $Dy_2Ti_2O_7$ preclude the existence of monopole excitations in dipolar spin ice. Instead, we suggest that magnetization decay experiments validating the magnetolyte theory need to be repeated, with the considerations outlined above. The analogy of spin ice to a magnetolyte is appealing and may yet be shown to be qualitatively correct. The current quantities associated with the theory, however, do not agree with this experiment. The μSR data which may have been used to shore up the magnetolyte/magnetricity theory in Ref. [7] has been refuted as well [83]. The disagreement with current Coulomb gas/dipolar spin ice theory at low temperatures does not rule out monopoles, either. The dipolar spin ice model remains a solid qualititative description of the relaxation. The Debye-Hückel theory is also a reasonable qualitative description of the relaxation. However, further work would be required to even just bring it to the level of agreement of the Coulomb gas/dipolar spin ice simulations. This work does not rule out monopoles, but instead calls for further understanding in the model for low temperatures.

Chapter 6

Conclusion

Using ac susceptibility, we have contributed new information adding to the already substantial body of work on spin ice, especially in the context of the monopole excitations which have been shown to be present there. Specifically, we have added the low temperature spin dynamics of the dilute Coulomb phase of the spin ice materials $Ho_2Ti_2O_7$ and $Dy_2Ti_2O_7$ using ac susceptibility. The relaxation there, where the monopole density is small, are suprisingly slower than simulated or calculated by theoretical works. This is an extremely important regime as it provides a 'stress test' of the dipolar spin ice model and the mapping of this model to that of a gas of monopole defects. This should be of interest for study of the differences between the two canonical spin ice materials, $Ho_2Ti_2O_7$ and $Dy_2Ti_2O_7$.

6.1 Summary

The relaxation of the spin ice has been charted as it freezes into the two-in, two-out ice rules state. Both $Ho_2Ti_2O_7$ and $Dy_2Ti_2O_7$ display thermally activated relaxation behaviour in the low temperature limit. The Arrhenius energy barrier was found to be 10.71 K and 9.79 K for $Ho_2Ti_2O_7$ and $Dy_2Ti_2O_7$ respectively, corresponding to $\sim 6\, J_{\text{eff}}$ and $\sim 8.9\, J_{\text{eff}}$. This shows that the J_{eff} energy scale is not universal in determining the low temperature energy cost, as had been suggested in $Dy_2Ti_2O_7$ [11] and measured in $Ho_2Ti_2O_7$.

$Ho_2Ti_2O_7$ and $Dy_2Ti_2O_7$ are different, not just by a scaling of microscopic tunneling time or J_{eff}, but through obvious differences in the shape of the absorption spectra. The broader, asymmetric relaxation spectrum of $Ho_2Ti_2O_7$ indicates there is more physics at

play than in $Dy_2Ti_2O_7$. Currently, it is not understood what the sources of these differences are. Further measurements are required to understand what is happening to the high frequency $Ho_2Ti_2O_7$ relaxation.

From an experimental standpoint, we find that timescales determined by the magnetocaloric effect [64] or thermal relaxation [82] experiments are not an extension, either quantitatively or qualitatively, of spin relaxation as determined by ac susceptibility. The spin and lattice systems have been shown to fall out of equilibrium in other works [81]. When accessing the spins via the lattice, the timescale for spin-lattice equilibrium appears to be convoluting the actual measured relaxation time. Further understanding of the temperature dependence of the timescale of spin-lattice coupling is required. However, as it stands these experiments cannot be effectively compared to equilibrium ac susceptibility measurements.

We find that there are no modes of relaxation corresponding to the timescales of magnetization decay measurements on $Dy_2Ti_2O_7$ supporting the magnetolyte theory [13]. Within the frequency range we are able to measure, which includes where relaxation on the timescales seen by Giblin *et al.* would occur, the frequency spectra is flat, which agrees with our observation of the relaxation disappearing in temperature. This casts doubt on the support this data provides the magnetolyte picture of spin ice, but does not necessarily rule out an Onsager-Wien type dissociation mechanism of magnetic relaxation. Further measurements are required to establish if this is the case in spin ice, which will require careful consideration of the equilibrium issues outlined above.

These measurements also show that theoretical work has not yet captured the spin freezing found in experimental work. The simulations of a Coulomb monopole gas [6] and of dipolar spin ice [11] do not describe the relaxation. While continuous thermally activated relaxation behaviour was expected by theoretical works, the Arrhenius relaxation we observe is freezing out much faster on account of a higher thermal activation energy than theory predicts. This may be due to not fully accounting for the loss of screening in these materials, or, not considering all of the long range Coulomb interactions a monopole defect is subject to. Applying the Debye-Hückel treatment to ac susceptibility in spin ice [12] does not capture the freezing seen here either. However, there may be improvements in the theory after inclusion of interaction between bound pairs as well as interactions between bound pairs and monopoles [12]. At the very least, these improvements will be required to make Debye-Hückel theory be as good as the Coulomb gas simulations of Jaubert *et al.*

It is important to note that the qualitative and quantitative disagreements this work finds with existing monopole theoretical and experimental work does not preclude the existence of monopole excitations in spin ice. The message of this work is one of encour-

agement to theorists and experimentalists alike, that the existing body of knowledge does not account for the discrepancy between previous experimental works and existing theory. What we find is current simulations do not capture the entire magnitude of the energy landscape which is the barrier to these thermal excitations, and might require a more complete treatment of the dipolar spin ice model. Alternatively, experimental and theoretical efforts could look to understand what it is that makes real-life spin ice materials deviate from the fundamental physics at hand.

6.2 Future Work

6.2.1 $Ho_2Ti_2O_7$ and $Dy_2Ti_2O_7$

Higher frequency measurements of $Ho_2Ti_2O_7$ are required in order to further understand what is occuring on the high frequency tail of the absorption spectra. This could be the emergence of another relaxation mode, tied to excited crystal field levels. Coaxing further bandwidth out of a SQUID magnetometer through using a high-frequency SQUID controller, optimized SQUID parameters, as well as removing bandwidth-limiting twisted pairs could yield another decade in bandwidth. Alternatively, a conventional coil magnetometer could be employed to study the relaxation above dilution fridge temperatures. Another decade added to the bandwidth at low frequencies could also help establish the nature of any Onsager-Wien type chemical kinetics which may be present. Previous measurements have used field to enhance the initial freezing temperature in $Ho_2Ti_2O_7$ [60]. Higher temperature frequency measurements could perhaps help resolve the mystery of the missing high temperature freezing point, which Ehlers *et al.* have used application of dc magnetic field to observe. It may in fact just be present at low temperatures and high frequencies, which have not yet been explored using ac susceptibility. Further high frequency information about $Dy_2Ti_2O_7$ would be useful for comparison, in terms of understanding the difference between the two in the plateau regime, which has not yet been observed in $Ho_2Ti_2O_7$. As a starting point, one could reconstruct the $\chi'(f,T)$ and $\chi''(f,T)$ parameter space from existing high temperature work and analyze along isothermals to find peaks in χ'', making comparison to frequency scan results easier.

An orientation study of $Ho_2Ti_2O_7$ and $Dy_2Ti_2O_7$ would be valuable as well. It would seem that currently, the low field limit has nothing to differentiate between directions, unlike high field measurements. However, it would be prudent to verify this with careful measurements of $\langle 100 \rangle$ and $\langle 111 \rangle$ orientations as well, for both dipolar spin ice materials.

A study of the effects of dilution on the energy barrier to relaxation of $Dy_2Ti_2O_7$ and $Ho_2Ti_2O_7$ at low temperatures could be very revealing. Not only might the energy barrier vary, but also seeing how the shape of the relaxation spectra change at low temperature. Currently, works by Snyder *et al.* [103] and Ke *et al.* [104] have largely focused on the high temperature measurements of the susceptibility, and have not undertaken low temperature measurements. It will be interesting to see if introducing disorder gradually leads to conventional glassy behaviour [14].

6.2.2 Other spin ice materials

Exploring other regions of dipolar spin ice parameter space, as we tried to do here with $Ho_2Ti_2O_7$ and $Dy_2Ti_2O_7$, could also be very valuable. Different materials may allow for different parts of the phase diagram to be accessible to our frequency range. For instance, a spin ice with well-isolated ground state, a smaller tunnelling time, and a larger, ferromagnetic J would freeze at higher temperatures (Fig. 2.12), which could be used to observe more of the dilute, Arrhenius limit of the relaxation within our frequency range. While spin ice candidates such as $Ho_2Sn_2O_7$ [49], $Dy_2Sn_2O_7$ [71], and $Pr_2Sn_2O_7$ [71] have been around for a while, they may provide further insight. Unfortunately, the stannates cannot be synthesized in single crystal form at this point [14]. Most recently, germanates $Dy_2Ge_2O_7$ and $Ho_2Ge_2O_7$, have been shown to exhibit spin ice behaviour [84]. While these materials may only be available in polycrystalline form, they could still provide extremely interesting insight. All of these materials could be worthwhile to examine to get more variance across the parameter space of spin ice, and could be used to assemble an understanding of the low temperature behaviour, as well provide examples of different magnetolytes upon which to test the theory.

APPENDICES

Appendix A

Experimental Details: Specific Heat Measurement

A.1 Heat Capacity Measurement

Heat capacity was measured using the quasi-adiabatic method. The quasi-adiabatic method utilizes a weak heat sink to the experimental stage of the fridge. The weak thermal link thermally isolates the sample on the timescale of the heat pulse introducted to the system and allows for a slow relaxation of the sample to the temperature of the fridge. When implemented correctly, the time constant of relaxation should be much longer than any internal time constants of the sample system. The method used by this group has been outlined previously by J. A. Quilliam [88, 91].

A 1 kΩ *Dale Electronics* RuO_2 thermometer and 10 kΩ metal oxide film resistor heater were mounted directly to the single crystal or polycrystalline sample using *General Electric* varnish 7301. The sample is then suspended, varnished to rest on nylon threads. Electrical connections to the heater and thermometer are made with 6 μm NbTi filaments. *Epotek* H20E two-component silver epoxy is used to connect contacts. A weak thermal link between the sample and the mixing chamber of a dilution refrigerator was fashioned using Pt-W (92% Pt, 8% W) wire for the smaller single crystals, and hard yellow brass foil for excessively large samples. The external time constant of relaxation was set using the length of the weak link, with the time constant set to approximately an hour for most systems studied, much longer than the internal relaxation time of the samples over the temperatures studied here, minimizing thermal gradients across the sample. Relative to the thermal conductance of the weak link, the nylon and NbTi filaments conduct negligible

amounts of heat [88]. The long time constant of relaxation also ensured that the sample cooled slowly into an equilibrium state, rather than a quenching. The RuO_2 thermometer resisitance was read by a *Linear Research* LR700 ac resistance bridge.

The sample was contained in a copper radiation shield, to avoid heat load through blackbody radiation, and mounted on the mixing chamber of the S.H.E. DRP-36 dilution refrigerator. The mixing chamber itself is contained within a lead shield and two μ-metal shields. Known heat pulses of length t were applied at t_0 to the sample, with temperature data taken at least 30 minutes before and after the pulse. The sample temperature was fit before and after with exponential fits. For long internal time constants of equilibration, a double exponential fit was utilized to fit the weak link time constant and the longest internal time constant. For shorter internal equilibration times, a single exponential fit was used. The heat capacity is given by $C = Q/\Delta T$. ΔT is given by extrapolating fitted temperature data to the middle of the pulse, time $t_0 + t/2$.

A new RuO_2 thermometer is used for each measurement, and calibrated while on the sample. The thermometer is calibrated to a *LakeShore* Ge resistance thermometer on the mixing chamber of the dilution refrigerator. The functional form of the calibration used is that from Pobell [89], to fourth order:

$$T = \sum A_n (ln(R))^n \tag{A.1}$$

Based upon previous studies of the addenda [88, 91] we can estimate that the addenda generally comprises a small portion ($< 1\%$) of the specific heat in the systems studied here.

Appendix B

Specific heat of $Yb_2Ti_2O_7$

B.1 Motivation

The ground state of the rare-earth pyrochlore ytterbium titanate ($Yb_2Ti_2O_7$) has recently become a topic of substantial interest. $Yb_2Ti_2O_7$ is the only known example of a ferromagnetic XY pyrochlore, where instead of the spins lying along the local $\langle 111 \rangle$ axes of individual tetraheda (as in spin ice), the spins lay in the plane perpendicular to the local $< 111 >$ direction. [105]. The crystal field lifts the ground state degeneracy of the Yb^{3+} ion (J = 7/2) to form a ground state Kramers doublet, with the next excited state a doublet as well. Conflicting experimental reports have found ferromagnetic order, or instead found it eludes order and maintains a spin liquid ground state. More recently, it has been suggested to be an exchange spin ice [106], proposed as a quantum spin ice which exhibits a Coulombic-like phase featuring magnetic monopole defects, 'electric' defects, and emergent photons [15], and proposed as a monopole Coulomb gas which freezes via a Higgs transition into a condensed monopole state [107].

Recent neutron scattering measurements by collaborators at McMaster had found a shift from 2D correlations at high temperature, to short-range 3D correlations, and an ordered state in applied field. This work was undertaken to provide a complimentary technique to assess specific heat of the single crystal samples for collaborators at McMaster University, and to further understand the nature of the ground state.

B.2 Background

A brief overview of the history of $Yb_2Ti_2O_7$ and relevant results will be given here. The first specific heat measurement was conducted on a powder sample by Blöte *et al.* in 1969, and observed a broad peak around 2 K and a sharp peak indicating a λ-type phase transition at $\sim$ 214mK [38]. Based upon this, it was assumed a ordered magnetic state had been obtained. Susceptibility measurements in the same work found a ferromagnetic Curie-Weiss temperature of +0.4 K. There has been some sample dependence in the temperature of this transition, as subsequent polycrystalline measurements by Siddharthan *et al.* in 1999 and Dalmas de Réotier *et al.* in 2006 found critical temperatures of 282 mK [42] and 250 mK [108] respectively. Even with this variation, the same type of transition is seen consistently, summarized in Fig. B.1.

Magnetization measurements by Bramwell *et al.* found a similar weakly ferromagnetic Curie-Weiss temperature of 0.59 K, and a ground state doublet. There were also indications of an easy plane anisotropy perpendicular to the $\langle 111 \rangle$ axis [25]. A set of studies by Hodges *et al.* really added quite a bit to the picture, as it found other techniques complicated the current understanding. Evidence of a freezing of the moments of the Yb^{3+} below the Mössbauer ^{170}Yb spectroscopy limit was found at $\sim$0.25 K, on a polycrystalline sample [109]. Neutron diffraction measurements found no long range order below 0.2 K coinciding with this drop. Later work established that the ground state is a Kramers doublet, well separated from the first excited state, by 620 K [110]. The Yb moments had planar anisotropy, with the easy plane perpendicular to the local $\langle 111 \rangle$ axis. The coupling is dominated by the exchange component. Subsequent measurements in 2002 by Hodges *et al.* added to the picture by confirming with μSR the presence of a first order transition in the spin dynamics at $\sim$0.24 K, but also that the μSR fluctuation rate remained temperature independent below the transition [111]. This was attributed to a regime of quantum fluctuations.

Further work contended the dynamic nature of the low temperature ordered phase and presented another view. Yasui *et al.* concluded a transition to ferromagnetic order below 240 mK using neutron diffraction, susceptibility, and magnetization data on single-crystal $Yb_2Ti_2O_7$, which found a weakly ferromagnetic +0.53 K for the Curie-Weiss temperature [112]. The neutron scattering found a Bragg scattering from a ferromagnetic state. Hysteresis was also found in the neutron scattering data, on the time scale of warming and cooling of the measurement. This was thought to be indicative of very slow dynamics out of equilibrium with the time scale of their measurement. Susceptibility found a peak, indicating some kind of transition, and some hysteresis in magnetization. However, following polycrystalline work by Gardner *et al.*, it was clear that the differences between previous

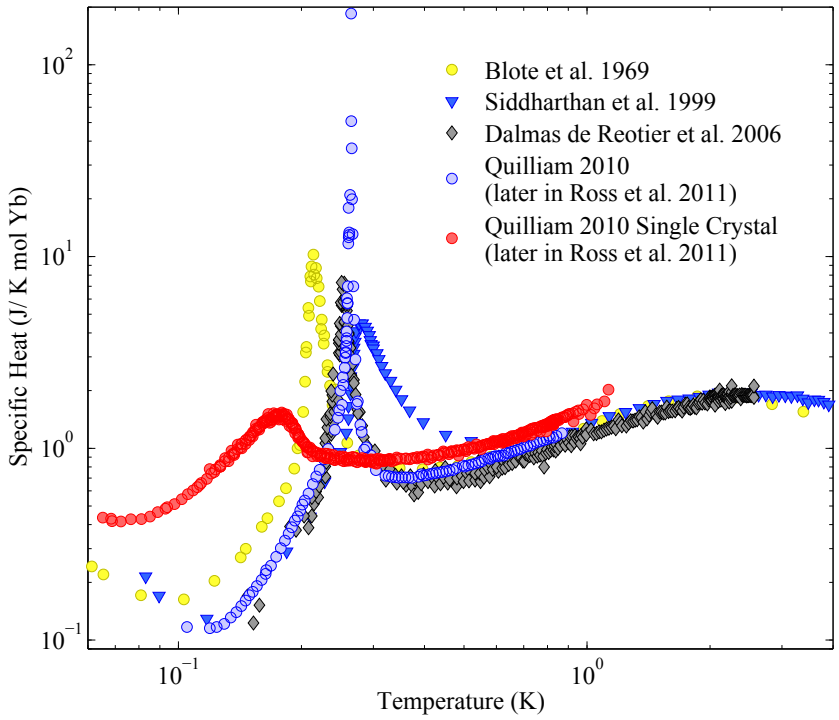

Figure B.1: Specific heat studies of $Yb_2Ti_2O_7$, showing a first order transition typically seen in polycrystalline samples, and a single crystal measurement showing instead a broad feature.

measurements would not be easily reconciled. They used polarized neutron diffraction and neutron spin echo to contend that the spins remain dynamic below this transition temperature. NSE showed no change within error bars below the transition temperatures down to 180 mK [113].

Neutron diffraction on a single crystal of $Yb_2Ti_2O_7$ by Bonville *et al.* found no magnetic Bragg peaks but instead rods of scattering appearing along the [111] direction, indicating correlations in those planes [114]. The transition was likened to that of the liquid-gas transition; no long range order is observed, but rather a change in correlations. Later neutron scattering work by Ross *et al.* had found the rods of scattering along the $\langle 111 \rangle$ direction correspond to decoupling of the system into kagome planes [105]. No sign of ferromagnetic order is seen in zero field, but application of field along the $[1\bar{1}0]$ axis brings

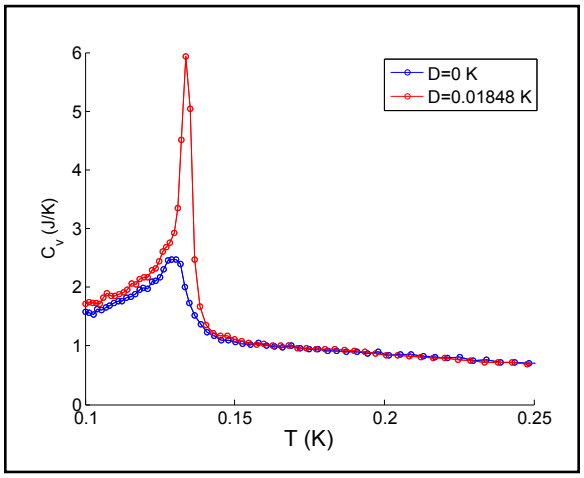

Figure B.2: Simulated $Yb_2Ti_2O_7$ specific heat by Thompson, using the Hamiltonian presented there. Using dipole-dipole interactions in the simulations yields a sharp feature in specific heat. From Ref. [116].

on long range order. The specific heat transition that had been typically seen around $\sim$ 240 mK seemed to correspond to a crossover from 2D correlations to short range 3D correlations. This work also does not find a long-range ordered ferromagnetic ground state as proposed by Yasui *et al.*

Recent work in this group by J. A. Quilliam had measured polycrystalline and single crystal samples [91] in collaboration with colleagues at McMaster University, as a complementary technique to the neutron scattering work of Ross *et al.* [105]. This resulted in a surprisingly substantial difference between the polycrystalline and single crystal samples (Fig. B.1). The polycrystalline sample showed an extremely high quality first order transition at 265 mK, an order of magnitude higher than the best previous measurement [38]. The single crystal showed no indication of this first order transition, but instead exhibited a broad bump centred around 180 mK (Fig. B.1). This was not the exact same single crystal as used in the neutron scattering results, but was grown using similar growth parameters.

Local susceptibility measurements by Cao *et al.* suggested the importance of anisotropic exchange in $Yb_2Ti_2O_7$[115]. Curiously, Cao *et al.* later found that the exchange is ferromagnetic and Ising-like at low temperatures, and coined the term exchange spin ice, in contrast to the dipolar spin ice discussed here [106].

A Hamiltonian was proposed recently by Thompson *et al.* based on simulations repro-

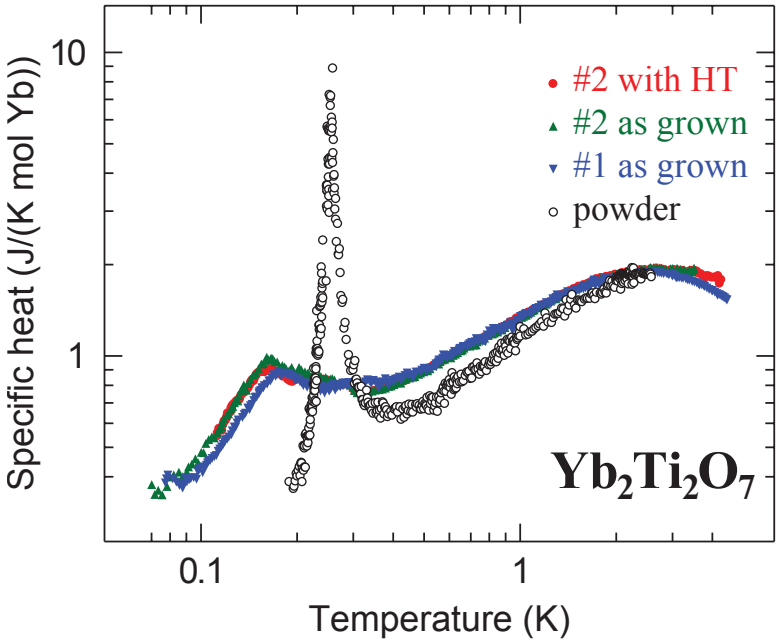

Figure B.3: Specific heat measurements of $Yb_2Ti_2O_7$ by Yaouanc *et al.*, which found a similar broad feature to the the single crystal measured by Quilliam. From Ref. [119].

ducing the neutron scattering data, specifically the [111] rod of scattering. This proposed Hamiltonian contained dipolar interactions, and four different flavours of exchange interaction, including anisotropy [117]. It was also used to calculate local spin susceptibility, to find good agreement with experimental data, while also showing a model with only isotropic exchange and dipolar interactions could not satisfy the experimental data [118]. Thompson's MSc. thesis also contains a very comprehensive review of the $Yb_2Ti_2O_7$ literature [116]. Monte Carlo simulations of specific heat were done by Thompson using his model Hamiltonian [116]. Shown in Fig. B.2, the simulations produced a rounded specific heat anomaly with no dipolar interactions, and exhibited a peak with dipolar interactions turned on.

Immediately prior to the specific heat presented here appearing in print [16], another single crystal work was published by Yaouanc *et al.* This found a broad feature (Fig. B.3, at $\sim$ 180 mK [119], with no sharp transition as had been seen in the polycrystalline measurement carried out by some of those authors [108]. This was very similar to that seen by Quilliam in [91].

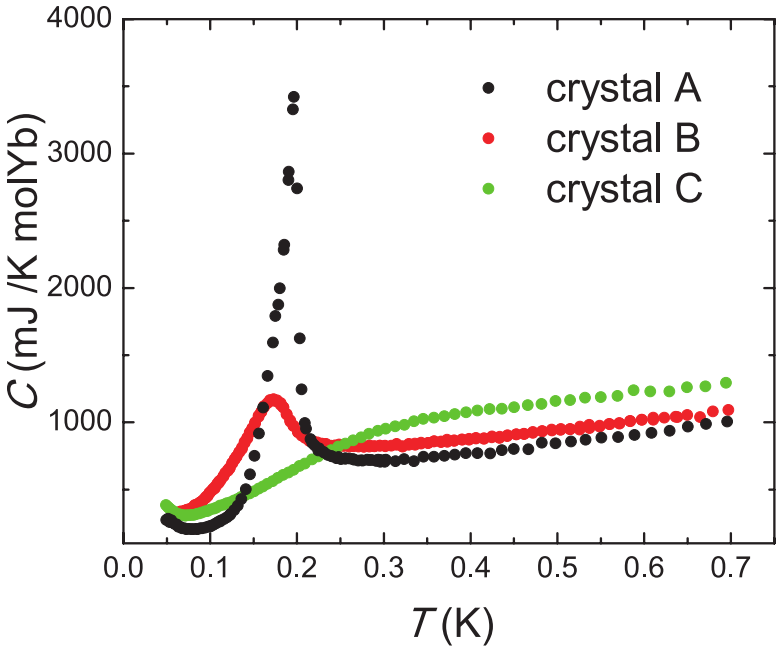

Figure B.4: Single crystal $Yb_2Ti_2O_7$ samples of varying quality presented by Chang *et al.* Off-stoichiometric Yb concentration in sample C was found to suppress the sharp transition. From Ref. [107].

Most recently, Chang *et al.* proposed a Higgs transition from a magnetic Coulomb phase, like the classical spin ices, to a ferromagnetic state, a Higgs phase of monopole excitations [107]. The ordering observed is said to be understood as a Bose-Einstein condensation of monopole spinons. They use low temperature polarized neutron studies and theoretical calculations to justify this. Specific heat measurements were included in the supplementary material of this work. They produced three different species of single crystal through variation of growth conditions: no transition, broad feature at 175 mK, and sharp λ-type transition at 200 mK, as shown in Fig. B.4. Extended x-ray fine structure measurements showed that the closer the material was to ideal stoichiometry, the sharper and more ideal the transition. The ferromagnetic state was only seen in the highest quality sample. They contended that the variety of behaviours observed in $Yb_2Ti_2O_7$ are due to proximity to a quantum phase transition.

Quality single crystal materials are invaluable for many measurements techniques which seek Q-dependent or orientation dependent properties which cannot be given by the bulk,

including neutron scattering work. The aim of this work was to provide a complementary technique to neutron scattering measurements in order to clarify the origin of any transitions seen there, and assess if the neutron scattering measurement was probing the broad feature found by Quilliam *et al.* In this way, any transitions observed in neutron scattering could be associated with any specific heat anomalies present in that exact sample growth. This new work by Ross *et al.*, featuring the specific heat measurements presented here, appeared in print in Ref. [16].

B.3 Experiment

The samples of $Yb_2Ti_2O_7$ were obtained from our collaborators at McMaster University, prepared there in an image furnace as described in the Experimental Details.[1] The starting material for the $Yb_2Ti_2O_7$ growth was created by mixing oxides Yb_2O_3 and TiO_2 in stoichiometric ratios. This was annealed at 1200°C for 24 hours, ramping temperature at a rate of 100°C/h. The single crystal growth was at a rate of 5 mm/h in an environment of 4 atm of oxygen. The single crystal used for neutron scattering measurements was measured after those measurements. The other single crystal samples were prepared in a similar fashion.

Three different samples of $Yb_2Ti_2O_7$ were studied as part of this work. Two single crystals, A and B, were cut from the same growth, in fact right next to each other. They were of mass 359.5 mg and 353.6 mg. Sample A was measured as is, but Sample B was annealed in oxygen for 10 days. A third sample, sample C, was actually used in neutron scattering work described by Ross *et al.* in Ref. [105] and Ref. [16]. This sample, with mass 7.0515 g, was mounted in a slightly different fashion than the prior samples due to its exceptionaly large mass: the sample had two weak links of high strength yellow brass foil in parallel. A coil of copper wire heat-sunk with *Epo-tek* H20E silver epoxy at either end of the sample was used to aid heat sinking.

The measured results are shown in Fig. B.5. The sample (No. 3) measured as part of this work was as-grown and un-treated. It displays two features in specific heat, a small, sharp peak at 269 mK and a broad peak at 196 mK. This was not the first time something of this nature was seen, as preliminary work in the group by J. A. Quilliam had seen these two features in a single crystal.[2] The oxygen-annealed sample (No. 4) exhibits the same features, but there is a noticeable enhancement (sharpening and narrowing) of the higher

[1] Prepared by K. A. Ross

[2] Unpublished, J. A. Quilliam

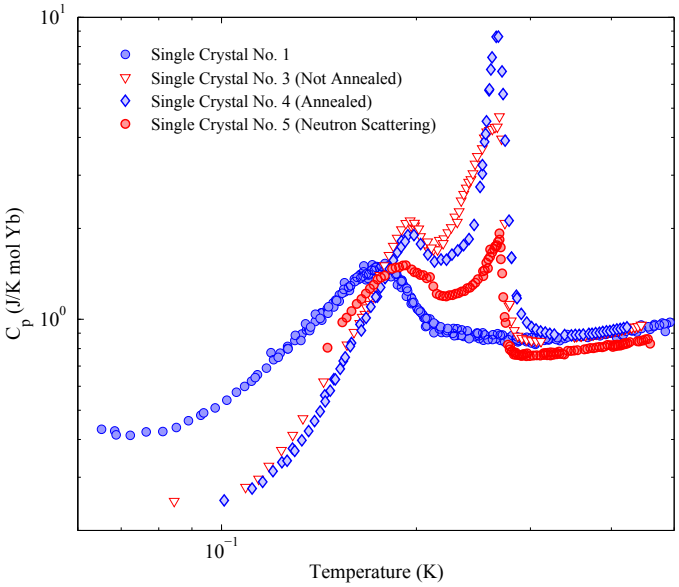

Figure B.5: Comparison of the measured single crystals of $Yb_2Ti_2O_7$. The sharp and broad anomalies are observed in all samples measured here.

temperature peak at 268 mK, while the lower peak at 198 mK remains largely unchanged. Also shown is the first measured single crystal, exhibiting the broad bump at 180 mK. The true test would be to measure the same sample (No. 5) which was measured by neutron scattering [105, 16]. Indeed, we see clearly that the neutron scattering sample also shows a noticeable peak at 265 mK, as well as a broad feature at 200 mK.

However, the results are confusing in light of the neutron scattering work by Ross *et al.*, which was completed prior to measuring the specific heat of sample No. 5. This neutron scattering work is shown in Fig. B.6 from Ref. [16]. The measurements found a change in scattering width of the at 400 mK, where the crossover to short range 3D correlations occurs, and a suppression of quasi-elastic scattering. Specific heat measurement find no feature at 400 mK! This indicates that whatever is causing this change in correlation length is not changing the entropy significantly.

B.4 Comparison and Discussion

The single crystals No. 3, No. 4, and No. 5 are qualitatively very consistent. Two features, a sharp (but small) peak, and a broad feature are prominent in both. The high temperature feature appears to be quite consistent in the location of the peak. The samples studied here appear to be unique in that they exhibit what appears to be both the characteristics of the single crystal No. 1 measured by J.A. Quilliam as well as the polycrystalline sample, which have been reasonably consistent in the nature of the transition to date. No other published work has observed both of these features as the same time. There are a few possible explanations for the co-existence of these features. The first, the sample in entirety is exhibiting two different transitions which are fundamentally part of the whole crystal. The second, there are two 'types' of single crystal which comprise the sample; one which exhibits typical single crystal behaviour, the other which shows polycrystalline behaviour.

The polycrystalline material seems to be the most consistent, as the λ-type transition is seen in all samples measured, to the best of the author's knowledge. There is some variation in the temperature at which this is seen: 214 mK [38], 250 mK [108], 265 mK [91], and 282 mK [42]. Overall, they are quite consistent. The single crystals, however, are problematic. The single crystalline work presented by Yaouanc *et al.* exhibits a broad feature very similar to what was observed in the first single crystal measured in Ref. [16]. It is substantially different compared to the polycrystalline sample they had previously measured [108]. Interestingly, annealing in oxygen does not seem to have had a substantial effect on the heat capacity. There is some hint of something at the temperatures at which we see a transition, but it is quite small in magnitude and there is no clear peak present. While sample A as measured by Chang *et al.* found a broad bump, they showed higher quality samples could evolve the feature into a peak. However, they do not see the appearance of a second peak, as in our single crystal sample.

There are a few discrepancies in Chang *et al.*'s treatment of the current sample quality picture. First, they are assuming no neutron scattering has ever been done on polycrystalline samples exhibiting first order transitions. This is erroneous, as Hodges *et al.* saw no indication of ferromagnetic order in their neutron diffraction work. Dalmas de Réotier *et al.* measured the Hodges *et al.* (2002) polycrystalline sample, and found a sharp first order transition. The powder samples seem to exhibit clear λ-type transitions, with no published exceptions. Second, they do not address the coexistence of the broad and sharp features in our work [16].

We will now discuss this specific heat result in the context of the neutron scattering work of which it was a part. Further measurements using elastic neutron scattering find

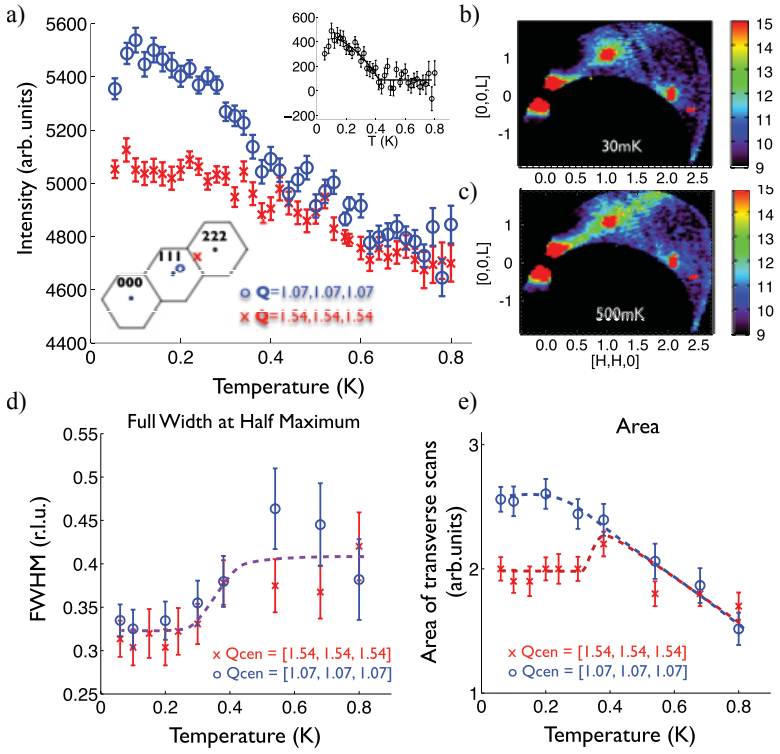

Figure B.6: Ross *et al.* show the scattering intensity at two Q points changes at 400 mK (a). The d) full width at half max and e) area of transverse scans are also parametrized, showing distinct shifts at 400 mK. From Ref. [16].

a noticeable change at 400 mK in the full width at half maximum and area of transverse scans across the [111] rod of scattering, after fitting the profile of the line of scattering with Lorentzian lineshapes. This change, however, does not occur at the same temperature of the transition. In Ref. [16], ground state correlations are found to be quite small, extending only over nearest neighbours of a kagomé star, and over only one kagomé-triangular-kagomé stack in 3D. Above 400 mK, the correlation only extends over the kagomé star. There is considerable off-rod diffuse scattering, which changes very little in temperature between 500 mK and 30 mK, unlike the rod of scattering.

Naturally, this raises the question of what is occuring structurally within the powder and single crystals that leads to such a substantial difference. Single crystal exhibiting the two peaked transition were measured using powder neutron diffraction, as well as poly-crystalline material which exhibited the clear first order transition, as part of Ref. [16].

Rietveld refinement showed that the two patterns agreed reasonably well, with slight differences. The crushed single crystal had a slightly larger lattice parameter, 10.0200 ± 0.00002 versus 10.01322(1) Å. The Bragg peaks were slightly wider indicating some lattice strain in the single crystal. There was no substantial site substitution in either sample, so it would seem that a small amount of disorder, site substitution, or lattice strain are the culprits in the sample dependence. It is interesting that annealing in oxygen was able to enhance the high temperature feature, indicating what may be oxygen deficiency in the single crystal.

Our powder sample still seems to have a distinctly stronger transition to long range order than any other sample studied, as well as the highest T_c. It is not immediately clear why we see both phases, so to speak, of the transitions at once, also. The No. 3 and No. 4 samples were cuts from a larger single crystal, right next to each other. It seems to make more sense that if there were to be any instabilities as the molten zone travels through the furnace, there could be variation of properties along the z-axis of the crystal. Here though, we see both features in the specific heat in short segments of the crystal, and not just in the entire neutron scattering sample. As well, the polycrystalline sintered sample seems to be very similar to the crushed single crystal, as shown in diffraction experiments.

The most typical single crystal (broad feature only) may be due to either a strain brought on in the lattice by the long range crystalline order. Annealing did not appear to significantly affect the broad feature. Rather, it definitely affected the first order transition peak. It would seem that the single crystal is subject to some form of oxygen deficiency which can be healed through annealing. Perhaps locally, oxygen defects affect the crystalline electric field surrounding the Yb^{3+} spins, changing the nature of the spins and allowing some different kind of ordering (or prevention of order). However, this could all be undone as it seems there is no order.

B.5 Conclusion

This study is the culmination of a comprehensive examination of specific heat dependence between polycrystalline and single crystal samples of $Yb_2Ti_2O_7$. The specific heat measurements of this material show a clear sample dependence. Polycrystalline samples exhibit a sharp first order transition with reports of the T_c varying from 214 mK to 280 mK, with the sharpest reported feature at 265 mK. Some single crystals exhibit a broad oeak at $\sim$ 200 mK, which seems to be related. In addition, some single crystals exhibit two features: One feature at $\sim$265 mK, with a second at $\sim$200 mK.

The neutron scattering work of our collaborators shows that for a two-peak sample, at transition from 2D to 3D correlations occurs at 400 mK. There is an absence of magnetic Bragg peaks at the low temperatures in this material. We have qualified that the specific heat of this material shows no feature at 400 mK, but instead we find a broad low temperature peak, and relatively sharp high temperature peak. We can see that this crystal exhibits characteristics of both the 'typical' powder and the broad feature of some single crystal samples. The existence of one does not preclude the existence of the other in the same crystal, as it may appear from prior work [119, 107].

The sample variation in those materials has made it difficult to interpret many results. Polycrystalline $Yb_2Ti_2O_7$ seems to exemplify the best possible realization of $Yb_2Ti_2O_7$, as the specific heat results seem relatively consistent, thus inferring things about the nature of $Yb_2Ti_2O_7$ before and after the first order transition from results based on polycrystalline samples can be done with some confidence. Further study using other techniques is needed in the transition regimes. The correlation of the specific heat features to signatures from other experimental probes is required to further understand what is happening. It is clear that the debate over the state of $Yb_2Ti_2O_7$ is not yet completely settled.

B.5.1 Future Work

Detailed ac susceptibility measurements would be valuable, both to establish the nature of the transitions and to determine if the spins remain dynamic within our ac susceptibility time window, like in Mössbauer spectroscopy [111]. If $Yb_2Ti_2O_7$ can indeed be viewed as a quantum spin ice [15], frequency spectra may reveal very interesting relaxation, which then could be compared to $Ho_2Ti_2O_7$ and $Dy_2Ti_2O_7$ as studied here. Sample quality will be very important for this. The current sample we study seems to exhibit both features with sufficient amplitude, and perhaps it will be best suited to an ac susceptibility study, for determining what effect each feature has on the frequency response. Along the [111] direction, we also may be able to see the change of spin correlations at 400 mK at zero field.

This is a promising material of study, as the ground state continues to be debated. There is still much to be understood, and it would be fascinating to see if the low temperature feature could be sharpened as in Ref. [107]. Other techniques are required to nail down what exactly is happening. A phase diagram is needed to understand how disorder, however small it may seem, can change the low temperature phase of this material. Following Chang *et al.* who proposed a phase diagram with Coulombic liquid and condensate phases [107], it may be that the variation in sample quality allow $Yb_2Ti_2O_7$ to cross the border between Coulombic liquid and Coulombic condensate.

Appendix C

Specific Heat of $Tb_2Ti_2O_7$

C.1 Background

The pyrochlore oxide terbium titanate ($Tb_2Ti_2O_7$) is the subject of a vast amount of literature, a review of which can be found in Ref. [14]. While also exhibiting strong local $\langle 111 \rangle$ anisotropy, $Tb_2Ti_2O_7$ was initially thought to order in an all-in or all-out long range ordered state, by virtue of its negative Curie-Weiss temperature [120], and therefore anticipated negative exchange interactions. However, long range order is not observed down to 50 mK. This refusal to order has led to extensive study of the properties of this apparent spin liquid.

Here, we will give a brief summary of the background of $Tb_2Ti_2O_7$. The cooperative paramagnetic state was first identified by Gardner *et al.* [121]. μSR, neutron scattering, and dc susceptibility verifed the existence of antiferromagnetic correlations, but determined that the paramagnetic state persisted until 0.07 K. A detailed study by Gingras *et al.* of $Tb_2Ti_2O_7$ was completed. They found the crystalline electric field lifts the $2J + 1$ degeneracy of the Tb^{3+} free-ion state and yields a ground state doublet, with the next excited states separated by a gap of 18 K [120]. The crystal field results in strong Ising behaviour along the local $\langle 111 \rangle$ axis. There is a distinctly antiferromagnetic Curie Weiss temperature, even when accounting for contributions from the crystalline electric field, with θ_{CW} is approximately -14 K. Finally, there is no evidence of any extensive residual entropy as observed in the spin ice materials, and more than the $R \ln 2$ expected for a ground state doublet is recovered [120].

The absence of order in a system in which interactions indicate ordering transition should have occurred has led to characterization as a spin liquid candidate. Taking this

further, a different approach to the behaviour exhibited by $Tb_2Ti_2O_7$ was proposed in 2007 by Molavian *et al.* They presented a renormalized Hamiltonian which takes the predicted long range order state which should exist in $Tb_2Ti_2O_7$ and instead allows virtual fluctuations between the doublet ground state and excited crystal field states [17]. This forces $Tb_2Ti_2O_7$ from the all-in all-out long range ordered state which can be seen in Fig. 2.12 to the spin ice regime, with a very low transition temperature. One of the predictions of this theory is a plateau in the magnetization of the $\langle 111 \rangle$ direction [122].

There has been a great deal of variation in sample quality, both of the single crystal [123] and polycrystalline variety, which is probably the source of much of the variability of experimental results. Measurements by Chapuis *et al.* proposed a ground state split singlet, separated by 1.8 K, based upon entropy measurements and simulations using a two singlet ground state [124]. Very recently, Gaulin *et al.* determined no splitting of the ground state doublet into two singlets, within a resolution of 0.2 K [125]. This is just a brief survey of some general experimental results. From here, we will discuss previous specific heat measurements.

C.2 Previous Experimental Work

Naturally, there have been numerous previous specific heat measurements as part of the volumes of work done on $Tb_2Ti_2O_7$. Consistency has not been a feature of these measurements. Not unlike $Yb_2Ti_2O_7$, an incredible variety of sample quality has been seen in specific heat measurements of both polycrystalline and single crystal samples. This can be assessed at glance through the presence (or absence) of several features.

The experimental measurements to date are shown in Figs. C.1 and C.2. The first, a polycrystalline measurement by Siddharthan *et al.*, found no ordering transition [42]. Subsequent meaurements of a single crystal sample by Gingras *et al.* also found no ordering, but instead two broad features centred around 1.5 K and 6 K. The 6 K feature was interpreted as a remnant of the excited crystal field doublet, while the lower feature is interpreted as a build-up of short range correlations based on the single ion ground state doublet.

A single crystal measurement by Hamaguchi *et al.* found a third feature [28]. They observe broad features at 5 K and 0.7 K, as well as a sharp peak at 0.37 K. The 0.7 K and 5 K features were associated with the two above features found by Gingras *et al.*, while the 0.37 K peak was thought to be a second order phase transition. Cornelius *et al.* measured, in 2005, a polycrystalline sample and found similar behaviour to Gingras *et al.*

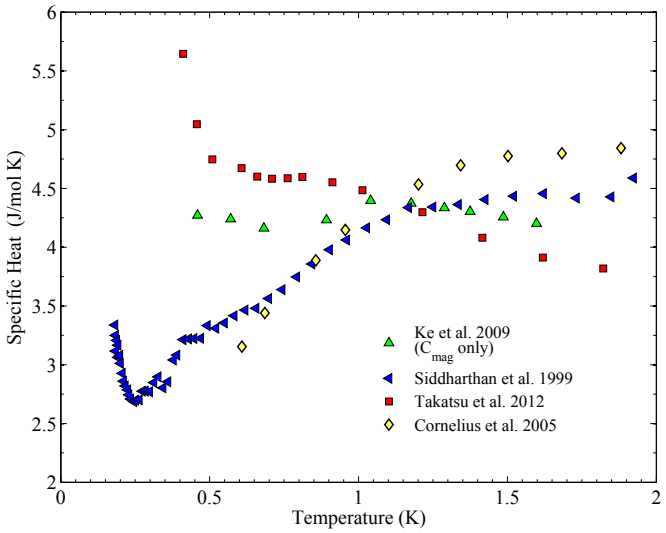

Figure C.1: Previous specific heat studies of polycrystalline $Tb_2Ti_2O_7$. There is clear sample quality dependence in the samples.

The doctoral thesis of Chapuis found substantial sample variation in single crystals [123]. The specific heat varied wildly between growth conditions, even within the same growth conditions [123]. A and B, of the same oxides and growth speed, exhibit very different features. One crystal, D, was grown with two different rates, and this found a significant growth rate dependence. The half grown at 3 mm/h developed the onset of a peak in specific heat very similar to that of Ref. [28]. The portion of the crystal grown at 8 mm/h showed no such feature, however. This lack of robust single crystal growth indeed proves problematic. With the variety of behaviours shown of these samples, it is difficult to ascertain what the benchmark sample should be. Some work by Ke *et al.* in 2009, studying polycrystalline $Dy_{2-x}Tb_xTi_2O_7$, also measured $Tb_2Ti_2O_7$, and found features similar to the two typical high temperature features, at $\sim$6 K and $\sim$1 K.

Most recently, Yaouanc *et al.* published a study using numerous techniques to characterize a TTO single crystal, and found an exotic shift in the μSR data at 0.15 K, but no trace in the specific heat [126]. They discuss the sample variation found in Ref. [123], but elect to use the highest quality sample determined by which has the lowest residual entropy. They find similar behaviour in specific heat in that the two higher temperature features are present, but also an upturn below $\sim$0.15 K, after subtraction of the nuclear

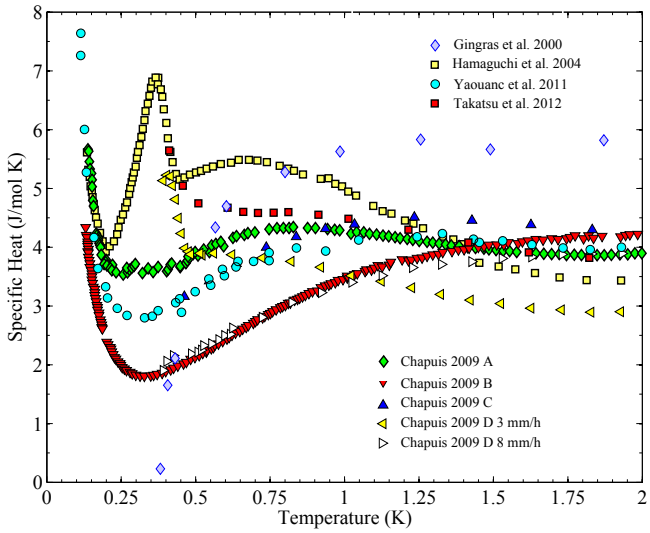

Figure C.2: Previous specific heat studies of single crystal $Tb_2Ti_2O_7$. As with the polycrystalline samples, significant differences are apparent between samples.

hyperfine contribution to specific heat. Truly, a cornucopia of variety, as can be seen in the specific heat measurements.

Neutron scattering results observed the emergence of an inelastic neutron scattering mode at 8 meV along with a mode at 0 meV at $\sim$ 400 mK, coupled with an upturn of specific heat below 500 mK [19]. This was understood as spin fluctuations between Tb spin states. There is agreement with estimates of the energy band of the excited states. Interestingly, this does not support a singlet-singlet ground state [124]. The variety of behaviours in different samples is ascribed to the proximity of the system to perhaps a quantum critical point, where minute changes in field, pressure, chemical pressure, slight disorder, strain, oxygen deficiency, or substitution seem to make for huge differences. The specific heat data only extended to 400 mK. Our measurement was intended to verify the presence of any thermodynamic signatures below this temperature.

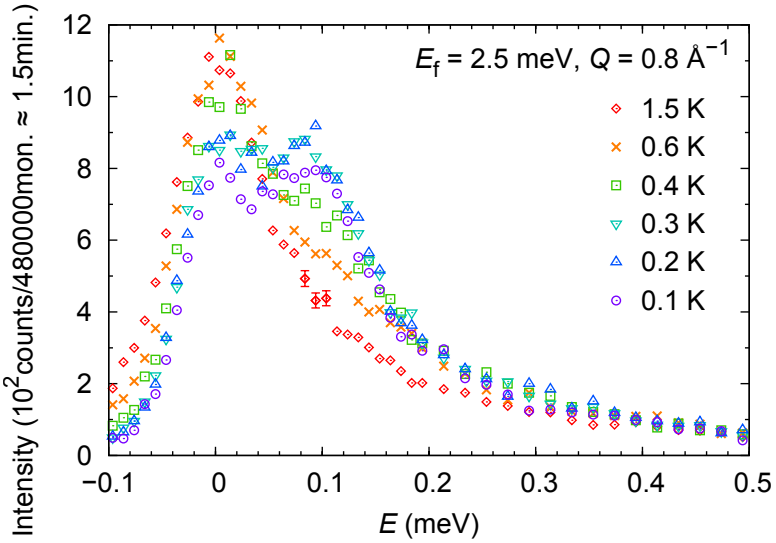

Figure C.3: The emergence of a mode of inelastic scattering found in neutron scattering by Takatsu *et al.* This correlates with the second order transition seen in specific heat.

C.3 Experiment

Polycrystalline samples of $Tb_2Ti_2O_7$ were prepared at Tokyo Metropolitan University [19] using the standard solid state reaction.[1] Oxides Tb_4O_7 and TiO_2 were fired in stoichiometric ratios at 1350 °C, in the manner described in Ref. [121]. A rectangular prism of polycrystalline $Tb_2Ti_2O_7$ with mass 9.04 mg was mounted in a specific heat cell, and measured using the quasi-adiabatic method.

Within the temperature range studied (200 and 550 mK), there is a clear peak at ∼400 mK observed in specific heat data and an indication of an upturn at the lowest temperatures studied, corresponding the nuclear component, as can be seen in Fig. C.4. Due to the magnitude of the nuclear component known to be present in Tb^{3+} compounds, it is difficult to calculate the magnetic contribution to the entropy without first subtracting the nuclear component of the specific heat. The lattice contribution to specific heat is quite negligible at these temperatures [120] and does not require consideration.

[1]Samples from H. Kadowaki

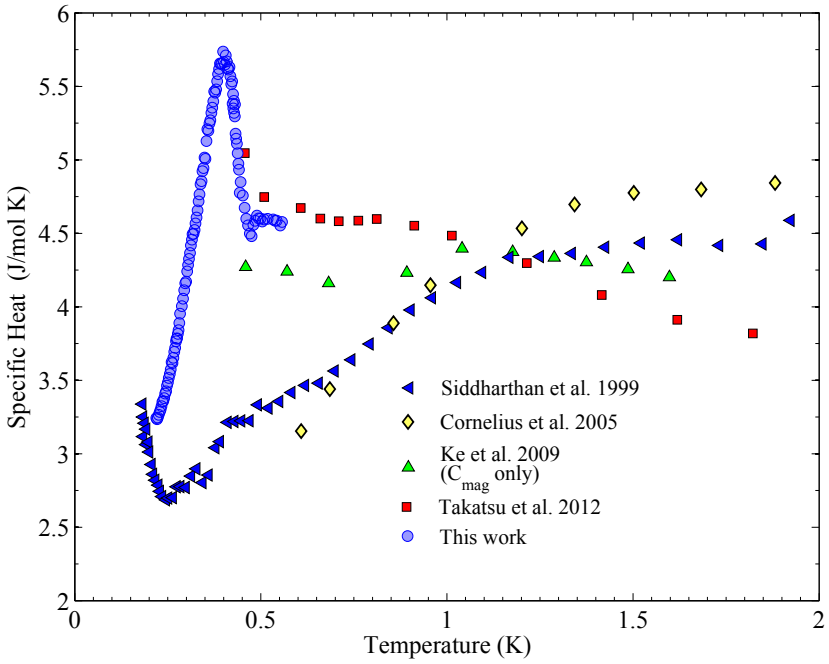

Figure C.4: The specific heat of polycrystalline $Tb_2Ti_2O_7$ as measured for this work, compared to previous measurement. The 400 mK transition has not been clearly observed in polycrystalline measurements up to this point.

C.4 Comparison and Discussion

The sample measured here is in complete contrast to previous powder sample measurements, which have never seen any clear indication of a second order phase transition in this temperature range (Fig. C.4). Siddharthan *et al.* seem to observe some minute feature at 400 mK in their powder sample measurements, but it seems to come from a very small portion of their sample in order to have such a small contribution to the specific heat.

The single crystals provide a few more examples of the feature seen here. Our sample seems to be most like that of Hamaguchi *et al.*, with the transition temperature of their material, 0.37 K, slightly lower than the sample measured here (Fig. C.5). Interestingly, we don't see the onset of the same 0.7 K broad feature, or, it is significantly diminished. In comparison to Chapuis' findings [123], we see the same characteristic as the sample grown

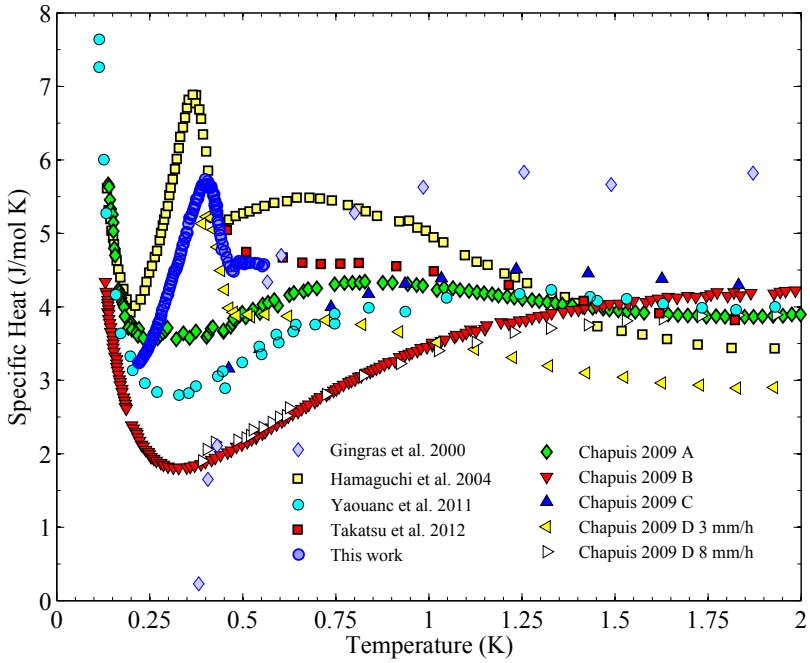

Figure C.5: The previous specific heat studies of single crystal $Tb_2Ti_2O_7$, compared to the polycrystalline sample studied here. This work resembles the result of Hamaguchi *et al.* [28] and that of Chapuis [123]

at 3 mm/h. However, this was the only crystal grown there that expressed the ∼400 mK feature. The rest is truly a variety of results, as can be seen in Fig. C.2.

Our results are not in agreement with single crystal measurements by Yaouanc *et al.*, which is not surprising with the current history between powder and single crystal samples. They do not see the transition at 0.4 K which we observe. Unfortunately, they are quite dismissive of the transition in other works [28] and seem to have neglected it in their own work, which they mention they observed as well [126]. If the nuclear hyperfine interaction was subtracted correctly from the specific heat, the upturn they observe at ∼0.17 K could be the onset of the suppressed 0.4 K transition. However, subtracting nuclear components is fraught with difficulties, as not only is it important to get the calculation of the Schottky anomaly right, but also thermometry can make or break the subtraction of such a steep feature. That upturn could only be the sign of a transition, if the nuclear component was

subtracted correctly.

This result fits well with that observed by Takatsu *et al.* Our measurement agrees well with their high temperature specific heat measurements. As well, we show a clear thermodynamic signature at 400 mK corresponds to the emergence of the double-peaked energy spectrum, with features at 0 and 0.8 K.

Just like $Yb_2Ti_2O_7$, we have a pyrochlore which seems to be extremely sensitive to slight variations in sample quality, such that the samples display very different behaviour. One very noticeable difference between these two systems is the lack of robustness of the polycrystalline phase. While in $Yb_2Ti_2O_7$, the powder seems to be relatively generic in its behaviour, the polycrystalline $Tb_2Ti_2O_7$systems display little to no consistency. $Tb_2Ti_2O_7$ may also contain some slight disorder, or site substitution which has a large effect on the specific heat. The constituent oxides used was varied in Ref. [123], finding some dependence. This may be due to the difference valence states of Tb, Tb(III) and Tb(IV). Ruff *et al.* had observed broadening of the specific heat feature with reducing temperature, which seemed to indicate the system was on the verge of a structural transition [127]. However, a structural transition would not be commensurate with the emergence of the inelastic neutron scattering mode.

C.5 Conclusion

Initial measurements of the specific heat of a $Tb_2Ti_2O_7$ showed an upturn at the lowest temperatures studied (500 mK), seemingly corresponding to the emergence of the inelastic mode in neutron scattering measurements. We find that there is indeed a second order transition at 0.4 K, which is thought to be a thermodynamic signature of the inelastic scattering mode. The nature of this transition seems to be associated with the condensation of spins from a paramagnetic state to one characterized by quantum fluctuations [19]. It would seem that this high quality powder samples capture the best character of $Tb_2Ti_2O_7$, but this remains disputed [126].

This measurement, similar to $Yb_2Ti_2O_7$, demonstrates the variability in sample behaviours and emphasizes the importance of characterizing samples using multiple techniques. The 400 mK feature had not previously been seen in polycrystalline samples, but a similar feature has been seen in some single crystal growths [28, 123]. There are fundamental differences between polycrystalline and single crystal samples which could explain the large amount of disparate results for both materials. For example, this could include the singlet vs. doublet ground state debate [124, 125].

The delicate nature of the low temperature phase of this material has been ascribed to the possibility of proximity to a quantum critical point [19]. If this is indeed the case, one sample should not rule out the other, as these different species of sample could be representing the variety of phases surrounding this transition.

C.5.1 Future Work

As with $Yb_2Ti_2O_7$, ac susceptibility measurements using our gradiometer would be very useful on $Tb_2Ti_2O_7$ to further characterize the various specific heat features, and determine how magnetic in nature. The magnetometer in our group would be well suited to study the energy and timescales of spin relaxation in $Tb_2Ti_2O_7$ and determine if it compares to that we see in the spin ice materials, only shifted to a lower temperature (i.e. $T_{ice} \sim 0.1\,K$). This order of magnitude in temperature could make the excited crystal field states inaccessible, and perhaps reduce dynamics to thermally activated. In any case, any sample should also be characterized by specific heat to determine what species it is.

Appendix D

Specific heat of $Pr_2Hf_2O_7$

D.1 Background

The praseodymium-based pyrochlores with A = Pr^{3+} (J = 4) have not historically had as much attention as the other rare-earth pyrochlores studied in this thesis, but this has changed recently.

$Pr_2Sn_2O_7$, first measured in 2002 by Matsuhira *et al.*, showed spin ice behaviour in the ac susceptibility, with a freezing at $\sim$ 0.35 K [71]. The D_{3d} crystal field symmetry was calculated to split the Pr^{3+} free-ion state $^3H_4$ into three doublets, and three singlets. DC susceptibility determined a ferromagnetic Curie-Weiss temperature of 0.32 K. The ground state was determined to be a non-Kramers doublet, with some mixing of other states, but largely Ising along the local $\langle 111 \rangle$ axis. Based upon this evidence, $Pr_2Sn_2O_7$ was suggested to be a spin ice.

Matsuhira *et al.* confirmed a frequency dependent spin freezing in ac susceptibility akin to spin ice at $\sim$ 0.35 K, with a barrier energy E_B = 3.54 K [128]. There is also a weak irreversibility at 90 mK indicative of a freezing on the time scale of the magnetization measurement. The saturation magnetization supported the existence of strong $\langle 111 \rangle$ Ising anisotropy.

$Pr_2Sn_2O_7$ was proposed to be a dynamic spin ice based upon neutron scattering and specific heat measurements by Zhou *et al.* [72]. Here, specific heat measurements found that even less of the residual entropy of the typical spin ice was recovered. Inelastic neutron scattering found the characteristic relaxation time had a shallow energy dependence, with no crossover to thermally activated freezing as seen in $Ho_2Ti_2O_7$ and $Dy_2Ti_2O_7$. Based

upon the Monte Carlo simulations of den Hertog and Gingras, the specific heat peak can be used to infer a nearest neighbour exchange of $J_{\rm nn} = 0.92$K, and an estimated $D_{\rm nn} = 0.13K$, much smaller than the dipole interaction of the Ho and Dy compounds.

$Pr_2Ir_2O_7$ is quite unlike most of the pyrochlores as it is metallic. This leads to its own host of interesting properties, including the Kondo effect and anomalous Hall effect [14] which will not be described in detail here.

$Pr_2Zr_2O_7$ was found by Matsuhira *et al.* to have an antiferromagnetic Curie-Weiss temperature of 0.55 K, but showed no ordering transition in specific heat [129]. Instead, a frequency dependent of dynamics around ∼0.2 K was observed in ac susceptibility. No ordering transition is seen in magnetic specific heat down to 0.35 K, though there is broad peak around 2 K. The theoretical ground state for antiferromagnetic exchange on the pyrochlore lattice with local ⟨111⟩ Ising anisotropy is supposed to be a unique four-in, four-out ground state. However, this has yet to be observed in an antiferromagnetic pyrochlore magnets, such as $Tb_2Ti_2O_7$ discussed above. Like $Pr_2Sn_2O_7$, they report a non-Kramers doublet ground state, with local ⟨111⟩ Ising spins. The exchange interactions were thought to be ferromagnetic, as the dipole-dipole interaction for this is very weakly ferromagnetic, based on the Pr^{3+} moment and the lattice spacing [129].

Theoretical work by Onoda and Tanaka has proposed a model of quantum melting of the spin ice to describe all of these phenomena [130]. This pseudospin 1/2 Hamiltonian they propose

$$H_{\rm eff} = J \sum [\sigma_r^z \sigma_{r'}^z + 2\delta(\sigma_r^+ \sigma_{r'}^- + \sigma_r^- \sigma_{r'}^+) + 2q(e^{i\Phi_{r,r'}} \sigma_r^+ \sigma_{r'}^+ + h.c.)] \qquad \text{(D.1)}$$

finds at low temperatures, a cooperative ferroquadrupolar ground state with a chirality. These systems are termed an analog to smectic liquid crystals.

No published works have examined Hf^{+4} as the B-site ion, with the exception of a report on growth and low temperature properties by Craig *et al.* [20]. Early specific heat measurements on $Pr_2Hf_2O_7$ show no ordering, a θ_{CW} = -2.04 K, and a broad feature around 2 K. These initial results showed promise for the absence of ordering in the same spirit as $Pr_2Zr_2O_7$. These materials were prepared with hydroxide starting materials.

D.2 Experimental Details

Polycrystalline samples of $Pr_2Hf_2O_7$ were provided by Alice Durand and Linton Corruccini at University of California-Davis. The samples were prepared using the standard solid

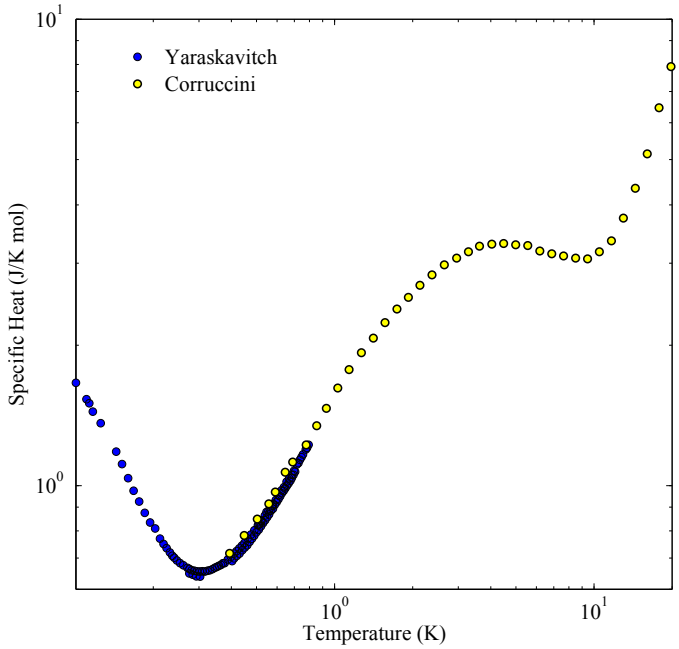

Figure D.1: The measured specific heat of $Pr_2Hf_2O_7$. Good agreement with the high temperature work by Corruccini is found. No ordering transition is seen to 100 mK.

state reaction, where constituent oxides Pr_6O_11 and HfO_2 were combined and ground in stoichiometric ratios. Pressed pellets were fired at 1600°, 1500°, 1400°, 1300°, and 1200° for 72 hours each. After an intermediate grinding and pressing, the firing was repeated. Powder x-ray diffraction patterns found the material to be of the $Fd\bar{3}m$ with a lattice constant of 10.651 Å. Two impurity peaks at the 1% level were apparent. Magnetic susceptibility measurements were consistent with all Pr ions being Pr^{3+}, not the tetravalent Pr^{4+}.

A polycrystalline sample of $Pr_2Hf_2O_7$, with mass 51.9 mg, was prepared using the method outlined in Appendix A, and measured using the quasi-adiabatic method. The specific heat of $Pr_2Hf_2O_7$ is plotted in Fig. D.1. No transition of any sort was observed between 100 mK and 800 mK. Pr+3 has a strong spin-orbit coupling between the nuclear and electronic spins [131] and so we can anticipate a nuclear hyperfine component to specific heat. This qualitatively explains the upturn at low temperatures, but does not solely account for it. The high temperature side of a nuclear hyperfine Schottky anomaly peak should behave as $C_{\text{nuclear}} \propto 1/T^2$ [132]. Curiously, the upturn clearly does not resemble

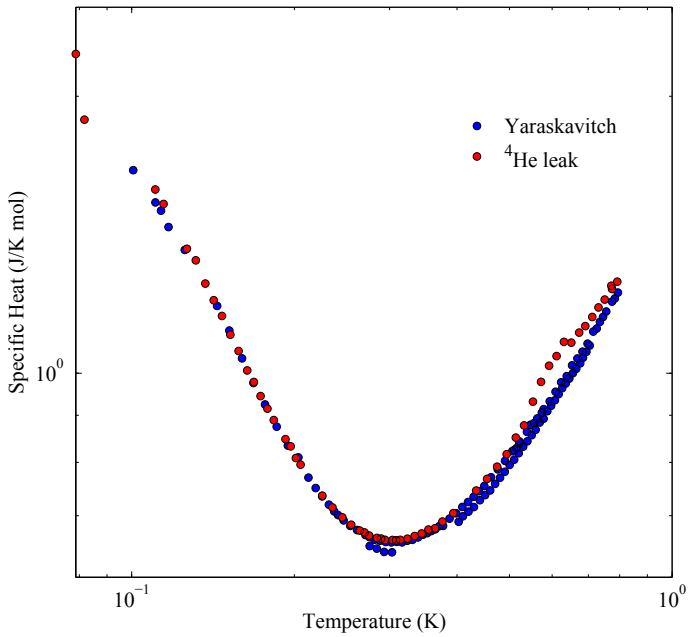

Figure D.2: The specific heat of $Pr_2Hf_2O_7$, including data taken with a helium leak in the vacuum space. The data taken with a leak shows a subtle anomaly due to ^{4}He leak in vacuum space.

this power law dependence, but instead a $\propto 1/T$ power law. This is likely coincidental, and can be taken as evidence that a significant amount of the electronic entropy remains, preventing a fit to the hyperfine contribution.

During the course of the measurement, one particular set of data taken all during one cooldown showed an anamolous feature around 0.6 K, shown in Fig. D.2. This was in contrast to previous data taken at those temperatures. As it turned out, a coworker, Borko Djurkovic, had previously seen a similar phenomenon on another dilution refrigerator in the group [133]. This was very apparent as a latent heat during his heat pulses, caused by the vapourization of a superfluid of helium which had crept over the sample. The effect wasn't nearly as severe, and only apparent after analysis of the data. However, after repair of a suspect solder joint at the 4 K flange of the fridge, the feature was no longer apparent. In any situation where a helium leak in the vacuum space may be anticipated, however slight, quasi-adiabatic specific heat seems to be able to provide a signature.

D.3 Comparison and Discussion

We see good agreement with the high temperature data provided by the Corruccini group. The specific heat also is very similarly to that seen in $Pr_2Zr_2O_7$, which is the most similar studied system, as mentioned in the Background. That measurement did not go low enough to observe the nuclear contribution [129].

Further understanding is required of the nuclear contribution specific heat, in order to subtract it from the electronic component and uncover if a ordering transition is indeed occurring. Any ordering feature occuring somewhere in that range could be obscured by the steep increase in specific heat. As mentioned in the previous discussion about $Tb_2Ti_2O_7$, estimating a nuclear hyperfine contribution to specific heat can be fraught with difficulties. The arrangement of nuclear levels woul be required in order to calculate the anticipated specific heat.

Ideally, Pr^{3+} ions would be substituted into, say, $Y_2Hf_2O_7$ in a low dilution, and electron spin resonance used to probe the local environment of the Pr^{3+} sites. This would yield the coupling between the nulclear and electron spins, from which then the contribution to specific heat could be determined. However, if we could see the peak of the nuclear anamoly, we could at least attempt a fit. A careful remeasurement of the sample with a re-configured sample size and weak link may be able to measure low enough in order to observe the peak temperature. A smaller sample will reduce the internal time constants of equilibration. Alternatively, the weak link time constant could be increased by reconfiguring the weak link. This would mean longer measurement time, but would allow measurement to lower temperatures.

Disorder may play a role in this refusal to order, but it seems unlikely, as the impurity phases seem to be at the 1% level according to the x-ray diffraction. Site substitution is probably not occurring on significant quantities, based upon the x-ray diffraction and susceptibility by Durand and Corruccini. Deviations from Ising-like behaviour could be potentially contributing to spin liquid behaviour.

D.4 Conclusion

This is the first specific heat measurement of this material at these temperatures to the best of our knowledge. We find no ordering transition down to 100 mK. The antiferromagnetic Curie-Weiss temperature should lead to an ordering transition, but there is no

transition observed, implying a spin liquid behaviour. Further work is required to understand this material, including a detailed calculation of the crystal electric field scheme, and the sensitivity of the system to any disorder as $Yb_2Ti_2O_7$ and $Tb_2Ti_2O_7$ seem to be.

Praseodymium-based pyrochlore oxides have already been the subject of substantial interest and numerous exhibitions of exotic physics, as mentioned in the background. The hafnates may represent a new frontier in the pyrochlore oxides, which have already been such a great area of research.

References

[1] L. Pauling, J. Am. Chem. Soc. **57**, 2680 (1935).

[2] P. G. Wolynes and W. A. Eaton, Physics World , 39 (1999).

[3] P. G. Debenedetti and F. H. Stillinger, Nature **410**, 259 (2001).

[4] S. T. Bramwell and M. J. Gingras, Science **294**, 1495 (2001).

[5] C. Castelnovo, R. Moessner, and S. L. Sondhi, Nature **451**, 42 (2008).

[6] L. Jaubert and P. Holdsworth, Nature Phys. **5**, 258 (2009).

[7] S. T. Bramwell, S. R. Giblin, S. Calder, R. Aldus, D. Prabhakaran, and T. Fennell, Nature **461**, 956 (2009).

[8] H. Kadowaki, N. Doi, Y. Aoki, Y. Tabata, T. J. Sato, J. Lynn, K. Matsuhira, and Z. Hiroi, J. Phys. Soc. Japan **78**, 103706 (2009).

[9] D. J. P. Morris, D. A. Tennant, S. A. Grigera, B. Klemke, C. Castelnovo, R. Moessner, C. Cztemasty, M. Meissner, K. C. Rule, J.-U. Hoffmann, K. Kiefer, S. Gerischer, D. Slobinsky, and R. S. Perry, Science **326**, 411 (2009).

[10] T. Fennell, P. Deen, A. Wildes, K. Schmalzl, D. Prabhakaran, A. Boothroyd, R. Aldus, D. F. McMorrow, and S. T. Bramwell, Science **326**, 415 (2009).

[11] L. D. C. Jaubert and P. C. W. Holdsworth, J. Phys.: Condens. Matter **23**, 164222 (2011).

[12] C. Castelnovo, R. Moessner, and S. L. Sondhi, Phys. Rev. B **84**, 144435 (2011).

[13] S. R. Giblin, S. T. Bramwell, P. C. W. Holdsworth, D. Prabhakaran, and I. Terry, Nature Phys. **7**, 252 (2011).

[14] J. Gardner, M. Gingras, and J. E. Greedan, Rev. Mod. Phys. **82**, 53 (2010).

[15] K. A. Ross, L. Savary, B. D. Gaulin, and L. Balents, Phys. Rev. X **1**, 021002 (2011).

[16] K. A. Ross, L. R. Yaraskavitch, M. Laver, J. S. Gardner, J. A. Quilliam, S. Meng, J. B. Kycia, D. K. Singh, T. Proffen, H. A. Dabkowska, and B. D. Gaulin, Phys. Rev. B **Accepted** (2011).

[17] H. R. Molavian, M. J. P. Gingras, and B. Canals, Phys. Rev. Lett. **98**, 157204 (2007).

[18] H. Takatsu, H. Kadowaki, T. J. Sato, Y. Tabata, and J. W. Lynn, arXiv:1106.3649 (2011).

[19] H. Takatsu, H. Kadowaki, T. J. Sato, J. W. Lynn, Y. Tabata, T. Yamazaki, and K. Matsuhira, J. Phys.: Condens. Matter **24**, 052201 (2012).

[20] H. A. Craig, UC Davis Explorations **12**, 23 (2009).

[21] G. H. Wannier, Phys. Rev. **79**, 357 (1950).

[22] R. M. F. Houtappel, Physica **26**, 425 (1950).

[23] P. W. Anderson, Phys. Rev. **102**, 1008 (1956).

[24] J. Villain, Z. Phys. B **33**, 31 (1979).

[25] S. T. Bramwell, M. N. Field, M. J. Harris, and I. P. Parkin, J. Phys.: Condens. Matter **12**, 483 (2000).

[26] N. W. Ashcroft and N. D. Mermin, *Solid State Physics* (Thompson Learning, 1976).

[27] L. Balents, Nature **464**, 199 (2010).

[28] N. Hamaguchi, T. Matsushita, N. Wada, Y. Yasui, and M. Sato, Phys. Rev. B **69**, 132413 (2004).

[29] N. P. Raju, E. Gmelin, and R. K. Kremer, Phys. Rev. B **46**, 5405 (1992).

[30] M. J. P. Gingras, C. V. Stager, N. P. Raju, B. D. Gaulin, and J. E. Greedan, Phys. Rev. Lett. **78**, 947 (1997).

[31] J. A. Quilliam, K. A. Ross, A. G. Del Maestro, M. J. P. Gingras, L. R. Corruccini, and J. B. Kycia, Phys. Rev. Lett. **99**, 097201 (2007).

[32] R. S. Freitas and J. S. Gardner, J. Phys.: Condens. Matter **23**, 164215 (2011).

[33] W. H. Bragg, Proc. Phys. Soc. London **34** (1921).

[34] W. F. Giauque and M. F. Ashley, Phys. Rev. **43**, 81 (1933).

[35] W. F. Giauque and J. W. Stout, J. Am. Chem. Soc. **58**, 1144 (1936).

[36] J. D. Bernal and R. H. Fowler, J. Chem. Phys. **1**, 515 (1933).

[37] J. D. Cashion, A. H. Cooke, M. J. M. Leask, T. L. Thorp, and M. R. Wells, Journal of Materials Science **3**, 402 (1968).

[38] H. W. Blöte, R. F. Wielinga, and W. J. Huiskamp, Physica **43**, 549 (1969).

[39] M. J. Harris, S. T. Bramwell, D. F. McMorrow, T. Zeiske, and K. W. Godfrey, Phys. Rev. Lett. **79**, 2554 (1997).

[40] M. J. Harris, S. T. Bramwell, T. Zeiske, D. F. McMorrow, and P. J. C. King, J. Magn. Magn. Mater. **177-181**, 757 (1998).

[41] A. Ramirez, A. Hayashi, R. Cava, R. Siddharthan, and B. Shastry, Nature **399**, 333 (1999).

[42] R. Siddharthan, B. Shastry, A. P. Ramirez, A. Hayashi, R. J. Cava, and S. Rosenkranz, Phys. Rev. Lett. **83**, 1854 (1999).

[43] Y. M. Jana and D. Ghosh, Phys. Rev. B **61**, 9657 (2000).

[44] S. Rosenkranz, A. Ramirez, A. Hayashi, R. J. Cava, R. Siddharthan, and B. S. Shastry, J. Appl. Phys. **87**, 5914 (2000).

[45] B. C. den Hertog and M. J. P. Gingras, Phys. Rev. Lett. **84**, 3430 (2000).

[46] S. T. Bramwell, M. J. Harris, B. C. den Hertog, M. J. P. Gingras, J. S. Gardner, D. F. McMorrow, A. R. Wildes, A. L. Cornelius, J. D. M. Champion, R. G. Melko, and T. Fennell, Phys. Rev. Lett. **87**, 047205 (2001).

[47] A. Cornelius and J. Gardner, Phys. Rev. B **64**, 060406 (2001).

[48] M. J. P. Gingras and B. C. den Hertog, Can. J. Phys **79**, 1339 (2001).

[49] K. Matsuhira, Y. Hinatsu, K. Tenya, and T. Sakakibara, J. Phys.: Condens. Matter **12**, L649 (2000).

[50] K. Matsuhira, Y. Hinatsu, and T. Sakakibara, J. Phys.: Condens. Matter **13**, L737 (2001).

[51] J. Snyder, J. S. Slusky, R. J. Cava, and P. Schiffer, Nature **413**, 48 (2001).

[52] R. G. Melko, B. C. den Hertog, and M. J. Gingras, Phys. Rev. Lett. **87**, 067203 (2001).

[53] J. Snyder, J. S. Slusky, R. J. Cava, and P. Schiffer, Phys. Rev. B **66**, 064432 (2002).

[54] R. Higashinaka, H. Fukazawa, D. Yanagishima, and Y. Maeno, Journal of Physics and Chemistry of Solids **63**, 1043 (2002).

[55] K. Matsuhira, Z. Hiroi, T. Tayama, S. Takagi, and T. Sakakibara, J. Phys.: Condens. Matter **14**, L559 (2002).

[56] Z. Hiroi, K. Matsuhira, S. Takagi, T. Tayama, and T. Sakakibara, J. Phys. Soc. Japan **72**, 411 (2003).

[57] R. Higashinaka, H. Fukazawa, and Y. Maeno, Phys. Rev. B **68**, 014415 (2003).

[58] J. S. Snyder, B. G. Ueland, J. S. Slusky, H. Karunadasa, R. J. Cava, A. Mizel, and P. Schiffer, Phys. Rev. Lett. **91**, 107201 (2003).

[59] G. Ehlers, A. L. Cornelius, M. Orendae, M. Kajnakova, T. Fennell, S. T. Bramwell, and J. S. Gardner, J. Phys.: Condens. Matter **15**, L9 (2003).

[60] G. Ehlers, A. L. Cornelius, T. Fennell, M. Koza, S. T. Bramwell, and J. S. Gardner, J. Phys.: Condens. Matter **16**, S635 (2004).

[61] J. Snyder, B. G. Ueland, J. S. Slusky, H. Karunadasa, R. J. Cava, and P. Schiffer, Phys. Rev. B **69**, 064414 (2004).

[62] R. G. Melko and M. J. P. Gingras, J. Phys.: Condens. Matter **16**, R1277 (2004).

[63] J. Shi, Z. Tang, B. Zhu, P. Huang, D. Yin, C. Li, Y. Wang, and H. Wen, J. Magn. Magn. Mater. **310**, 1322 (2007).

[64] M. Orendáč, J. Hanko, E. Čižmár, A. Orendáčová, M. Shirai, and S. T. Bramwell, Phys. Rev. B. **75**, 104425 (2007).

[65] T. Fennell, O. A. Petrenko, B. Føak, J. S. Gardner, S. T. Bramwell, and B. Ouladdiaf, Phys. Rev. B **72**, 224411 (2005).

[66] J. P. Clancy, J. P. C. Ruff, S. R. Dunsiger, Y. Zhao, H. A. Dabkowska, J. S. Gardner, Y. Qiu, J. R. D. Copley, T. Jenkins, and B. D. Gaulin, Phys. Rev. B **79**, 014408 (2009).

[67] J. P. Sutter, S. Tsutsui, R. Higashinaka, Y. Maeno, O. Leupold, and A. Q. R. Baron, Phys. Rev. B **75**, 140402(R) (2007).

[68] J. Lago, S. Blundell, and C. Baines, J. Phys.: Condens. Matter **19**, 326210 (2007).

[69] T. Yavors'kii, T. Fennell, M. J. P. Gingras, and S. T. Bramwell, Phys. Rev. Lett. **101**, 037204 (2008).

[70] H. Kadowaki, Y. Ishii, K. Matsuhira, and Y. Hinatsu, Phys. Rev. B **65**, 144421 (2002).

[71] K. Matsuhira, Y. Hinatsu, K. Tenya, H. Amitsuka, and T. Sakakibara, J. Phys. Soc. Japan **71**, 1576 (2002).

[72] H. D. Zhou, C. R. Wiebe, J. A. Janik, L. Balicas, Y. J. Yo, Y. Qiu, J. R. D. Copley, and J. S. Gardner, Phys. Rev. Lett. **101**, 227204 (2008).

[73] Y. M. Jana, A. Sengupta, and D. Ghosh, J. Magn. Magn. Mater. **248**, 7 (2002).

[74] K. A. Milton, Rep. Prog. Phys. **69**, 1637 (2006).

[75] P. A. M. Dirac, Proceedings of the Royal Society of London **133**, 60 (1931).

[76] C. L. Henley, Annu. Rev. Condens. Matter Phys. **1**, 179 (2010).

[77] I. A. Ryzhkin, Journal of Experimental and Theoretical Physics **101**, 481 (2005).

[78] T. Sakakibara, T. Tayama, Z. Hiroi, K. Matsuhira, and S. Takagi, Phys. Rev. Lett. **90**, 207205 (2003).

[79] L. Chang, Y. Su, H. Schneider, R. Mittal, M. R. Lees, G. Balakrishnan, and Brückel, J. Phys.: Conf. Series **211**, 012013 (2010).

[80] C. Castelnovo, R. Moessner, and S. L. Sondhi, Phys. Rev. Lett. **104**, 107201 (2010).

[81] D. Slobinsky, C. Castelnovo, R. A. Borzi, A. S. Gibbs, A. P. Mackenzie, R. Moessner, and S. A. Grigera, Phys. Rev. Lett. **105**, 267205 (2010).

[82] B. Klemke, M. Meissner, P. Strehlow, K. Keifer, S. A. Grigera, and D. A. Tennant, J. Low Temp. Phys. **163**, 345 (2011).

[83] S. R. Dunsiger, A. A. Aczel, C. Arguello, H. A. Dabkowska, A. Dabkowski, M.-H. Du, T. Goko, B. Javanprast, T. Lin, F. L. Ning, H. M. L. Noad, D. J. Singh, T. J. Williams, Y. J. Uemura, M. J. P. Gingras, and G. M. Luke, Phys. Rev. Lett. **107**, 207207 (2011).

[84] H. D. Zhou, S. T. Bramwell, J. G. Cheng, C. R. Wiebe, G. Li, L. Balicas, J. A. Bloxsom, H. J. Silverstein, J. S. Zhou, J. B. Goodenough, and J. S. Gardner, Nature Comm. **2**, 478 (2011).

[85] J. Costa-Quintana and F. López-Aguilar, Progress in Electromagnetics Research **121**, 159 (2011).

[86] S. Ladak, D. E. Read, G. K. Perkins, L. F. Cohen, and W. R. Branford, Nature Physics **6**, 359 (2010).

[87] J. S. Gardner, B. D. Gaulin, and D. McK. Paul, J. Cryst. Growth **191**, 740 (1998).

[88] J. A. Quilliam, Specific heat of the dilute, dipolar-coupled, ising magnet $\mathrm{liho}_x\mathrm{y}_{1-x}\mathrm{f}_4$, Master's thesis, University of Waterloo, 2006.

[89] F. Pobell, *Matter and Methods at Low Temperatures, Third Edition* (Springer, 2007).

[90] R. Richardson and E. Smith, editors, *Experimental Techniques in Condensed Matter Physics at Low Temperatures* (Addison-Wesley, 1998).

[91] J. A. Quilliam, *Disorder, Geometric Frustration and Dipolar Interactions in Rare Earth Magnets*, PhD thesis, University of Waterloo, 2010.

[92] J. A. Quilliam, S. Meng, C. G. A. Mugford, and J. B. Kycia, Phys. Rev. Lett. **101**, 187204 (2008).

[93] J. A. Quilliam, L. R. Yaraskavitch, H. A. Dabkowska, B. D. Gaulin, and J. B. Kycia, Phys. Rev. B **83**, 094424 (2011).

[94] L. R. Yaraskavitch, H. M. Revell, S. Meng, K. A. Ross, H. M. L. Noad, H. A. Dabkowska, B. D. Gaulin, and J. B. Kycia, Phys. Rev. B **85**, 020410(R) (2012).

[95] J. Clarke and A. I. Braginski, editors, *The SQUID Handbook* (Wiley-VCH, 2004).

[96] H. Weinstock, editor, *SQUID Sensors: Fundamentals, Fabrication, and Applications* (Kluwer Academic, 1996).

[97] A. Aharoni, J. Appl. Phys. **83**, 3432 (1998).

[98] S. Yoshida, K. Nemoto, and K. Wada, J. Phys. Soc. Japan **73**, 1619 (2004).

[99] L. D. C. Jaubert, *Topological Constraints and Defects in Spin Ice*, PhD thesis, Ecole Normale Supérieure de Lyon, 2009.

[100] H. Fukazawa, R. G. Melko, R. Higashinaka, Y. Maeno, and M. J. P. Gingras, Phys. Rev. B **65**, 054410 (2002).

[101] O. A. Petrenko, M. R. Lees, and G. Balakrishnan, Phys. Rev. B **68**, 012406 (2003).

[102] H. Diep, editor, *Frustrated Spin Systems* (World Scientific, 2004).

[103] J. Snyder, B. G. Ueland, A. Mizel, J. S. Slusky, H. Karunadasa, R. J. Cava, and P. Schiffer, Phys. Rev. B **70**, 184431 (2004).

[104] X. Ke, R. S. Freitas, B. G. Ueland, G. C. Lau, M. L. Dahlberg, R. J. Cava, R. Moessner, and P. Schiffer, Phys. Rev. Lett. **99**, 137203 (2007).

[105] K. A. Ross, J. P. C. Ruff, C. P. Adams, J. S. Gardner, H. A. Dabkowska, Y. Qiu, J. R. D. Copley, and B. D. Gaulin, Phys. Rev. Lett. **103**, 227202 (2009).

[106] H. B. Cao, A. Gukasov, I. Mirebeau, and P. Bonville, J. Phys.: Condens. Matter **21**, 492202 (2009).

[107] L.-J. Chang, S. Onoda, Y. Su, Y.-J. Kao, K.-D. Tsuei, Y. Yasui, K. Kakurai, and M. R. Lees, **arXiv:111.5406v1**.

[108] P. Dalmas de Réotier, V. Glazkov, C. Marin, A. Yaouanc, P. C. M. Gubbens, S. Sakarya, P. Bonville, A. Amato, C. Baines, and P. J. C. King, Physica B **374-375**, 145 (2006).

[109] J. A. Hodges, P. Bonville, A. Forget, and G. André, Can. J. Phys **79**, 1373 (2001).

[110] J. A. Hodges, P. Bonville, A. Forget, M. Rams, K. Królas, and G. Dhalenne, J. Phys.: Condens. Matter **13**, 9301 (2001).

[111] J. A. Hodges, P. Bonville, A. Forget, A. Yaouanc, P. Dalmas de Réotier, G. André, M. Rams, K. Królas, C. Ritter, P. C. M. Gubbens, C. T. Kaiser, P. J. C. King, and C. Baines, Phys. Rev. Lett. **88**, 077204 (2002).

[112] Y. Yasui, M. Soda, S. Iikubo, M. Ito, M. Sato, N. Hamaguchi, T. Matsushita, N. Wada, T. Takeuchi, N. Aso, and K. Kakurai, J. Phys. Soc. Japan **72**, 3014 (2003).

[113] J. S. Gardner, G. Ehlers, N. Rosov, R. W. Erwin, and C. Petrovic, Phys. Rev. B **70**, 180404 (2004).

[114] P. Bonville, J. A. Hodges, E. Bertin, and J.-P. Bouchaud, Hyperfine Interactions **156**, 103 (2004).

[115] H. Cao, A. Gukasov, I. Mirebeau, P. Bonville, C. Decorse, and G. Dhalenne, Phys. Rev. Lett. **103**, 056402 (2009).

[116] J. D. Thompson, Searching for the magnetic interactions in the rare earth pyrochlore oxide $yb_2ti_2o_7$, Master's thesis, University of Waterloo, 2011.

[117] J. D. Thompson, P. A. McClarty, H. M. Ronnow, L. P. Regnault, A. Sorge, and M. J. P. Gingras, Phys. Rev. Lett. **106**, 187202 (2011).

[118] J. D. Thompson, P. A. McClarty, and M. J. P. Gingras, J. Phys.: Condens. Matter **23**, 164219 (2011).

[119] A. Yaouanc, P. Dalmas de Réotier, C. Marin, and V. Glazkov, Phys. Rev. B **Accepted** (2011).

[120] M. J. P. Gingras, B. C. den Hertog, M. Faucher, J. S. Gardner, S. R. Dunsiger, L. J. Chang, B. D. Gaulin, N. P. Raju, and J. E. Greedan, Phys. Rev. B **62**, 6496 (2000).

[121] J. S. Gardner, B. D. Gaulin, S.-H. Lee, C. Broholm, N. P. Raju, and J. E. Greedan, Phys. Rev. Lett. **83**, 211 (1999).

[122] H. R. Molavian and M. J. P. Gingras, J. Phys.: Condens. Matter **21**, 172201 (2009).

[123] Y. Chapuis, *Frustration géomeétrique, transitions de phase et ordre dynamique*, PhD thesis, Université Joseph Fourier, 2010.

[124] Y. Chapuis, A. Yaouanc, P. Dalmas de Réotier, C. Marin, S. Vanishri, S. H. Curnoe, C. Vâju, and A. Forget, Phys. Rev. B **82**, 100402(R) (2010).

[125] B. D. Gaulin, J. S. Gardner, P. A. McClarty, and M. J. P. Gingras, Phys. Rev. B **84**, 140402(R) (2011).

[126] A. Yaouanc, P. Dalmas de Réotier, Y. Chapuis, C. Marin, S. Vanishri, D. Aoki, L.-P. Føok, Regnault, C. Buisson, A. Amato, C. Baines, and A. D. Hillier, Phys. Rev. B **84**, 184403 (2011).

[127] J. P. C. Ruff, B. D. Gaulin, J. P. Castellan, K. C. Rule, J. P. Clancy, J. Rodriguez, and H. A. Dabkowska, Phys. Rev. Lett. **99**, 237202 (2007).

[128] K. Matsuhira, C. Sekine, C. Paulsen, and Y. Hinatsu, J. Magn. Magn. Mater. **272-276**, e981 (2004).

[129] K. Matsuhira, C. Sekine, C. Paulsen, M. Wakeshima, Y. Hinatsu, T. Kitazawa, Y. Kiuchi, Z. Hiroi, and S. Takagi, J. Phys. Conf. Series **145**, 012031 (2009).

[130] S. Onoda and Y. Tanaka, Phys. Rev. Lett. **105**, 047201 (2010).

[131] A. Abragam and B. Bleaney, *Electron Paramagnetic Resonance of Transition Ions* (Oxford University Press, 1970).

[132] A. Tari, *The Specific Heat of Matter at Low Temperatures* (Imperial College Press, 2003).

[133] B. Djurkovic, Specific heat of unconventional superconductors, Master's thesis, University of Waterloo, 2010.